

Graph-Cover Decoding and Finite-Length Analysis of Message-Passing Iterative Decoding of LDPC Codes*

Pascal O. Vontobel[†] and Ralf Koetter[‡]

Abstract

The goal of the present paper is the derivation of a framework for the finite-length analysis of message-passing iterative decoding of low-density parity-check codes. To this end we introduce the concept of graph-cover decoding. Whereas in maximum-likelihood decoding all codewords in a code are competing to be the best explanation of the received vector, under graph-cover decoding all codewords in all finite covers of a Tanner graph representation of the code are competing to be the best explanation.

We are interested in graph-cover decoding because it is a theoretical tool that can be used to show connections between linear programming decoding and message-passing iterative decoding. Namely, on the one hand it turns out that graph-cover decoding is essentially equivalent to linear programming decoding. On the other hand, because iterative, locally operating decoding algorithms like message-passing iterative decoding cannot distinguish the underlying Tanner graph from any covering graph, graph-cover decoding can serve as a model to explain the behavior of message-passing iterative decoding.

Understanding the behavior of graph-cover decoding is tantamount to understanding the so-called fundamental polytope. Therefore, we give some characterizations of this polytope and explain its relation to earlier concepts that were introduced to understand the behavior of message-passing iterative decoding for finite-length codes.

Index Terms: Graph-cover decoding, iterative decoding, message-passing algorithms, linear programming decoding, fundamental polytope, fundamental cone, pseudo-codewords, minimal pseudo-codewords, pseudo-weight.

*The work of P. O. Vontobel was supported by NSF Grants CCR 99-84515 and CCR-0105719 at UIUC and by and by NSF Grants CCR 99-84515, CCR 01-05719, ATM-0296033, DOE SciDAC, and ONR Grant N00014-00-1-0966 at UW-Madison. The work of R. Koetter was partially supported by NSF Grants CCR 99-84515 and CCR-0105719. The material in this paper was presented in part at the 3rd International Conference on Turbo Codes and Related Topics, Brest, France, September 2003.

[†]Was with ECE Department, University of Wisconsin-Madison, 1415 Engineering Drive Madison, WI 53706, USA. E-Mail: pascal.vontobel@ieee.org. P. O. Vontobel is the corresponding author.

[‡]Coordinated Science Laboratory and ECE Department, University of Illinois at Urbana-Champaign, 1308 West Main Street, Urbana, IL 61801, USA. E-mail: koetter@uiuc.edu.

1 Introduction

Low-density parity-check (LDPC) codes were introduced by Gallager [1, 2]. As important as the codes themselves was also a class of decoding algorithms that he presented. These algorithms had two common features. Firstly, based on the observed channel output, these algorithms tried to *iteratively* find the codeword that was sent over the channel. Secondly, these algorithms operated *locally* in the sense that they combined partial information that could then be used in other partial-information combining.

Although revolutionary, these codes and decoding algorithms were forgotten for a long time. The main reason being that, although these algorithms were computationally far less demanding than maximum a-posterior decoding (MAPD) and maximum-likelihood decoding (MLD), they were nevertheless too complex for that time. Besides some work by Zyablov [3], Zyablov and Pinsker [4], Tanner [5], and Margulis [6], Gallager’s ideas lay dormant for about 30 years. Then, in the mid-1990’s, the discovery of turbo codes by Berrou, Glavieux, and Thitimajshima [7], the rediscovery of LDPC codes by MacKay and Neal [8, 9, 10], and the work of Wiberg, Loeliger, and Koetter [11, 12] on codes on graphs and message-passing iterative decoding (MPID) initiated a flurry of research on iterative decoders and codes amenable to such decoders that continues to these days. They lead to new and practical approaches not only in communications but also in signal processing and artificial intelligence. Many of these developments can be explained nowadays with the help of concepts like the generalized distributive law as formulated by Aji and McEliece [13] or factor graphs and the sum-product algorithm (SPA) by Kschischang, Frey, and Loeliger [14, 15].

While MPID has had unparalleled success, it is fair to say that its behavior for the case of finite-length codes is, at present, not well understood and many results are based on simulations alone. Before delineating what is known about the finite-length case, let us however first turn to the infinite-length case. For LDPC codes with block length going to infinity (where it is assumed that the length of the smallest cycle in the underlying Tanner graph also goes to infinity, or where at least the fraction of finite-length cycles vanishes) it turned out that there is an elegant analysis technique, the so-called density evolution: this technique was first introduced by Luby et al. [16] for the binary erasure channel and then by Richardson, Shokrollahi, and Urbanke [17, 18] for more general channels. These results were very valuable in guiding code designers how to tweak LDPC codes into well-performing (finite-length) irregular LDPC codes. There are, however, some drawbacks of these techniques: firstly, it is not clear, if these results give the best finite-length irregular codes, and secondly, and more importantly, they do not say if a specific code exhibits an error floor and if yes, where this error floor is.

Early techniques that tried to tackle the finite-length case focused on specific families of codes and/or restricted classes of channels. In that direction, let us mention the analysis of so-called cycle codes¹ by Wiberg [12], tail-biting trellises and graphs with a single cycle by Anderson and Hladik [19], by Aji et al. [20], and by Forney et al. [21]. For the binary erasure channel, influential work was done by Di et al. [22] utilizing the notion of *stopping sets*. Finally, for more general channels, the idea of *near-codewords*, *trapping sets*, *extrinsic message degree (EMD)*, and *instantons* were used by MacKay and Postol [23], by Richardson [24], by Tian et al. [25, 26], and by Chernyak et al. [27, 28], respectively, to empirically characterize problematic situations for MPID.

¹Cycle codes are codes with a Tanner graph where all bit nodes have degree two.

A complete understanding of MPID of finite-length codes with finitely many iterations is essentially given by *computation trees* [12], i.e. by the valid configurations of such computation trees. Some work on analyzing computation trees was done by Wiberg [12], with subsequent work by Frey et al. [29] and Forney et al. [30]. Although this approach is intuitively very appealing, it seems to be very difficult to get a simple characterization of the valid configurations on computation trees, a necessary requirement if one wants to understand MPID. In fact, only extremely simple codes were analyzed with this technique so far.

Experimental results for codes of reasonable length and rate show that decision boundaries can be of a rather complex nature, a fact that makes the above-mentioned problems in trying to analyze the valid configurations on computation trees not completely unexpected. A complete understanding of MPID of a given code is probably an illusionary task, therefore we will settle here for a more modest goal.

In this paper we present an analysis technique for MPID of a given code. Although the underlying principle of our analysis technique is very simple, experimentally it seems to give very good predictions of the decoding behavior; in fact, it gives the correct answers for all the cases where MPID behavior is understood analytically. The predicted decision boundaries are hyperplanes in the log-likelihood ratio vector space and it turns out that the decision boundaries are exactly the same as the ones under so-called linear programming decoding (LPD) that was recently introduced by Feldman, Wainwright, and Karger [31, 32]. In the light of this coincidence one might actually argue that the various MPID algorithms are nothing else than low-complexity, very efficient, and aggressive LP solvers that most of the time “decide” for the same (pseudo-)codeword as LPD, but not always.² We have done some work towards showing the nearness of min-sum algorithm (MSA) decoding and LPD [33] but in this paper we will not discuss this aspect any further.

The analysis technique that was mentioned in the previous paragraph will be called graph-cover decoding (GCD): its name stems from the fact that during GCD all codewords in all finite covers of a given Tanner graph are competing to be the best explanation of the received vector. Analyzing all the codes in all the finite covers seems at first to be an infeasible task. However, it turns out that they can be characterized by the so-called fundamental polytope. Among other things, we will see in this paper how this fundamental polytope unifies the notions of stopping sets, pseudo-codewords, near-codewords, and trapping sets.³

The outline of this paper is as follows. In Sec. 1.1 we will discuss the iterative decoding of a simple code and show the underlying philosophy behind our analysis technique. After some notational remarks in Sec. 1.2, the main part of the paper starts in Sec. 2 which introduces graph covers and the fundamental polytope. In Sec. 3 we review MAPD/MLD of codes and by considering relaxations of optimization problems we make the link to LPD. Then, in Sec. 4 we will show that GCD is essentially equivalent to LPD and we will see how GCD can be seen as a model for MPID. Whereas Sec. 5 will discuss various descriptions and properties of the fundamental polytope and cone, Sec. 6 will focus on a variety of pseudo-weights and their properties. A simple upper bound on the AWGNC pseudo-weight will be presented in Sec. 7 which implies a sub-linear asymptotic behavior of the AWGNC pseudo-weight for any family of regular LDPC codes (under some mild conditions). Finally, in Sec. 8 we explain the relationship of GCD to other concepts that have been used in the past to explain the

²When LPD decides for a pseudo-codeword that is not a codeword, the dynamical behavior of MPID depends very much on the type of the MPID under consideration.

³For more references on these topics, see also [34].

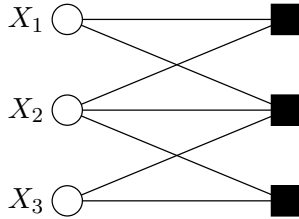


Figure 1: Tanner graph T of the length-3 code under consideration.

finite-length behavior of MPID, and in Sec. 9 we offer some conclusions and mention some open problems.

1.1 Motivating Example

Because we are using binary codes, we can without loss of optimality assume that a decoding algorithm bases its decision on the log-likelihood ratio (LLR) vector which is given by the observed channel output sequence. The understanding of a particular decoding algorithm is then tightly related to the understanding the decision regions in the space of LLR vectors. While the visualization of decision regions is a very intuitive way of showing how a decoder works (and of showing differences between different decoders), it is usually infeasible to show all the aspects of the decision regions since practical codes have a length of several tens of bits to several ten thousands of bits which implies that the space of LLR vectors has a dimension of several tens to several ten thousands.

However, some of the key differences between MAPD/MLD and iterative decoding can already be seen for very short codes. The aim of this section is to discuss such a very short code and to introduce an approximate analysis based on graph covers that explains the main characteristics of the decision regions of iterative decoding like sum-product algorithm (SPA) and the min-sum algorithm (MSA) decoding. (Note that the notation that we will use in this subsection will be properly introduced in Sec. 1.2 and in later sections.)

We consider a code \mathcal{C} of length $n = 3$ defined by the parity-check matrix

$$\mathbf{H} \triangleq \begin{pmatrix} 1 & 1 & 0 \\ 1 & 1 & 1 \\ 0 & 1 & 1 \end{pmatrix}, \quad (1)$$

whose Tanner graph $T \triangleq T(\mathbf{H})$ is depicted in Fig. 1. Because \mathbf{H} has rank 3, the dimension of the code is 0 and therefore \mathcal{C} contains only one codeword:

$$\mathcal{C} \triangleq \left\{ (x_1, x_2, x_3) \in \mathbb{F}_2^3 \mid (x_1, x_2, x_3) \cdot \mathbf{H}^T = \mathbf{0} \right\} = \{(0, 0, 0)\}.$$

While it, at first, may seem strange to consider a zero-rate code, it is indeed an ideal candidate to investigate problematic behaviors of iterative decoding. Assume that we are using the code for data transmission over an additive white Gaussian noise channel (AWGNC) and that the LLR vector is $\boldsymbol{\lambda} = (\lambda_1, \lambda_2, \lambda_3)$.

Consider first block-wise MAPD (which is equivalent to block-wise MLD since we assume that all codewords are transmitted equally likely). It is immediately apparent that for such

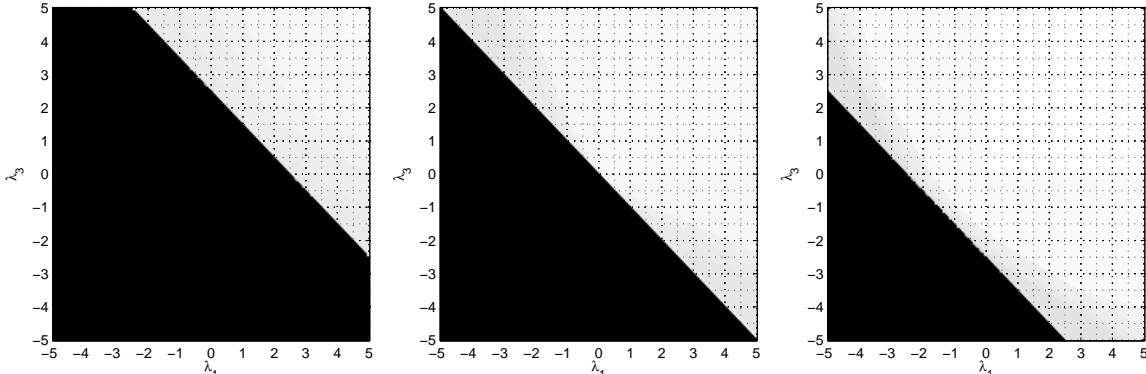


Figure 2: SPA decoding with maximally 60 iterations of the code \mathcal{C} that is represented by the Tanner graph \mathbb{T} in Fig. 1. The gray-scale indicates after how many iterations the algorithm converged to the all-zeros codeword with the implication that in the black region the decoder did not converge (see text for more details). From left to right: (λ_1, λ_3) -plane for $\lambda_2 = -2.5, 0, +2.5$.

a decoder there is only one decision region: we decide $\hat{\mathbf{x}} = (0, 0, 0)$ independently of $\boldsymbol{\lambda}$.⁴

We now turn to MPID, more precisely decoding based on the SPA and MSA [14] where one iteration consists in updating the messages at all variable nodes and then updating the messages at all check nodes. The SPA decoding convergence behavior as a function of $(\lambda_1, \lambda_2, \lambda_3)$ is depicted in Fig. 2: the gray-scale indicates after how many iterations the SPA converged to the all-zeros codeword.

In practical applications, the SPA and the MSA are performed for a certain pre-defined number of iterations. The binary vector that is obtained at the end of these iterations is then considered to be the decision on the transmitted codeword. Very often, the following termination rule is used additionally: the algorithm terminates if the binary vector found by the algorithm is a codeword, i.e. the syndrome is the all-zeros vector.

However, for our investigations of the code \mathcal{C} we did not adopt this latter termination rule: the reason is that there are only eight binary vectors of length 3 and therefore it is not unlikely that at some point the algorithm obtains the all-zeros vector even if the internal state of the iterative process has not converged to a stable point.⁵ So, for obtaining the plots in Fig. 2 we did the following: for each $(\lambda_1, \lambda_2, \lambda_3)$ point we performed 60 iterations of the SPA and we considered the algorithm to have converged once the decision vector remained the all-zeros codeword over subsequent iterations. Fig. 2 shows then the decision regions and the convergence times under SPA decoding after performing 60 iterations. It is evident that these decision regions are clearly *different* from the decision regions for block-wise MAPD/MLD! Indeed, the plots in Fig. 2 suggest that there is a decision boundary described by the equation $\lambda_1 + \lambda_2 + \lambda_3 = 0$: for $\lambda_1 + \lambda_2 + \lambda_3 > 0$ the SPA does converge and for $\lambda_1 + \lambda_2 + \lambda_3 < 0$ the SPA does not converge to the all-zeros codeword.

How can these differences in the decision regions between MAPD/MLD on the one hand

⁴Note that using a *symbol-wise* maximum a-posteriori decoder has also only one decision region: we decide for $\hat{x}_1 = 0, \hat{x}_2 = 0, \hat{x}_3 = 0$ independently of $\boldsymbol{\lambda}$.

⁵For reasonably long codes this is hardly an issue. E.g. for a rate-1/2 code of length 200, the probability that the algorithm accidentally finds a codeword is $2^{100}/2^{200} = 2^{-100}$.

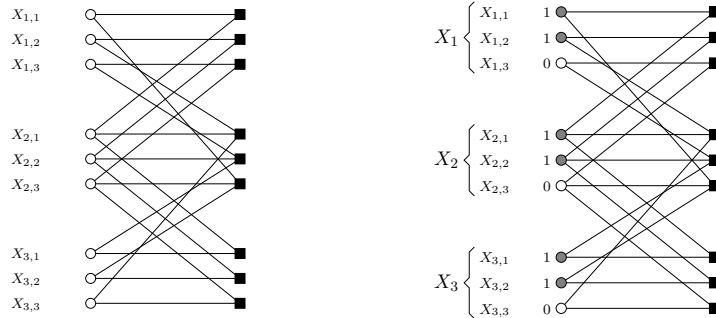


Figure 3: Left: a possible triple cover \tilde{T} of the Tanner graph T . Right: a non-zero codeword of the code defined by \tilde{T} .

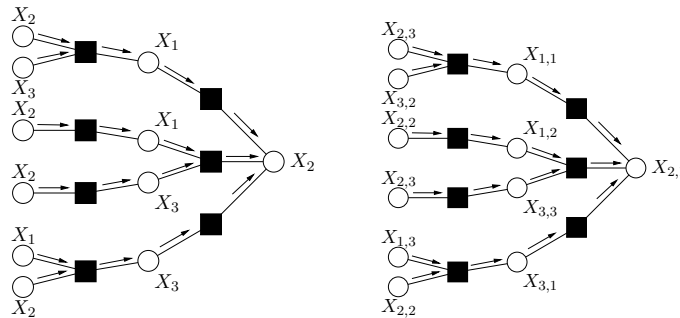


Figure 4: Left: computation tree with root X_2 after two iterations when decoding code \mathcal{C} . Right: computation tree with root $X_{2,1}$ after two iterations when decoding code $\tilde{\mathcal{C}}$.

and MPID on the other hand be explained? In this paper we argue that the key difference between the block-wise MAPD/MLD (or symbol-wise MAPD/MLD) and any MPID algorithm is the following: whereas the former algorithms use *global* information and constraints to find the optimal solution, the latter algorithms base their decisions on information that was gathered by processing information *locally*. This locality, which on one hand leads to huge savings in terms of the number of computations needed, is on the other hand also the main weakness of any MPID algorithm.

Let us briefly outline how we will use this global-vs-local perspective to obtain an understanding of the differences between MAPD/MLD and MPID. Consider the code $\tilde{\mathcal{C}}$ of length 9 that is defined by the Tanner graph \tilde{T} in Fig. 3 (left). Assume that we use this code for data transmission over an AWGNC and assume that at the receiver the hypothetical LLR vector is

$$\tilde{\lambda} \triangleq (\lambda_{1,1}:\lambda_{1,2}:\lambda_{1,3}, \lambda_{2,1}:\lambda_{2,2}:\lambda_{2,3}, \lambda_{3,1}:\lambda_{3,2}:\lambda_{3,3}).$$

In the same way that we used the SPA for decoding the code \mathcal{C} whose Tanner graph is shown in Fig. 1, we can use the analogous message-passing-based decoding algorithm for decoding the code $\tilde{\mathcal{C}}$.

For both cases we can draw the computation trees [12]: Fig. 4 (left) shows the computation tree with root X_2 after two iterations when decoding code \mathcal{C} whereas Fig. 4 (right) shows the

computation tree with root $X_{2,1}$ after two iterations when decoding code $\tilde{\mathcal{C}}$. The topological equivalence with the computation tree in Fig. 4 (left) might at first appear as a coincidence. However, this is not a coincidence. The reason is that the Tanner graph $\tilde{\mathbb{T}}$ has a special relationship with respect to the Tanner graph \mathbb{T} ; in fact, $\tilde{\mathbb{T}}$ is a so-called 3-cover of \mathbb{T} . This means that $\tilde{\mathbb{T}}$ has three times more nodes but locally it is indistinguishable from \mathbb{T} .

Moreover, if we assume that

$$\tilde{\lambda} = (\lambda_1:\lambda_1:\lambda_1, \lambda_2:\lambda_2:\lambda_2, \lambda_3:\lambda_3:\lambda_3)$$

then not only are the computation trees topologically equivalent, but also the messages are identical! Therefore, for this special choice of $\tilde{\lambda}$ (in relation to a given λ), the message-passing-based decoding algorithm cannot distinguish if it is decoding code \mathcal{C} or $\tilde{\mathcal{C}}$. In fact, it cannot distinguish if it is decoding code \mathcal{C} or any code defined by any graph cover of \mathbb{T} . The harmful effect of the codes that are given by the graph covers is that they contain codewords that *cannot* be explained as liftings of codewords in \mathcal{C} . E.g. code $\tilde{\mathcal{C}}$ contains the codeword $(0:0:0, 0:0:0, 0:0:0)$ which is a lifting of the codeword $(0, 0, 0)$ in \mathcal{C} . However, code $\tilde{\mathcal{C}}$ contains also the codeword $(1:1:0, 1:1:0, 1:1:0)$, cf. Fig. 3 (right), which is *not* a lifting of a codeword in \mathcal{C} .⁶

We emphasize two crucial observations:

- In principle, locally operating decoding algorithms *cannot distinguish* if they are operating on a Tanner graph \mathbb{T} or any finite cover of this graph as, for example, the cubic cover depicted in Fig. 3 (left).
- In general, the binary codes defined by finite covers of a Tanner graph support codewords that are not liftings of codewords in the original Tanner graph. Such a codeword is indicated in Fig. 3 (right) for the cubic cover in Fig. 3 (left).

It is clear, that any locally operating MPID will automatically take into account all possible codewords in all finite graph covers of the original graph. In other words, whereas in MAPD/MLD decoding all the codewords are competing to be the best explanation of the received vector, under MPID all codewords in all finite graph covers compete to be the best explanation of the received vector. In the case of our example code, the existence of non-zero codewords in finite covers of the original graph explains to large extents the observed behavior of SPA- and MSA-based decoding: indeed, for the specific code at hand it can be shown that *any* non-zero codeword in a finite cover of \mathbb{T} (like the codeword in the triple cover shown in Fig. 3 (right)) has the same effect as a virtually present, all-one codeword.

At first glance it seems to be a formidable task to characterize all possible codewords being introduced by the union of finite covers of any degree. (The number of finite covers of a graph grows faster than exponential with the covering degree). However, it turns out that this becomes an object that itself is elegantly described and compactly represented in the original Tanner graph.

Let us emphasize that this paper uses graph covers as an *analysis* technique. In the past, there have been various researchers who have used graph covers (sometimes also called graph liftings) but they used them for *constructing* LDPC codes that have some desirable symmetries, see e.g. Tanner et al. [35, 36].

⁶In total, $\tilde{\mathcal{C}}$ contains four codewords, three of them are not liftings of any codeword of \mathcal{C} .

Before concluding this motivating example let us mention some unexplained behaviour of SPA decoding for larger LLR values, see Fig. 5. Besides the decision boundary $\lambda_1 + \lambda_2 + \lambda_3 = 0$ that we have already discussed above, there appears an oval-shaped region where the SPA seems to have a problem in converging to the all-zeros codeword. Upon applying a slight modification to the SPA decoder, these oval-shaped regions disappear however, see Fig. 6. The modification that we applied was the following. Letting $\boldsymbol{\mu}^{(t)}$ and $\tilde{\boldsymbol{\mu}}^{(t)}$ be the LLR messages at iteration t from the bit nodes to the check nodes and from check to bit nodes, respectively, the usual SPA message updates can be written as $\boldsymbol{\mu}^{(t)} := f(\tilde{\boldsymbol{\mu}}^{(t-1)}, \boldsymbol{\lambda})$, $\tilde{\boldsymbol{\mu}}^{(t)} := \tilde{f}(\boldsymbol{\mu}^{(t)})$ for some suitably chosen functions f and \tilde{f} . The modified SPA message update rules are then $\boldsymbol{\mu}^{(t)} := \alpha \cdot f(\tilde{\boldsymbol{\mu}}^{(t-1)}, \boldsymbol{\lambda}) + (1 - \alpha) \cdot \boldsymbol{\mu}^{(t-1)}$, $\tilde{\boldsymbol{\mu}}^{(t)} := \tilde{f}(\boldsymbol{\mu}^{(t)})$ for some α where $0 \leq \alpha \leq 1$.⁷ Note that this modified SPA still operates locally and so it cannot distinguish if it is decoding the code described by the base Tanner graph or any of the codes described by the finite covers of the base Tanner graph.

1.2 Notation

This section discusses the various notations that we will use in this paper. We start with some sets. We let \mathbb{Z} , \mathbb{Z}_+ , \mathbb{Z}_{++} , \mathbb{Q} , \mathbb{Q}_+ , \mathbb{Q}_{++} , \mathbb{R} , \mathbb{R}_+ , and \mathbb{R}_{++} be the set of integers, the set of non-negative integers, the set of positive integers, the set of quotients, the set of non-negative quotients, the set of positive quotients, the set of real numbers, the set of non-negative real numbers, and the set of positive real numbers, respectively. We let $\mathbb{F}_2 \triangleq \{0, 1\}$ be the Galois field with two elements; as a set, \mathbb{F}_2 will be considered as a subset of \mathbb{R} . The size of a set \mathcal{S} is denoted by $|\mathcal{S}|$.

In the following, all scalars, entries of vectors, and entries of matrices will be considered to be in \mathbb{R} , unless noted otherwise. So, if an addition or a multiplication is not in the real field, we will indicate this, e.g. by writing $a + b$ (in \mathbb{F}_2) or $\mathbf{a} + \mathbf{b}$ (in \mathbb{F}_2). Moreover, when $\mathcal{T} \in \mathbb{Z}^N$ and $\mathcal{S} \subseteq \mathbb{F}_2^N$ then an expression like $\mathcal{T} \subseteq \mathcal{S}$ (in \mathbb{F}_2) means that $\mathbf{t} \pmod{2}$ lies in \mathcal{S} for all $\mathbf{t} \in \mathcal{T}$. As usually done in coding theory, we use only row vectors. An inequality of the form $\mathbf{a} \geq \mathbf{b}$ involving two vectors of length N is to be understood component-wise, i.e. $a_i \geq b_i$ for all $1 \leq i \leq N$. We let $\mathbf{1}_N$ be the row-vector of length N and the matrix \mathbf{I}_N be the identity matrix of size $N \times N$; when the length (size) of this vector (matrix) are obvious from the context, we will omit the index. The support $\text{supp}(\mathbf{x})$ of a vector will be the set of indices where \mathbf{x} is nonzero.

Square brackets will be used in different ways: if L is some positive integer then $[L]$ will denote the set $\{1, 2, \dots, L\}$. If \mathbf{A} is some matrix then $[\mathbf{A}]_{k,\ell}$ will denote the element in the k -th row and ℓ -th column of \mathbf{A} . If S is a statement (for example $\mathbf{x} \in \mathcal{C}$) then $[S] = 1$ if S is true and $[S] = 0$ otherwise.

By $\langle \mathbf{x}, \mathbf{y} \rangle \triangleq \sum_i x_i y_i$ we will denote the standard inner product of two vectors having the same length. The ℓ_1 -norm of a vector \mathbf{x} is $\|\mathbf{x}\|_1 \triangleq \sum_i |x_i|$, the ℓ_2 -norm of a vector \mathbf{x} is $\|\mathbf{x}\|_2 \triangleq \sqrt{\sum_i |x_i|^2}$, and the ℓ_∞ -norm (also called the max-norm) of a vector \mathbf{x} is $\|\mathbf{x}\|_\infty \triangleq \max_i |x_i|$. Note that $\|\mathbf{x}\|_1 = \langle \mathbf{x}, \mathbf{1} \rangle$ if and only if $\mathbf{x} \geq \mathbf{0}$. Let $\mathbf{x}, \mathbf{y} \in \mathbb{F}_2^N$ be two vectors of length N . The Hamming weight $w_H(\mathbf{x})$ of \mathbf{x} is the number of non-zero positions of \mathbf{x} , and the Hamming distance $d_H(\mathbf{x}, \mathbf{y})$ between \mathbf{x} and \mathbf{y} is the number of positions where \mathbf{x} and \mathbf{y} disagree.

⁷Let us mention that while discussing trapping sets and their influence, Laendner and Milenkovic [37] observed a similar slight change in behavior upon modifying the SPA slightly. However, whereas they are “averaging” the probability messages, we are “averaging” the LLR messages.

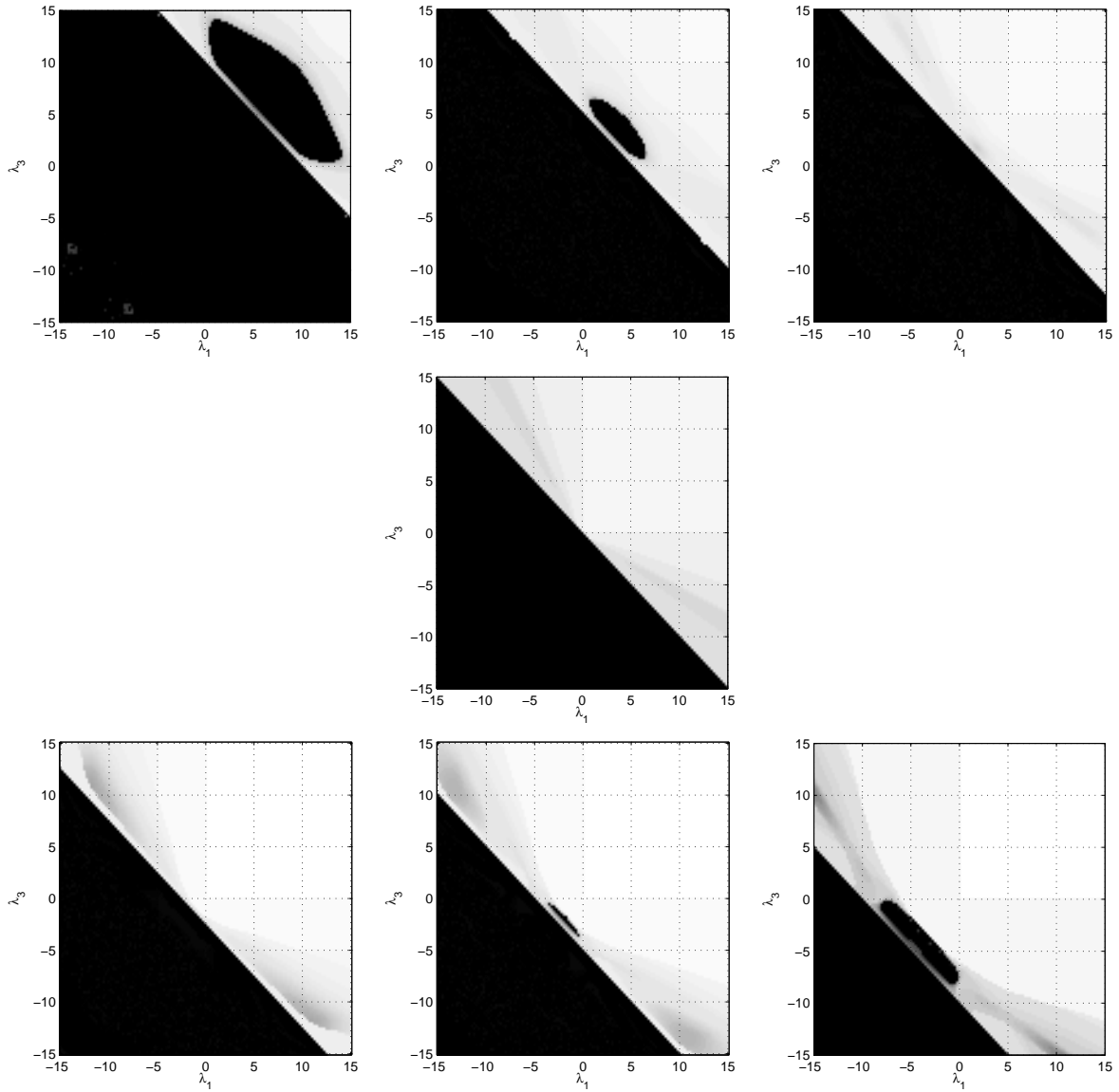


Figure 5: SPA decoding with maximally 60 iterations of the code \mathcal{C} that is represented by the Tanner graph \mathbb{T} in Fig. 1. The gray-scale indicates after how many iterations the algorithm converged to the all-zeros codeword with the implication that in the black region the decoder did not converge (see text for more details). From top-left to bottom-right: (λ_1, λ_3) -plane for $\lambda_2 = -10, -5, -2.5, 0, +2.5, +5, +10$.

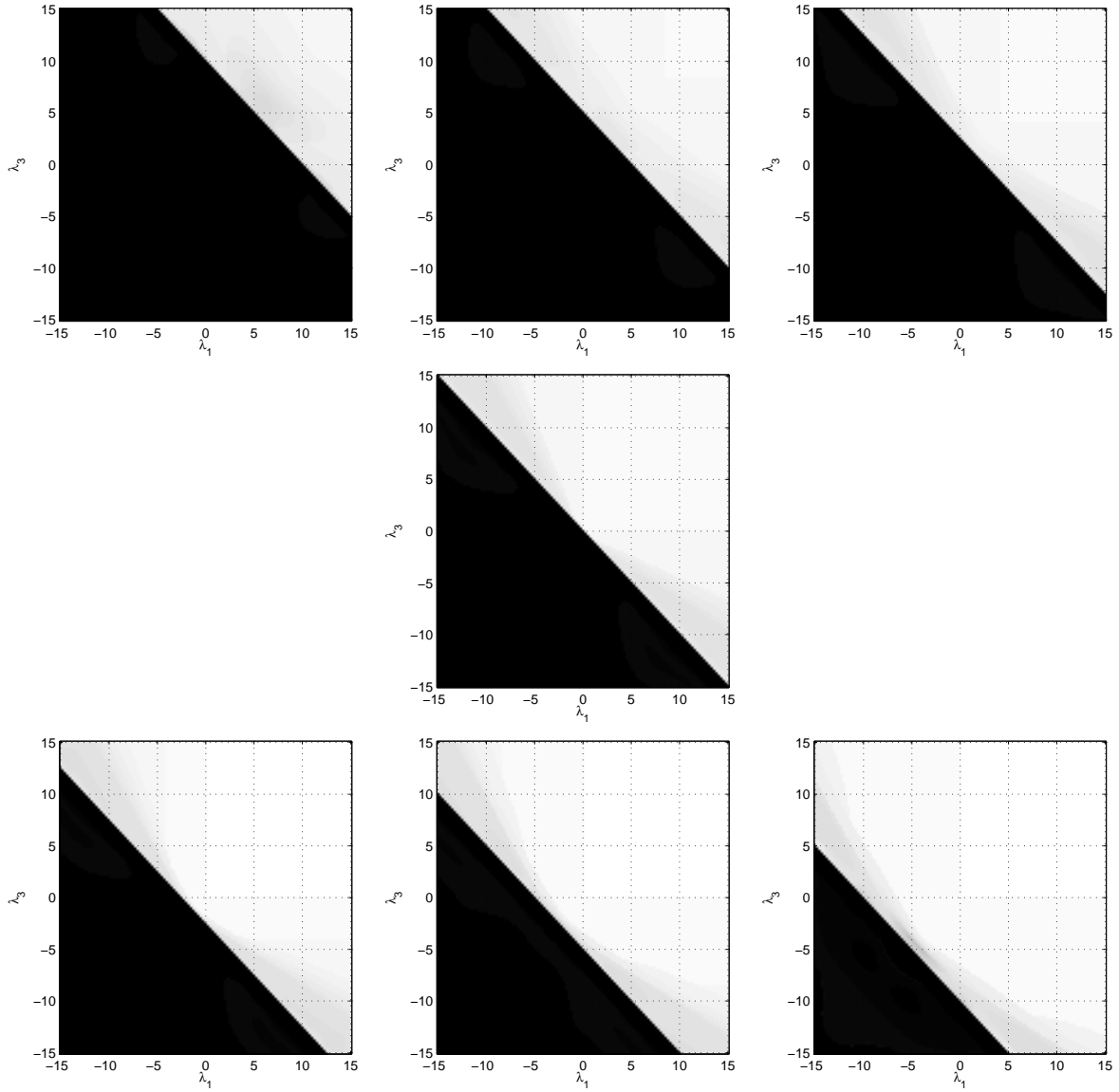


Figure 6: Modified SPA decoding ($\alpha = 0.85$) with maximally 60 iterations of the code \mathcal{C} that is represented by the Tanner graph \mathbb{T} in Fig. 1. The gray-scale indicates after how many iterations the algorithm converged to the all-zeros codeword with the implication that in the black region the decoder did not converge (see text for more details). From top-left to bottom-right: (λ_1, λ_3) -plane for $\lambda_2 = -10, -5, -2.5, 0, +2.5, +5, +10$.

Unless stated otherwise, the code \mathcal{C} will be a binary linear code of length n and will be defined by some $m \times n$ parity-check matrix \mathbf{H} , i.e. $\mathcal{C} \triangleq \{\mathbf{x} \in \mathbb{F}_2^n \mid \mathbf{x}\mathbf{H}^T = \mathbf{0}\}$.⁸ We let $\mathcal{I} \triangleq \mathcal{I}(\mathbf{H}) \triangleq \{1, \dots, n\}$ be the set of codeword indices, $\mathcal{J} \triangleq \mathcal{J}(\mathbf{H}) \triangleq \{1, \dots, m\}$ be the set of check indices, $\mathcal{J}_i \triangleq \mathcal{J}_i(\mathbf{H}) \triangleq \{j \in \mathcal{J} \mid [\mathbf{H}]_{j,i} = 1\}$ be the set of check indices that involve the i -th codeword position, and $\mathcal{I}_j \triangleq \mathcal{I}_j(\mathbf{H}) \triangleq \{i \in \mathcal{I} \mid [\mathbf{H}]_{j,i} = 1\}$ be the set of codeword positions that are involved in the j -th check.

If $\mathbf{x} \in \mathbb{F}_2^n$ and $\mathcal{S} \subseteq \mathcal{I}$, we let $\mathbf{x}_{\mathcal{S}}$ be the sub-vector of those positions of \mathbf{x} whose indices are elements of \mathcal{S} , i.e. the projection of \mathbf{x} onto \mathcal{S} . Similarly, $\mathcal{C}_{\mathcal{S}} \triangleq \{\mathbf{x}_{\mathcal{S}} \mid \mathbf{x} \in \mathcal{C}\}$ will be the projection of \mathcal{C} onto the index set \mathcal{S} .⁹ A $(w_{\text{col}}, w_{\text{row}})$ -regular binary LDPC code is a code that has a parity-check matrix \mathbf{H} where all columns have weight w_{col} and all rows have weight w_{row} . The dimension of a code \mathcal{C} is the logarithm (to the base 2) of the number of codeword and the rate is the ratio of the dimension divided by the length. Note that the dimension of \mathcal{C} is at least $1 - |\mathcal{J}|/n$, with equality if and only if \mathbf{H} has full rank.

If \mathcal{C} is a code then the minimum Hamming weight $w_{\mathbf{H}}^{\min}(\mathcal{C})$ is the minimum Hamming weight of all nonzero codewords of \mathcal{C} , and the minimum Hamming distance $d_{\mathbf{H}}^{\min}(\mathcal{C})$ is the minimum Hamming distance between any two distinct codewords of \mathcal{C} . It is well known that for linear codes $w_{\mathbf{H}}^{\min}(\mathcal{C}) = d_{\mathbf{H}}^{\min}(\mathcal{C})$. A code of length n , dimension k , and minimum distance d will be called an $[n, k, d]$ code.

Let us introduce some notions from convex geometry (see e.g. [39]). Let $\mathbf{x}^{(1)}, \dots, \mathbf{x}^{(k)}$ be k points in \mathbb{R}^N . A point of the form $\theta_1 \mathbf{x}^{(1)} + \dots + \theta_k \mathbf{x}^{(k)}$ with $\theta_1 + \dots + \theta_k = 1$ and $\theta_i \geq 0$, $i \in [k]$ is called a convex combination of $\mathbf{x}^{(1)}, \dots, \mathbf{x}^{(k)}$. A set $\mathcal{S} \subseteq \mathbb{R}^N$ is called convex if every possible convex combination of two points of \mathcal{S} is in \mathcal{S} . By $\text{conv}(\mathcal{S})$ we denote the convex hull of the set \mathcal{S} , i.e. the set that consists of all possible convex combinations of all the points in \mathcal{S} ; equivalently, $\text{conv}(\mathcal{S})$ is the smallest convex set that contains \mathcal{S} .

Again, let $\mathbf{x}^{(1)}, \dots, \mathbf{x}^{(k)}$ be k points in \mathbb{R}^N . A point of the form $\theta_1 \mathbf{x}^{(1)} + \dots + \theta_k \mathbf{x}^{(k)}$ with $\theta_i \geq 0$, $i \in [k]$, is called a conic combination of $\mathbf{x}^{(1)}, \dots, \mathbf{x}^{(k)}$. A set $\mathcal{K} \subseteq \mathbb{R}^N$ is called a cone if every possible conic combination of two points of \mathcal{K} is in \mathcal{K} . A cone \mathcal{K} is called a proper cone if it satisfies the following conditions: \mathcal{K} is convex, \mathcal{K} is closed, \mathcal{K} is solid (i.e. it has nonempty interior), and \mathcal{K} is pointed (i.e., it contains no line or, equivalently, if $\mathbf{x} \in \mathcal{K}$ and $-\mathbf{x} \in \mathcal{K}$, then $\mathbf{x} = \mathbf{0}$). By $\text{conic}(\mathcal{S})$ we denote the conic hull of the set \mathcal{S} , i.e. the set that consists of all possible conic combinations of all the points in \mathcal{S} ; equivalently, $\text{conic}(\mathcal{S})$ is the smallest conic set that contains \mathcal{S} .

Let us now introduce polytopes and polyhedra. On the one hand, a polytope in \mathbb{R}^N is defined to be the convex hull of a finite set of points in \mathbb{R}^N . On the other hand, a polyhedron \mathcal{P} in \mathbb{R}^N is defined as the solution set of a finite number of linear equalities and inequalities:

$$\mathcal{P} \triangleq \left\{ \mathbf{x} \in \mathbb{R}^N \mid \langle \mathbf{a}^{(j)}, \mathbf{x} \rangle \leq b_j, j \in [m], \langle \mathbf{c}^{(j)}, \mathbf{x} \rangle = d_j, j \in [p] \right\},$$

where $\mathbf{a}^{(j)}$, $j \in [m]$, and $\mathbf{c}^{(j)}$, $j \in [p]$, are vectors of the same length as \mathbf{x} and b_j , $j \in [m]$, and d_j , $j \in [p]$, are scalars. From this definition we see that a polyhedron is the intersection of a finite number of half-spaces and hyperplanes and it is also easy to see that a polyhedron is a convex set. By the Weyl-Minkowski Theorem, cf. e.g. [40, p. 55], a bounded polyhedron is a polytope.

⁸Note the following convention: a row index of \mathbf{H} will be denoted by j and a column index of \mathbf{H} will be denoted by i .

⁹In coding language, this is often called puncturing the code \mathcal{C} at positions $\mathcal{I} \setminus \mathcal{S}$ [38].

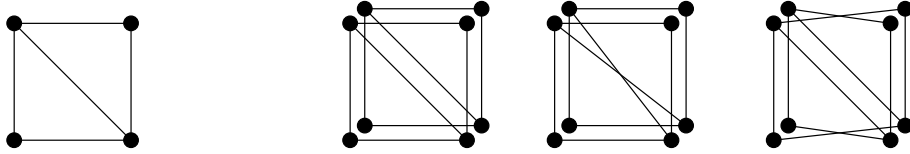


Figure 7: Left: base graph G . Right: sample of possible 2-covers of G .

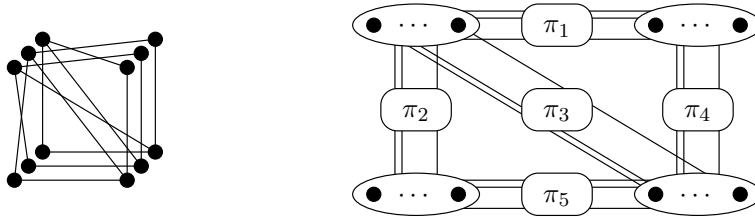


Figure 8: Left: a possible 3-cover of G . Right: a possible M -cover of G .

An *undirected* graph $G = G(\mathcal{V}(G), \mathcal{E}(G))$ consists of a vertex-set $\mathcal{V}(G)$ and an edge-set $\mathcal{E}(G)$ whereby the elements of $\mathcal{E}(G)$ are 2-subsets of $\mathcal{V}(G)$. By a graph (without further qualifications) we will always mean an undirected graph without loops and multiple edges. The smallest length of any cycle will be called the girth $g(G)$ and the largest graph distance between any two vertices will be called the diameter $\delta(G)$. If the graph has more than one component then $\delta(G) = \infty$. The neighborhood $\partial(v)$ of a vertex $v \in G$ is the set of vertices of G that are adjacent to v . It follows that $|\partial(v)|$ is the degree of the vertex v .

2 Graph Covers and the Fundamental Polytope

After recalling the definitions of finite graph covers and Tanner graphs, we will introduce the fundamental polytope, a notion that will turn out to be the crucial definition for the rest of the present paper.

Definition 1 (Graph cover, see e.g. [41, 42]) An unramified, finite cover, or, simply, a cover of a (base) graph G is a graph \tilde{G} along with a surjective map $\phi : \tilde{G} \rightarrow G$ which is a graph homomorphism, i.e., which takes adjacent vertices of \tilde{G} to adjacent vertices of G , such that for each vertex $v \in \mathcal{V}(G)$ and each $\tilde{v} \in \phi^{-1}(v)$, the neighborhood $\partial(\tilde{v})$ of \tilde{v} is mapped bijectively to $\partial(v)$. For a positive integer M , an M -cover of G is an unramified finite cover $\phi : \tilde{G} \rightarrow G$ such that for each vertex $v \in \mathcal{V}(G)$ of G , $\phi^{-1}(v)$ contains exactly M vertices of \tilde{G} . An M -cover of G is sometimes also called an M -sheeted covering of G or a cover of G of degree M .¹⁰ \square

A consequence of this definition is that if \tilde{G} is an M -cover of G then we can choose $\mathcal{V}(\tilde{G})$ to be $\mathcal{V}(\tilde{G}) \triangleq \mathcal{V}(G) \times [M]$: if $(v, m) \in \mathcal{V}(\tilde{G})$ then $\phi((v, m)) = v$ and if $((v_1, m_1), (v_2, m_2)) \in \mathcal{E}(\tilde{G})$ then $\phi(\{(v_1, m_1), (v_2, m_2)\}) = \{v_1, v_2\}$. Another consequence is that any M_2 -cover of any M_1 -cover of the base graph is an $(M_1 \cdot M_2)$ -cover of the base graph.

¹⁰It is important not to confuse the degree of a covering and the degree of a vertex.

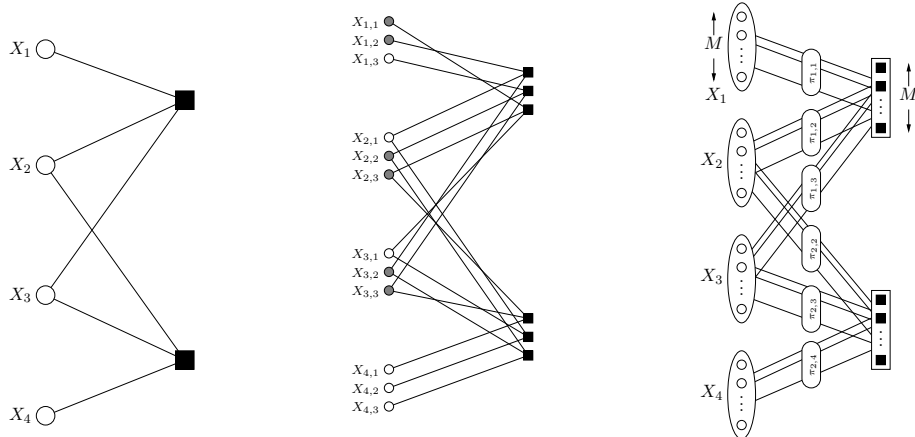


Figure 9: Left: Tanner graph $\mathsf{T}(\mathbf{H})$ of the simple binary linear code in Ex. 4. Middle: Possible 3-cover of $\mathsf{T}(\mathbf{H})$. The shading of the symbol nodes indicates the codeword $\tilde{\mathbf{x}}$ found in Ex. 5. Right: Possible M -cover of $\mathsf{T}(\mathbf{H})$.

Example 2 Let G be a (base) graph with 4 vertices and 5 edges as shown in Fig. 7 (left). Figs. 7 (right) and 8 (left), show possible 2- and 3-covers of G , respectively. Any M -cover of G is entirely specified by $|\mathcal{E}(G)|$ permutations: this is represented by Fig. 8 (right). Note that any 2-cover of G must have $8 = 2 \cdot 4$ vertices and $10 = 2 \cdot 5$ edges and any 3-cover of G must have $12 = 3 \cdot 4$ vertices and $15 = 3 \cdot 5$ edges. \square

In general, a graph G has $(M!)^{|\mathcal{E}(G)|}$ possible M -covers, some of them might be isomorphic. Moreover, an M -cover of G may consist of several components also if G consists of only one component. Before we can consider graph covers of Tanner graphs, we briefly recall the definition of Tanner graphs.

Definition 3 (Tanner graph [5, 11, 14]) *To a binary parity-check matrix \mathbf{H} that defines the code \mathcal{C} we can associate a bipartite graph $\mathsf{T}(\mathbf{H})$, the so-called Tanner graph of \mathbf{H} . This graph has vertex set $\mathcal{V} \triangleq \{X_i \mid i \in \mathcal{I}\} \cup \{B_j \mid j \in \mathcal{J}\}$ and edge set $\mathcal{E} \triangleq \{(X_i, B_j) \mid i \in \mathcal{I}, j \in \mathcal{J}_i\} = \{(X_i, B_j) \mid j \in \mathcal{J}, i \in \mathcal{I}_j\}$. On the other hand, given a Tanner graph T we can associate to T a code $\mathcal{C}(\mathsf{T})$ with parity-check matrix $\mathbf{H}(\mathsf{T})$ in the obvious manner. \square*

We will use some language from behavioral theory [43]: an assignment of \mathbb{F}_2 -values to the variable nodes will be called a configuration, and a configuration that fulfills all the checks will be called valid. In that sense, a codeword corresponds to a valid configuration and a code corresponds to the set of all valid configurations.

From the above definition of a Tanner graph it follows that $\partial(X_i) = \{B_j \mid j \in \mathcal{J}_i\}$ for all $i \in \mathcal{I}(\mathbf{H})$ and $\partial(B_j) = \{X_i \mid i \in \mathcal{I}_j\}$ for all $j \in \mathcal{J}(\mathbf{H})$. Moreover, the degree $|\partial(X_i)|$ of the node X_i is equal to the Hamming weight of the i -th column of \mathbf{H} and the degree $|\partial(B_j)|$ of the node B_j is equal to the Hamming weight of the j -th row of \mathbf{H} . Therefore, Tanner graphs of LDPC codes are sparse because of the sparseness of the parity-check matrix of LDPC codes.

Example 4 Let \mathcal{C} be a binary $[4, 2]$ code with parity-check matrix¹¹

$$\mathbf{H} \triangleq \begin{pmatrix} 1 & 1 & 1 & 0 \\ 0 & 1 & 1 & 1 \end{pmatrix}.$$

Obviously, $\mathcal{C} = \{(0, 0, 0, 0), (0, 1, 1, 0), (1, 0, 1, 1), (1, 1, 0, 1)\}$, $\mathcal{J} = \{1, 2\}$, $\mathcal{J}_1 = \{1\}$, $\mathcal{J}_2 = \{1, 2\}$, $\mathcal{J}_3 = \{1, 2\}$, $\mathcal{J}_4 = \{2\}$, $\mathcal{I} = \{1, 2, 3, 4\}$, $\mathcal{I}_1 = \{1, 2, 3\}$, and $\mathcal{I}_2 = \{2, 3, 4\}$. The Tanner graph $\mathbb{T}(\mathbf{H})$ that is associated to \mathbf{H} is shown in Fig. 9 (left).

An M -fold cover $\tilde{\mathbb{T}}$ (as shown in Fig. 9 (right)) of \mathbb{T} is specified by defining the permutations $\pi_{1,1}$, $\pi_{1,2}$, $\pi_{1,3}$ (corresponding to the first row of \mathbf{H}) and the permutations $\pi_{2,2}$, $\pi_{2,3}$, $\pi_{2,4}$ (corresponding to the second row of \mathbf{H}). \square

Let \mathcal{C} be a binary code with parity-check matrix \mathbf{H} and Tanner graph $\mathbb{T} \triangleq \mathbb{T}(\mathbf{H})$. For a positive integer M , let $\tilde{\mathbb{T}}$ be an arbitrary M -fold cover of \mathbb{T} , let $\tilde{\mathcal{C}} \triangleq \mathcal{C}(\tilde{\mathbb{T}})$ be the binary code described by $\tilde{\mathbb{T}}$, and let the codeword positions of $\tilde{\mathcal{C}}$ be indexed by $\tilde{\mathcal{I}} \triangleq \mathcal{I} \times [M]$ and the check equations by $\tilde{\mathcal{J}} \triangleq \mathcal{J} \times [M]$.

Knowing the graph \mathbb{T} , the graph $\tilde{\mathbb{T}}$ is completely specified by defining for all $j \in \mathcal{J}$, $i \in \mathcal{I}_j$ the permutations $\pi_{j,i}$ that map $[M]$ onto itself. The meaning of $\pi_{j,i}(m)$, $m \in [M]$, is the following: the m^{th} copy of check node j is connected to the $\pi_{j,i}(m)^{\text{th}}$ copy of codeword symbol X_i , i.e. check node $\tilde{B}_{j,m}$ is connected to codeword symbol $\tilde{X}_{i,\pi_{j,i}(m)}$. It follows that $\tilde{\mathbf{x}} \in \tilde{\mathcal{C}}$ if and only if

$$\sum_{i \in \mathcal{I}_j} \tilde{x}_{i,\pi_{j,i}(m)} = 0 \quad (\text{in } \mathbb{F}_2) \quad (2)$$

for all $(j, m) \in \tilde{\mathcal{J}}$. The parity check matrix $\tilde{\mathbf{H}}$ that expresses this fact can be defined as follows. Let the entries of $\tilde{\mathbf{H}}$ be indexed by $(j, m) \in \tilde{\mathcal{J}}$ and $(i, m') \in \tilde{\mathcal{I}}$. Then

$$[\tilde{\mathbf{H}}]_{(j,m),(i,m')} \triangleq \begin{cases} 1 & \text{if } i \in \mathcal{I}_j \text{ and } m' = \pi_{j,i}(m) \\ 0 & \text{otherwise.} \end{cases} \quad (3)$$

Example 5 We continue Ex. 4. The parity-check matrix $\tilde{\mathbf{H}} \triangleq \mathbf{H}(\tilde{\mathbb{T}})$ associated to a possible 3-fold cover Tanner graph $\tilde{\mathbb{T}}$ as shown in Fig. 9 (middle) looks like

$$\tilde{\mathbf{H}} \triangleq \left(\begin{array}{ccc|ccc|ccc|ccc} 0 & 1 & 0 & 1 & 0 & 0 & 0 & 1 & 0 & 0 & 0 & 0 & 0 \\ 0 & 0 & 1 & 0 & 1 & 0 & 0 & 0 & 1 & 0 & 0 & 0 & 0 \\ 1 & 0 & 0 & 0 & 0 & 1 & 1 & 0 & 0 & 0 & 0 & 0 & 0 \\ \hline 0 & 0 & 0 & 0 & 0 & 1 & 0 & 0 & 1 & 1 & 0 & 0 & 0 \\ 0 & 0 & 0 & 1 & 0 & 0 & 1 & 0 & 0 & 0 & 1 & 0 & 0 \\ 0 & 0 & 0 & 0 & 1 & 0 & 0 & 1 & 0 & 0 & 0 & 0 & 1 \end{array} \right).$$

This parity-check matrix defines a code $\tilde{\mathcal{C}} = \mathcal{C}(\tilde{\mathbb{T}})$: e.g. the configuration $\tilde{\mathbf{x}} = (1:1:0, 0:1:1, 0:1:1, 0:0:0)$ that is highlighted in Fig. 9 (middle) is a codeword in this code. Note also that $\tilde{\mathcal{C}}$ contains the liftings of all codewords to $\tilde{\mathbb{T}}$, namely if $(x_1, x_2, x_3, x_4) \in \mathcal{C}$ then $(x_1:x_1:x_1, x_2:x_2:x_2, x_3:x_3:x_3, x_4:x_4:x_4) \in \tilde{\mathcal{C}}$. The last statement follows from the following argument: since \mathbb{T} and $\tilde{\mathbb{T}}$ look locally the same, the fact that a codeword \mathbf{x} in \mathcal{C} fulfills the checks imposed by \mathbb{T} implies that the lifting of \mathbf{x} to $\tilde{\mathbb{T}}$ fulfills all the checks imposed by $\tilde{\mathbb{T}}$, i.e. that it is a codeword in $\tilde{\mathcal{C}}$. \square

¹¹Note that this is the same parity-check matrix as in the Example after Th. 2 in [44].

Definition 6 Let \mathcal{C} be a binary linear (base) code with parity-check matrix \mathbf{H} and let $\mathbb{T} \triangleq \mathbb{T}(\mathbf{H})$ be the corresponding Tanner graph. For any positive integer M , let $\tilde{\mathbb{T}}$ be an M -fold cover of \mathbb{T} and let $\tilde{\mathcal{C}} \triangleq \mathcal{C}(\tilde{\mathbb{T}})$. The (scaled) pseudo-codeword associated to $\tilde{\mathbf{x}}$ is the rational vector $\boldsymbol{\omega}(\tilde{\mathbf{x}}) \triangleq (\omega_1(\tilde{\mathbf{x}}), \omega_2(\tilde{\mathbf{x}}), \dots, \omega_n(\tilde{\mathbf{x}}))$ with

$$\omega_i(\tilde{\mathbf{x}}) \triangleq \frac{1}{M} \sum_{m \in [M]} \tilde{x}_{i,m}, \quad (4)$$

where the sum is taken in \mathbb{R} (not in \mathbb{F}_2). In fact, any multiple (by a positive scalar) of $\boldsymbol{\omega}(\tilde{\mathbf{x}})$ will be called a pseudo-codeword associated with $\tilde{\mathbf{x}}$. Because of its importance, we give a special name to the vector $M \cdot \boldsymbol{\omega}(\tilde{\mathbf{x}})$, namely we will call it the unscaled pseudo-codeword associated to $\tilde{\mathbf{x}}$. Additionally, we define $\boldsymbol{\omega}(\tilde{\mathcal{C}})$ to be the set

$$\boldsymbol{\omega}(\tilde{\mathcal{C}}) \triangleq \left\{ \boldsymbol{\omega}(\tilde{\mathbf{x}}) \mid \tilde{\mathbf{x}} \in \tilde{\mathcal{C}} \right\}.$$

Obviously, $\boldsymbol{\omega}(\tilde{\mathcal{C}}) \subseteq [0, 1]^n \cap \mathbb{Q}^n$. □

Note that whereas a pseudo-codeword as defined in Def. 6 has length $|\mathcal{I}(\mathbf{H})|$, i.e. equal to the length of the code \mathcal{C} , a codeword like $\tilde{\mathbf{c}} \in \tilde{\mathcal{C}}$ has length $M \cdot |\mathcal{I}(\mathbf{H})|$ where M is the degree of the corresponding cover Tanner graph. Because \mathbb{T} is a 1-cover of a Tanner graph \mathbb{T} we see that any codeword is also a pseudo-codeword.

Example 7 We continue Ex. 4. We saw that $\tilde{\mathbf{c}} = (1:1:0, 0:1:1, 0:1:1, 0:0:0)$ was a codeword of the code $\tilde{\mathcal{C}}$. Applying Def. 6 we see that the corresponding pseudo-codeword is $\boldsymbol{\omega}(\tilde{\mathbf{c}}) = (\frac{2}{3}, \frac{2}{3}, \frac{2}{3}, 0)$. (Note that this pseudo-codeword cannot be written as a convex combination of the codewords in \mathcal{C} .) The corresponding unscaled pseudo-codeword is $3 \cdot \boldsymbol{\omega}(\tilde{\mathbf{c}}) = (2, 2, 2, 0)$ and comparing this vector with Fig. 9 (middle), we see the intuitive meaning of its components: the first component corresponds to the number of shaded variable nodes $X_{1,m}$, $m \in [M]$, the second component corresponds to the number of shaded variable nodes $X_{2,m}$, $m \in [M]$, etc. □

We would like to investigate the question if it is possible to characterize the union of the set of all (scaled) pseudo-codewords obtained by all finite covers of the Tanner graph of a binary linear code, i.e. we would like to understand the set

$$\tilde{\mathcal{Q}}(\mathbf{H}) \triangleq \bigcup_{\substack{M \in \mathbb{Z}_{++} \\ \tilde{\mathbb{T}}: \tilde{\mathbb{T}} \text{ is an } M\text{-fold cover of } \mathbb{T}(\mathbf{H}) \\ \tilde{\mathbf{x}} \in \mathcal{C}(\tilde{\mathbb{T}})}} \left\{ (M, \tilde{\mathbb{T}}, \tilde{\mathbf{x}}) \right\} \quad (5)$$

and its “projection”¹²

$$\mathcal{Q}(\mathbf{H}) \triangleq \bigcup_{(M, \tilde{\mathbb{T}}, \tilde{\mathbf{x}}) \in \tilde{\mathcal{Q}}(\mathbf{H})} \left\{ \boldsymbol{\omega}(\tilde{\mathbf{x}}) \right\}. \quad (6)$$

¹²We could have defined

$$\mathcal{Q}(\mathbf{H}) \triangleq \bigcup_{(M, \tilde{\mathbb{T}}, \tilde{\mathbf{x}}) \in \tilde{\mathcal{Q}}(\mathbf{H})} \left\{ (M, \tilde{\mathbb{T}}, \boldsymbol{\omega}(\tilde{\mathbf{x}})) \right\},$$

but the definition of $\mathcal{Q}(\mathbf{H})$ in (6) contains enough information for our purposes.

From the properties of $\omega(\tilde{\mathcal{C}})$ it follows that $\mathcal{Q}(\mathbf{H}) \subseteq [0, 1]^n \cap \mathbb{Q}^n$. Observe that

$$\mathcal{Q}(\mathbf{H}) = \bigcup_{\tilde{\mathbf{T}}: \tilde{\mathbf{T}} \text{ is a finite-cover graph of } \mathbf{T}(\mathbf{H})} \left\{ \omega(\mathcal{C}(\tilde{\mathbf{T}})) \right\}. \quad (7)$$

This set has a surprisingly simple characterization. It will turn out that $\mathcal{Q}(\mathbf{H})$ is essentially given by the fundamental polytope introduced in the next definition. Before we turn to that definition, let us observe that the code \mathcal{C} can be written as the intersection

$$\mathcal{C} = \bigcap_{j \in \mathcal{J}} \mathcal{C}_j$$

of the codes

$$\mathcal{C}_j \triangleq \mathcal{C}_j(\mathbf{H}) \triangleq \{ \mathbf{x} \in \mathbb{F}_2^n \mid \langle \mathbf{x}, \mathbf{h}_j \rangle = 0 \text{ (in } \mathbb{F}_2) \} = \{ \mathbf{x} \in \mathbb{F}_2^n \mid \langle \mathbf{x}_{\mathcal{I}_j}, \mathbf{1} \rangle = 0 \text{ (in } \mathbb{F}_2) \}, \quad (8)$$

where for each $j \in \mathcal{J}$ we let \mathbf{h}_j be the j -th row of \mathbf{H} . For $j \in \mathcal{J}$, we will also use the codes

$$\mathcal{C}'_j \triangleq \mathcal{C}'_j(\mathbf{H}) \triangleq \{ \mathbf{x}' \in \mathbb{F}_2^{|\mathcal{I}_j|} \mid \langle \mathbf{x}', (\mathbf{h}_j)_{\mathcal{I}_j} \rangle = 0 \text{ (in } \mathbb{F}_2) \} = \{ \mathbf{x}' \in \mathbb{F}_2^{|\mathcal{I}_j|} \mid \langle \mathbf{x}', \mathbf{1} \rangle = 0 \text{ (in } \mathbb{F}_2) \}. \quad (9)$$

The codes \mathcal{C}_j and \mathcal{C}'_j are related as follows. First, \mathcal{C}'_j is the projection of \mathcal{C}_j onto \mathcal{I}_j , i.e. $\mathcal{C}'_j = (\mathcal{C}_j)_{\mathcal{I}_j}$. Secondly, the convex hulls of \mathcal{C}_j and of \mathcal{C}'_j fulfill

$$\text{conv}(\mathcal{C}_j) = \{ \boldsymbol{\omega} \in \mathbb{R}^n \mid \mathbf{0} \leq \boldsymbol{\omega} \leq \mathbf{1}, \boldsymbol{\omega}_{\mathcal{I}_j} \in \text{conv}(\mathcal{C}'_j) \}. \quad (10)$$

We are now ready for the main definition of this paper.

Definition 8 *The fundamental polytope $\mathcal{P} \triangleq \mathcal{P}(\mathbf{H})$ of \mathbf{H} is defined to be the set*

$$\mathcal{P} \triangleq \bigcap_{j \in \mathcal{J}} \text{conv}(\mathcal{C}_j) \quad (11)$$

$$= \bigcap_{j \in \mathcal{J}} \{ \boldsymbol{\omega} \in \mathbb{R}^n \mid \mathbf{0} \leq \boldsymbol{\omega} \leq \mathbf{1}, \boldsymbol{\omega}_{\mathcal{I}_j} \in \text{conv}(\mathcal{C}'_j) \} \quad (12)$$

$$= [0, 1]^n \cap \bigcap_{j \in \mathcal{J}} \{ \boldsymbol{\omega} \in \mathbb{R}^n \mid \boldsymbol{\omega}_{\mathcal{I}_j} \in \text{conv}(\mathcal{C}'_j) \}. \quad (13)$$

□

As can be seen from the notation $\mathcal{P}(\mathbf{H})$, the fundamental polytope is a function of the parity-check matrix \mathbf{H} that describes the code \mathcal{C} . This means that different parity-check matrices for the same code can (and usually do) yield different fundamental polytopes.

In the same way as all codewords of a code described by a parity-check matrix \mathbf{H} are all the valid configurations in a Tanner graph $\mathbf{T}(\mathbf{H})$, we see that (13) yields a similar description for all pseudo-codewords, i.e. for all the vectors that lie in the fundamental polytope $\mathcal{P}(\mathbf{H})$. Indeed, we redefine the Tanner graph as follows: each bit node X_i is now labeled Ω_i and can take on values in the interval $[0, 1]$ and each check node B_j is replaced by the indicator function of the convex hull of \mathcal{C}'_j . (We can use the results of Lemmas 25 and 26 in Sec. 5 to formulate these indicator functions.)

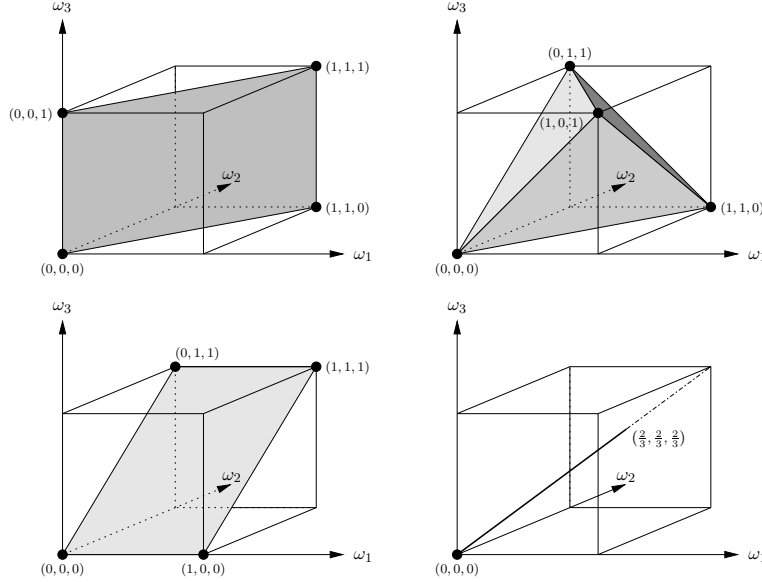


Figure 10: $\mathcal{C}_j(\mathbf{H})$, $j \in \mathcal{J}$ and $\mathcal{P}(\mathbf{H})$ for the parity-check matrix \mathbf{H} in (1). Top left: $\text{conv}(\mathcal{C}_1(\mathbf{H}))$. Top right: $\text{conv}(\mathcal{C}_2(\mathbf{H}))$. Bottom left: $\text{conv}(\mathcal{C}_3(\mathbf{H}))$. Bottom right: $\mathcal{P}(\mathbf{H}) = \bigcap_{j \in \mathcal{J}} \text{conv}(\mathcal{C}_j(\mathbf{H}))$.

Example 9 We continue discussing the code that was introduced in Sec. 1.1 whose parity-check matrix is shown in (1). For this parity-check matrix the codes \mathcal{C}_j , $j \in \mathcal{J}$ turn out to be

$$\begin{aligned} \mathcal{C}_1 &= \{(0, 0), (1, 1)\} \times \{(0), (1)\} = \{(0, 0, 0), (0, 0, 1), (1, 1, 0), (1, 1, 1)\}, \\ \mathcal{C}_2 &= \{(0, 0, 0), (0, 1, 1), (1, 0, 1), (1, 1, 0)\}, \\ \mathcal{C}_3 &= \{(0), (1)\} \times \{(0, 0), (1, 1)\} = \{(0, 0, 0), (1, 0, 0), (0, 1, 1), (1, 1, 1)\}. \end{aligned}$$

We can easily check that $\mathcal{C} = \bigcap_{j \in \mathcal{J}} \mathcal{C}_j = \{(0, 0, 0)\}$. Fig. 10 visualizes these codes, their convex hulls, and the fundamental polytope $\mathcal{P}(\mathbf{H}) = \bigcap_{j \in \mathcal{J}} \text{conv}(\mathcal{C}_j) = \{(\omega, \omega, \omega) \mid 0 \leq \omega \leq \frac{2}{3}\}$. Note that here the fundamental polytope has only two vertices: $(0, 0, 0)$ and $(\frac{2}{3}, \frac{2}{3}, \frac{2}{3})$ where the former is the pseudo-codeword corresponding to the all-zeros assignment in any finite cover and where the latter is e.g. the pseudo-codeword corresponding to the configuration in the triple cover shown Fig. 3 (right).

Moreover, using Prop. 10 below, it can be shown that $\mathcal{Q}(\mathbf{H})$ equals the set of all the rational points of $\mathcal{P}(\mathbf{H})$. Accepting this fact, we can also verify the statement made in Prop. 10 that all vertices of $\mathcal{P}(\mathbf{H})$ are in $\mathcal{Q}(\mathbf{H})$. \square

Note that usually the effective dimension of the fundamental polytope equals the length n of the code. In cases where the parity-check matrix has checks that involve only one or two codeword symbols, there is a reduction in effective dimensionality. The above example is a witness of this fact.

After having seen the definition of the fundamental polytope we are in a position to formulate the main theorem of this paper which relates the set $\mathcal{Q}(\mathbf{H})$ with the fundamental polytope $\mathcal{P}(\mathbf{H})$.

Proposition 10 *Let \mathcal{C} be an arbitrary binary linear code and let \mathbf{H} be its parity-check matrix. It holds that*

$$\mathcal{Q}(\mathbf{H}) = \mathcal{P}(\mathbf{H}) \cap \mathbb{Q}^n, \quad (14)$$

$$\mathcal{P}(\mathbf{H}) = \overline{\mathcal{Q}(\mathbf{H})}, \quad (15)$$

where the over-bar denotes the closure of the corresponding set under the usual topology of \mathbb{R}^n . Moreover, all vertices of $\mathcal{P}(\mathbf{H})$ are in $\mathcal{Q}(\mathbf{H})$.

Proof: See Sec. A.1. □

Before finishing this section let us mention that the fundamental polytope and related concepts can not only be defined for a code whose Tanner graph consists only of single parity-check codes but also for codes described by a Tanner graph where some or all of the check nodes represent more complicated subcodes or for codes described by a factor graph that represents a tail-biting trellis. The generalization is relatively straightforward and will not be discussed any further in this paper.

3 Channels, MAP Decoding, and LP Decoding

We consider the problem of data communication over a memoryless channel with input alphabet \mathcal{X} , output alphabet \mathcal{Y} , and with channel law $P_{Y|X}(y|x)$. In this paper we only consider channels with binary input, i.e. with $\mathcal{X} = \{0, 1\}$. In order to achieve reliable communication over such a channel, we will use a binary code $\mathcal{C} \subseteq \mathbb{F}_2^n$ of length n and rate R that is defined by some parity-check matrix \mathbf{H} . We assume that every codeword $\mathbf{x} \in \mathcal{C}$ is transmitted with equal probability, i.e. $P_{\mathbf{X}}(\mathbf{x}) = 2^{-nR}$ if $\mathbf{x} \in \mathcal{C}$ and $P_{\mathbf{X}}(\mathbf{x}) = 0$ otherwise, where R is the rate of the code.

Upon observing the output $\mathbf{Y} = \mathbf{y}$, block-wise maximum a-posteriori decoding (MAPD) can be formulated as the following optimization problem:¹³

$$\begin{aligned} \hat{\mathbf{x}}^{\text{MAPD}}(\mathbf{y}) &= \arg \max_{\mathbf{x} \in \mathbb{F}_2^n} P_{\mathbf{X}, \mathbf{Y}}(\mathbf{x}, \mathbf{y}) = \arg \max_{\mathbf{x} \in \mathbb{F}_2^n} P_{\mathbf{X}}(\mathbf{x}) \cdot P_{\mathbf{Y}|\mathbf{X}}(\mathbf{y}|\mathbf{x}) \\ &= \arg \max_{\mathbf{x} \in \mathcal{C}} P_{\mathbf{Y}|\mathbf{X}}(\mathbf{y}|\mathbf{x}) = \arg \min_{\mathbf{x} \in \mathcal{C}} -\log P_{\mathbf{Y}|\mathbf{X}}(\mathbf{y}|\mathbf{x}), \end{aligned} \quad (16)$$

where $P_{\mathbf{X}, \mathbf{Y}}(\mathbf{x}, \mathbf{y}) = P_{\mathbf{X}}(\mathbf{x}) \cdot P_{\mathbf{Y}|\mathbf{X}}(\mathbf{y}|\mathbf{x})$ is the joint pmf/pdf of the the coded (but unmodulated) channel input \mathbf{X} and the channel output \mathbf{Y} . Ties are resolved in a systematic way.

In the following we will use the fact that $P_{\mathbf{Y}|\mathbf{X}}(\mathbf{y}|\mathbf{x}) = \prod_{i \in \mathcal{I}} P_{Y_i|X_i}(y_i|x_i) = \prod_{i \in \mathcal{I}} P_{Y|X}(y_i|x_i)$ holds for memoryless channels (that are used without feedback). The random variable

$$\Lambda_i \triangleq \Lambda_i(Y_i) \triangleq \log \frac{P_{Y|X}(Y_i|0)}{P_{Y|X}(Y_i|1)} \quad (17)$$

with realization $\boldsymbol{\lambda}$ will be called the channel log-likelihood ratio for the i -th codeword

¹³Note that the resulting decision rule equals also the maximum-likelihood decision rule because all possible codewords \mathbf{x} occur with the same probability.

symbol.¹⁴ Block-wise MAPD can therefore be rewritten to read

$$\hat{\mathbf{x}}^{\text{MAPD}}(\mathbf{y}) = \arg \min_{\mathbf{x} \in \mathcal{C}} \log \frac{P_{\mathbf{Y}|\mathbf{X}}(\mathbf{y}|\mathbf{0})}{P_{\mathbf{Y}|\mathbf{X}}(\mathbf{y}|\mathbf{x})} = \arg \min_{\mathbf{x} \in \mathcal{C}} \sum_{i \in \mathcal{I}} x_i \lambda_i = \arg \min_{\mathbf{x} \in \mathcal{C}} \langle \mathbf{x}, \boldsymbol{\lambda} \rangle, \quad (18)$$

where ties are resolved in a systematic manner.

From this expression it is not far anymore to linear programming decoding (LPD) [31, 32]. In a first step, let us reformulate (18) as

$$\hat{\mathbf{x}}^{\text{MAPD}}(\mathbf{y}) = \arg \min_{\mathbf{x} \in \text{conv}(\mathcal{C})} \langle \mathbf{x}, \boldsymbol{\lambda} \rangle, \quad (19)$$

where ties are resolved in a systematic manner. This expression follows from two facts: all codewords in \mathcal{C} are vertices of $\text{conv}(\mathcal{C})$ and because the cost function is linear, the set of optimal solutions must always include at least one vertex of $\text{conv}(\mathcal{C})$.¹⁵ The resulting optimization problem on the right-hand side of (19) is a linear program (LP). Although it is of course desirable to solve such a problem, for arbitrary codes this problem turns out to be hard, a reason being that the number of inequalities needed to describe $\text{conv}(\mathcal{C})$ usually grows exponentially in the block length. A standard way in optimization theory to circumvent such complexity issues is to solve a closely related problem: instead of minimizing over $\text{conv}(\mathcal{C})$ we will minimize over a relaxation polytope $\text{relax}(\text{conv}(\mathcal{C}))$ of this polytope, i.e. over a larger polytope:

$$\hat{\boldsymbol{\omega}}^{\text{LPD}}(\mathbf{y}) = \arg \min_{\boldsymbol{\omega} \in \text{relax}(\text{conv}(\mathcal{C}))} \langle \boldsymbol{\omega}, \boldsymbol{\lambda} \rangle, \quad (20)$$

Of course, this new polytope should have a low description complexity, yet be a good approximation of $\text{conv}(\mathcal{C})$ so that it is highly likely that $\hat{\mathbf{x}}^{\text{LPD}}(\mathbf{y}) = \hat{\mathbf{x}}^{\text{MAPD}}(\mathbf{y})$. In particular, all codewords in \mathcal{C} should be vertices of $\text{relax}(\text{conv}(\mathcal{C}))$.

Probably one of the easiest ways of obtaining a reasonable relaxation is the following. Observe that

$$\mathcal{C} = \bigcap_{j \in \mathcal{J}(\mathbf{H})} \mathcal{C}_j(\mathbf{H}),$$

where $\mathcal{C}_j(\mathbf{H})$ was defined in (8). Consider now the set

$$\mathcal{R}(\mathbf{H}) \triangleq \bigcap_{j \in \mathcal{J}(\mathbf{H})} \text{conv}(\mathcal{C}_j(\mathbf{H})). \quad (21)$$

The fact that the set $\mathcal{R}(\mathbf{H})$ is a relaxation of $\text{conv}(\mathcal{C})$ can be seen from the following chain of reasoning: firstly, the set $\mathcal{R}(\mathbf{H})$ is the intersection of convex sets and is therefore convex itself; secondly, the set $\mathcal{R}(\mathbf{H})$ contains all codewords in \mathcal{C} ; thirdly, $\text{conv}(\mathcal{C})$ is the smallest convex set that contains \mathcal{C} ; combining these three observations leads to the conclusion that $\text{conv}(\mathcal{C}) \subseteq \mathcal{R}(\mathbf{H})$. Note that $\text{conv}(\mathcal{C}) = \mathcal{R}(\mathbf{H})$ is possible though strict inclusion turns out to be what happens usually. Of course, the set $\mathcal{R}(\mathbf{H})$ in (21) equals the set $\mathcal{P}(\mathbf{H})$ defined in Def. 8: the solution of the LP decoder when choosing $\text{relax}(\text{conv}(\mathcal{C})) \triangleq \mathcal{R}(\mathbf{H}) = \mathcal{P}(\mathbf{H})$ will henceforth be called $\hat{\boldsymbol{\omega}}^{\text{LPD}(\mathbf{H})}(\mathbf{y})$.

The next definition introduces another class of relaxations.

¹⁴Because of the memoryless property of the channel it also follows that $p_{\Lambda|\mathbf{X}}(\boldsymbol{\lambda}|\mathbf{x}) = \prod_{i \in \mathcal{I}} p_{\Lambda_i|X_i}(\lambda_i|x_i) = \prod_{i \in \mathcal{I}} p_{\Lambda|X}(\lambda_i|x_i)$.

¹⁵In case a whole face of $\text{conv}(\mathcal{C})$ is optimal we decide in favor of one of the vertices in it.

Definition 11 Let \mathbf{H} be an arbitrary parity-check matrix that defines a code \mathcal{C} . For some $r \geq 1$, let

$$\mathcal{R}_r(\mathbf{H}) \triangleq \bigcap_{\mathbf{h}} \text{conv}(\mathcal{C}(\mathbf{h})),$$

where the intersection is over all vectors $\mathbf{h} \in \mathbb{F}_2^n$ that can be written as the modulo-2 sum of at most r rows of \mathbf{H} . We call $\mathcal{R}_r(\mathbf{H})$ the r -th relaxation of $\text{conv}(\mathcal{C})$ with respect to \mathbf{H} . Note that $\mathcal{R}_r(\mathbf{H}) = \mathcal{P}(\mathbf{H}')$ where \mathbf{H}' is the parity-check matrix consisting of all rows of \mathbf{H} , the modulo-2 sums of all pairs of rows of \mathbf{H} , ..., the modulo-2 sum of all r -tuples of rows of \mathbf{H} . \square

Some of the consequences of this definition will be explored in Sec. 8.3.

Let us define three channels that will be of prime interest in this paper: the binary-input additive white Gaussian noise channel (BI-AWGNC or simply AWGNC), the binary symmetric channel (BSC), and the binary erasure channel (BEC).

Example 12 The binary input additive white Gaussian noise channel (BI-AWGNC) with input energy per channel symbol E_c and noise power σ^2 has output alphabet $\mathcal{Y} = \mathbb{R}$ and channel law¹⁶

$$P_{\bar{Y}|X}(\bar{y}|x) = \begin{cases} \frac{1}{\sqrt{2\pi\sigma}} \exp\left(-\frac{(\bar{y}-\sqrt{E_c})^2}{2\sigma^2}\right) & (\text{if } x = 0) \\ \frac{1}{\sqrt{2\pi\sigma}} \exp\left(-\frac{(\bar{y}+\sqrt{E_c})^2}{2\sigma^2}\right) & (\text{if } x = 1) \end{cases}. \quad (22)$$

Defining the input energy per information symbol to be E_b , this quantity is related to E_c through $E_c = R \cdot E_b$. Introducing $N_0 \triangleq 2\sigma^2$, two different signal-to-noise ratios can be defined, namely $\text{SNR}_b \triangleq E_b/N_0$ and $\text{SNR}_c \triangleq E_c/N_0$, which are related through $\text{SNR}_c = R \cdot \text{SNR}_b$. Defining $\bar{x}(x) \triangleq \sqrt{E_c} \cdot (1 - 2x)$ for $x \in \mathbb{F}_2 \subset \mathbb{R}$ we can write (22) as

$$P_{Y|X}(y|x) = \frac{1}{\sqrt{2\pi\sigma}} \exp\left(-\frac{(\bar{y} - \bar{x}(x))^2}{2\sigma^2}\right).$$

If $\mathbf{x} \in \mathbb{F}_2^n \subset \mathbb{R}^n$ is the codeword to be transmitted, then the modulated word is $\bar{\mathbf{x}} \triangleq \bar{\mathbf{x}}(\mathbf{x}) \triangleq \sqrt{E_c} \cdot (\mathbf{1} - 2\mathbf{x})$. So, upon sending \bar{x}_i we receive $\bar{Y}_i = \bar{x}_i + \bar{Z}_i$ where \bar{Z}_i is normally distributed with mean zero and variance σ^2 . Therefore, \bar{Y}_i given $X_i = 0$ is normally distributed with mean $+\sqrt{E_c}$ and variance σ^2 , whereas \bar{Y}_i given $X_i = 1$ is normally distributed with mean $-\sqrt{E_c}$ and variance σ^2 . For the BI-AWGNC we have a simple relationship between $\bar{\mathbf{Y}}$ and Λ , namely by simplifying the definition of LLR for the i -th symbol we see that

$$\Lambda_i \triangleq \Lambda_i(\bar{Y}_i) \triangleq \log \frac{P_{\bar{Y}_i|X_i}(\bar{Y}_i|0)}{P_{\bar{Y}_i|X_i}(\bar{Y}_i|1)} = \log \frac{P_{\bar{Y}_i|\bar{X}_i}(\bar{Y}_i + \sqrt{E_c})}{P_{\bar{Y}_i|\bar{X}_i}(\bar{Y}_i - \sqrt{E_c})} = 4 \cdot \frac{\sqrt{RE_b}}{N_0} \cdot \bar{Y}_i,$$

i.e. Λ is just a scaled version of $\bar{\mathbf{Y}}$. From this, it can easily be calculated that Λ_i given $X_i = 0$ is normally distributed with mean $4R \cdot \text{SNR}_b$ and variance $8R \cdot \text{SNR}_b$, whereas Λ_i given $X_i = 1$ is normally distributed with mean $-4R \cdot \text{SNR}_b$ and variance $8R \cdot \text{SNR}_b$.

¹⁶In the case of the AWGNC we will denote the output symbols by \bar{Y}_i and not by Y_i so that all (random) variables that can be represented in a signal space have an over-bar.

Finally, let us note that block-wise MAPD can not only be written as in (16) and (18) but also as

$$\hat{\mathbf{x}}^{\text{MAPD}}(\bar{\mathbf{y}}) = \arg \max_{\mathbf{x} \in \mathcal{C}} \sum_{i \in \mathcal{I}} \bar{x}_i(x_i) \lambda_i = \arg \max_{\mathbf{x} \in \mathcal{C}} \langle \bar{\mathbf{x}}(\mathbf{x}), \boldsymbol{\lambda} \rangle, \quad (23)$$

i.e. decoding can be written as finding the $\bar{\mathbf{x}}(\mathbf{x})$, $\mathbf{x} \in \mathcal{C}$, with the largest standard inner product with $\boldsymbol{\lambda}$. The decoding rule in (23) is also known as the correlation decoding rule. \square

Example 13 The binary symmetric channel (BSC) with cross-over probability $0 \leq \varepsilon \leq \frac{1}{2}$ has output alphabet $\mathcal{Y} = \{0, 1\}$ and channel law $P_{Y|X}(y|x) = 1 - \varepsilon$ if $y = x$ and $P_{Y|X}(y|x) = \varepsilon$ otherwise. The log-likelihood ratio for the i -th bit is the random variable

$$\Lambda_i \triangleq \Lambda_i(Y_i) \triangleq \log \frac{P_{Y_i|X_i}(Y_i|0)}{P_{Y_i|X_i}(Y_i|1)} = \begin{cases} +\log \frac{1-\varepsilon}{\varepsilon} & (\text{if } Y_i = 0) \\ -\log \frac{1-\varepsilon}{\varepsilon} & (\text{if } Y_i = 1) \end{cases}. \quad (24)$$

Note that $\log \frac{1-\varepsilon}{\varepsilon} \geq 0$. Upon sending $X_i = 0$, $\Lambda_i(Y_i)$ takes on the value $+\log \frac{1-\varepsilon}{\varepsilon}$ with probability $1 - \varepsilon$ and the value $-\log \frac{1-\varepsilon}{\varepsilon}$ with probability ε . \square

Example 14 The binary erasure channel (BEC) with erasure probability $0 \leq \epsilon \leq 1$ has output alphabet $\mathcal{Y} = \{0, 1, ?\}$ and channel law $P_{Y|X}(y|x) = 1 - \epsilon$ if $y = x$, $P_{Y|X}(y|x) = \epsilon$ if $y = ?$, and $P_{Y|X}(y|x) = 0$ otherwise. The log-likelihood ratio for the i -th bit is the random variable

$$\Lambda_i \triangleq \Lambda_i(Y_i) \triangleq \log \frac{P_{Y_i|X_i}(Y_i|0)}{P_{Y_i|X_i}(Y_i|1)} = \begin{cases} +\infty & (\text{if } Y_i = 0) \\ -\infty & (\text{if } Y_i = 1) \\ 0 & (\text{if } Y_i = ?) \end{cases}. \quad (25)$$

Upon sending $X_i = 0$, $\Lambda_i(Y_i)$ takes on the value $+\infty$ with probability $1 - \epsilon$ and the value 0 with probability ϵ . \square

Definition 15 A binary-input memoryless channel $(\mathcal{X} \triangleq \{0, 1\}, \mathcal{Y}, P_{Y|X})$ is called output-symmetric if there is an involution¹⁷ $\sigma : \mathcal{Y} \rightarrow \mathcal{Y}$ and two (possibly overlapping) sets \mathcal{Y}' and \mathcal{Y}'' such that:

- $\mathcal{Y}'' = \sigma(\mathcal{Y}')$, $\mathcal{Y}' = \sigma(\mathcal{Y}'')$, $\mathcal{Y}' \cup \mathcal{Y}'' = \mathcal{Y}$.
- For every $y' \in \mathcal{Y}'$ we have $P_{Y|X}(y'|0) = P_{Y|X}(y''|1)$ and $P_{Y|X}(y'|1) = P_{Y|X}(y''|0)$ where $y'' \triangleq \sigma(y')$.

\square

It is easy to see that the three previously discussed channels are output-symmetric. For the AWGNC one can e.g. choose $\mathcal{Y}' = \mathbb{R}_+$ and $\sigma(y') = -y'$, for the BSC one can e.g. choose $\mathcal{Y}' = \{0\}$ and $\sigma(y') = 1 - y'$, and for the BEC one can e.g. choose $\mathcal{Y}' = \{0, ?\}$, $\sigma(0) = 1$, $\sigma(1) = 0$, and $\sigma(?) = ?$.

In the rest of this paper we will focus on a specific class of codes, channels, and decoders:

¹⁷An involution is a mapping of order two, i.e. $\sigma(\sigma(y)) = y$ for all $y \in \mathcal{Y}$.

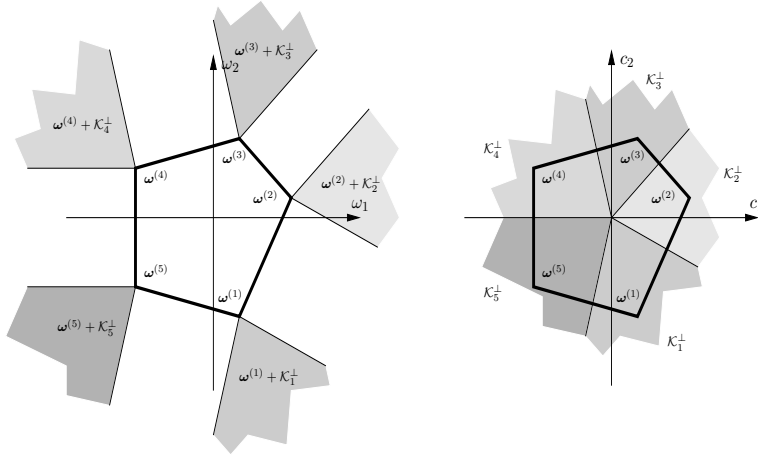


Figure 11: The set $\mathcal{A} = \text{conv}(\{\boldsymbol{\omega}^{(1)}, \boldsymbol{\omega}^{(2)}, \boldsymbol{\omega}^{(3)}, \boldsymbol{\omega}^{(4)}, \boldsymbol{\omega}^{(5)}\})$ used in Ex. 16. When the cost vector lies in \mathcal{K}_i^\perp then the linear program decides in favor vertex $\boldsymbol{\omega}^{(i)}$. Note that the half-rays that constitute the boundaries between the decision regions are perpendicular to the corresponding edge of the polytope. (In n -dimensional space the half-rays that span a decision cone are perpendicular to the corresponding facets of the polytope.)

- The codes are assumed to be binary and linear. (Note that a binary code that is defined by a parity-check matrix is automatically binary and linear.)
- The channels are assumed to be binary-input output-symmetric memoryless channels.
- The decoders are symmetric with respect to codewords.

For this scenario it turns out that the conditional decoding error probability is independent of the codeword that was sent. Therefore, for understanding decoders it is sufficient to analyze the case where the all-zeros codeword was transmitted.

The rest of this section will be devoted to recalling some facts from linear programming that will help to better understand the LPD. Let n be some positive integer. Consider the following optimization problem

$$\max_{\boldsymbol{\omega} \in \mathcal{A}} \langle \boldsymbol{\omega}, \mathbf{c} \rangle \quad (26)$$

where \mathcal{A} is a polyhedron in \mathbb{R}^n and cost vector $\mathbf{c} \in \mathbb{R}^n$. Such an optimization problem is called a linear program (LP) and the set of all $\boldsymbol{\omega}$ that achieve the maximum for a give \mathbf{c} is called the optimum set. Because the polyhedra that we are interested in are bounded we can actually assume that \mathcal{A} is a polytope.¹⁸

Example 16 Fig. 11 (left) shows a possible polytope \mathcal{A} in $n = 2$ dimensions with vertices $\boldsymbol{\omega}^{(i)}$, $i \in [5]$. One way to describe the set \mathcal{A} is as the convex combination of the set of

¹⁸Here are some commonly used terms when talking about polytopes: the intersection of an n -dimensional polytope with a tangent hyperplane is called a face, zero-dimensional faces are known as vertices, one-dimensional faces as edges, $(n - 2)$ -dimensional faces as ridges, and $(n - 1)$ -dimensional faces as facets. Note that edges and facets of two-dimensional polytopes are both one-dimensional objects; therefore one must be careful when generalizing a certain setup to a higher-dimensional space.

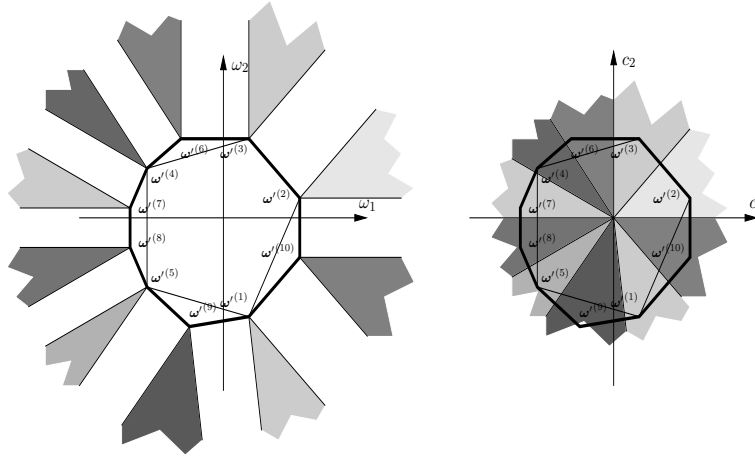


Figure 12: The set $\mathcal{A} = \text{conv}(\{\omega^{(1)}, \dots, \omega^{(10)}\})$ used in Ex. 19.

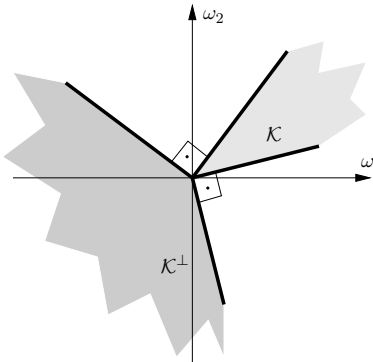


Figure 13: A cone \mathcal{K} in \mathbb{R}^2 and its dual cone \mathcal{K}^\perp . Because \mathcal{K} is a proper cone it holds that $\mathcal{K}^{\perp\perp} = \mathcal{K}$.

vertices: $\mathcal{A} = \text{conv}(\{\boldsymbol{\omega}^{(1)}, \boldsymbol{\omega}^{(2)}, \boldsymbol{\omega}^{(3)}, \boldsymbol{\omega}^{(4)}, \boldsymbol{\omega}^{(5)}\})$. Another way is to describe the set \mathcal{A} as the intersection of half-spaces where each of the half-spaces is described by a single linear (affine) inequality. \square

A special feature of an LP as in (26) is that for any given \mathbf{c} there is always a vertex that is optimal.¹⁹ Let $\boldsymbol{\omega}^{(*)}$ be a vertex of \mathcal{A} . An interesting question to ask is for which vectors \mathbf{c} the vertex $\boldsymbol{\omega}^{(*)}$ will be in the optimal set. To answer this question it is useful to introduce so-called dual cones.

Definition 17 Let \mathcal{K} be a cone in \mathbb{R}^n . The dual cone \mathcal{K}^\perp is then defined to be set²⁰

$$\mathcal{K}^\perp \triangleq \{\boldsymbol{\omega}' \in \mathbb{R}^n \mid \langle \boldsymbol{\omega}', \boldsymbol{\omega} \rangle \leq 0 \ \forall \boldsymbol{\omega} \in \mathcal{K}\}. \quad (27)$$

\square

If \mathcal{K} is a proper cone (cf. Sec. 1.2) it turns out that \mathcal{K}^\perp is also proper and that $\mathcal{K}^{\perp\perp} = \mathcal{K}$. Fig. 13 shows a possible cone in two dimensions along with its dual cone. Cones can either be described as the conic hull of a set of vectors, as the intersection of half-spaces, or a combination of both. When a cone is described as the conic hull of a set of vectors then this yields immediately the representation of the dual cone as the intersection of certain half-spaces. On the other hand, when a cone is described as the intersection of half-spaces then this yields immediately the representation of the dual cone as the conic hull of a certain set of vectors.

Example 18 Consider the same setup as in Ex. 16 and fix some $i \in [5]$. It turns out that the set of vectors \mathbf{c} where $\boldsymbol{\omega}^{(i)}$ is in the optimal set is the set \mathcal{K}_i^\perp where $\mathcal{K}_i \triangleq \text{conic}(\mathcal{A} - \boldsymbol{\omega}^{(i)})$. The set \mathcal{K}_i^\perp is shown in Fig. 11 (right). It is also instructive to plot the translated set $\boldsymbol{\omega}^{(i)} + \mathcal{K}_i^\perp$ in Fig. 11 (left). (Note that when the maximum operator in (26) is replaced by a minimum operator then the optimal set is $-\mathcal{K}_i^\perp$ where $\mathcal{K}_i \triangleq \text{conic}(\mathcal{A} - \boldsymbol{\omega}^{(i)})$ as above.) \square

Often it turns out that the linear program in (26) is too complicated to be solved. A possibility is then to solve a tightly related problem and then to try to infer the solution of the original problem from the related problem. A popular way of obtaining a related problem is to relax the set \mathcal{A} to the set \mathcal{A}' and to solve

$$\max_{\boldsymbol{\omega} \in \mathcal{A}'} \langle \boldsymbol{\omega}, \mathbf{c} \rangle \quad (28)$$

Of course, the set \mathcal{A}' should have some desirable properties: \mathcal{A}' should not be much larger than \mathcal{A} and all vertices of \mathcal{A} should be vertices of \mathcal{A}' .

Example 19 Consider the same setup as in Ex. 16. Instead of solving (26) for the set \mathcal{A} as in Fig. 11 (left) we can solve the relaxed linear program (28) with the set $\mathcal{A}' = \text{conv}(\{\boldsymbol{\omega}'^{(1)}, \dots, \boldsymbol{\omega}'^{(10)}\})$ as in Fig. 12 (left). We see that \mathcal{A}' fulfills the desirable properties that were listed above: \mathcal{A}' is not much larger than \mathcal{A} and $\boldsymbol{\omega}'^{(i)} = \boldsymbol{\omega}^{(i)}$, $i \in [5]$. Fig. 12 (right) shows for which \mathbf{c} we decide for which vertex. Of course, the regions fulfill $\mathcal{K}_i'^\perp \subseteq \mathcal{K}_i^\perp$ for $i \in [5]$. Moreover, the fact that \mathcal{A}' tightly resembles \mathcal{A} can also be seen from the fact that $\mathcal{K}_i'^\perp$ is nearly as large as \mathcal{K}_i^\perp for $i \in [5]$. \square

¹⁹For a generic vector \mathbf{c} the set of optimal points will contain exactly one vertex of the polytope. However, for any face of the polytope there is at least one cost vector \mathbf{c} such that this face is the optimal set.

²⁰The dual cone can be defined by $\langle \mathbf{x}, \mathbf{y} \rangle \leq 0$ or by $\langle \mathbf{x}, \mathbf{y} \rangle \geq 0$, here we have chosen the first possibility.

Contemplating Figs. 11 and 12, it does not look as if this relaxation really bought us anything. In fact, the optimization has to be carried out over a more complex region. However, for higher-dimensional problems the relaxation approach can work very nicely. E.g. the fundamental polytope $\mathcal{P}(\mathbf{H})$ is a relaxation of the set $\text{conv}(\mathcal{C})$ [31, 32] which seems to be quite tight especially in the case of LDPC codes. Whereas $\text{conv}(\mathcal{C})$ is usually very difficult to describe²¹, we will see that the fundamental polytope has a relatively simple description.

We conclude this section with a warning to the uninitiated reader: whereas two-dimensional pictures of polytopes and cones are very useful to get an initial understanding of the various definitions, higher dimensional polytopes and cones can behave quite differently. Note that in the channel coding case the high-dimensional spaces are unavoidable since it is well known from information theory that well-performing codes need to have a certain length.

4 Graph-Cover Decoding

This section introduces graph-cover decoding (GCD) which is the theoretical tool that will help to link LPD and MPID. On the one hand, GCD will be shown to be essentially equivalent to LPD. On the other hand, we will discuss how GCD can serve as a model of what is going on in MPID. Sometimes it is an exact model but usually it is just a very good approximation. The findings in this section will be corroborated by some simulation results that will be presented at the end of Sec. 5.

In the following we assume that we consider data transmission over a channel as discussed in Sec. 3.

Definition 20 (Lifting) *Let $\tilde{\mathbb{T}}$ be an arbitrary M -cover of $\mathbb{T}(\mathbf{H})$. The M -lifting of a length- n vector \mathbf{v} is the vector $\tilde{\mathbf{v}} \triangleq \mathbf{v}^{\uparrow M}$ with entries $\tilde{v}_{i,m} \triangleq v_i$ for all $(i, m) \in \mathcal{I}(\mathbf{H}) \times [M]$, i.e. $\tilde{\mathbf{v}}$ is a vector of length Mn where each entry is repeated M times. \square*

We remind the reader of the MAPD/MLD decision rule formulation in (16) and (18). That rule aims to find the codeword that gives the largest log-likelihood ratio given that \mathbf{y} was received. GCD extends this idea in the following way: instead of trying to find the codeword that gives the largest log-likelihood ratio that \mathbf{y} was received we want to find the codeword in any finite graph cover that gives the largest log-likelihood ratio that \mathbf{y} was received. In order to obtain a fair comparison we will rescale the log-likelihood ratios by the order of the cover degree.

However, before formulating GCD more precisely we have to extend the definition of the channel law. Let $P_{Y|X}(y|x)$ be the channel law of a memoryless channel. We define the extended joint conditional pmf/pdf of receiving a vector $\tilde{\mathbf{y}}$ of length Mn upon sending a vector $\tilde{\mathbf{x}}$ of length Mn to be

$$P_{\tilde{\mathbf{Y}}|\tilde{\mathbf{X}}}(\tilde{\mathbf{y}}|\tilde{\mathbf{x}}) = \prod_{i \in [n]} \prod_{m \in [M]} P_{Y|X}(y_{i,m}|x_{i,m}) \quad (29)$$

Definition 21 *We define graph-cover decoding (GCD) to be the following decision rule:*

$$(\hat{M}, \hat{\mathbb{T}}, \hat{\tilde{\mathbf{x}}})^{\text{GCD}(\mathbf{H})}(\mathbf{y}) = \arg \max_{(M, \mathbb{T}, \tilde{\mathbf{x}}) \in \tilde{\mathcal{Q}}(\mathbf{H})} \frac{1}{M} \log P_{\tilde{\mathbf{Y}}|\tilde{\mathbf{X}}}(\mathbf{y}^{\uparrow M}|\tilde{\mathbf{x}}), \quad (30)$$

²¹An exception are e.g. convolutional codes with not too many states.

where ties are resolved in a systematic or arbitrary way. Moreover, let $\hat{\omega}^{\text{GCD}(\mathbf{H})}(\mathbf{y}) \triangleq \omega(\hat{\mathbf{x}}^{\text{GCD}(\mathbf{H})}(\mathbf{y}))$. \square

The $1/M$ factor on the right-hand side of (30) is the promised rescaling factor that makes a fair comparison of the log-likelihood ratios. Note that the expression in (30) is also well-defined in the following sense: let \mathbf{x} be a codeword in \mathcal{C} . Then, for any M -cover graph $\tilde{\mathbb{T}}$ of $\mathbb{T}(\mathbf{H})$ the vector $\tilde{\mathbf{x}} \triangleq \mathbf{x}^{\uparrow M}$ is a codeword in $\mathcal{C}(\tilde{\mathbb{T}})$ with the property that

$$\log P_{\mathbf{Y}|\mathbf{X}}(\mathbf{y}|\mathbf{x}) = \frac{1}{M} \log P_{\tilde{\mathbf{Y}}|\tilde{\mathbf{X}}}(\mathbf{y}^{\uparrow M}|\tilde{\mathbf{x}}). \quad (31)$$

(A similar statement can be made about the relationship of a codeword in some finite cover to its liftings in finite covers of that finite cover.)

The next proposition shows that GCD and the LPD are essentially equivalent.

Proposition 22 *For a given received vector \mathbf{y} , let $\hat{\omega}^{\text{GCD}(\mathbf{H})}(\mathbf{y})$ be the GCD decision as defined as in Def. 21 and let $\hat{\omega}^{\text{LPD}(\mathbf{H})}(\mathbf{y})$ be the LPD decision as given in (20) with $\text{relax}(\text{conv}(\mathcal{C})) = \mathcal{P}(\mathbf{H})$. Then*

$$\hat{\omega}^{\text{GCD}(\mathbf{H})}(\mathbf{y}) = \hat{\omega}^{\text{LPD}(\mathbf{H})}(\mathbf{y}). \quad (32)$$

(For this statement we assume that if ties appear in either decoder that they are resolved in the same way.)

Proof: See Sec. A.2. \square

Let us now turn our attention to the connection between GCD and MPID. Recall our discussion about MPID for the trivial code in Sec. 1.1. On the one hand, we considered MPID of the received vector \mathbf{y} on the base Tanner graph \mathbb{T} shown in Fig. 1 and on the other hand, we considered MPID of $\tilde{\mathbf{y}}$ on the triple cover $\tilde{\mathbb{T}}$ shown in Fig. 3 (left). Because \mathbb{T} and $\tilde{\mathbb{T}}$ look locally the same, the computation tree for variable node X_i after t iterations will be identical to the computation tree for variable node $X_{i,m}$ after t iterations, where $m \in [3]$ is arbitrary. This is shown in Fig. 4 for the variable node X_2 and after $t = 2$ iterations. Moreover, under the assumption that $\tilde{\mathbf{y}} = \mathbf{y}^{\uparrow 3}$ it can readily be verified that the messages on the two computation trees are the same. In that way we see that because MPID is operating locally on Tanner graphs, MPID cannot distinguish if it is decoding the code defined by the base Tanner \mathbb{T} graph or any of the codes defined by the finite covers of \mathbb{T} . If the decoding of these codes is done in a MAPD/MLD fashion, then MPID is essentially equivalent to GCD, otherwise GCD is just a (usually very good) approximation to MPID.

There are cases where GCD is the right model for MPID. The list includes Tanner graphs that are trees (i.e. have no cycle), codes represented by trellises, codes represented by tail-biting trellises, and cycle codes (i.e. codes where all bit nodes have degree two). Additionally, when we transmit over the BEC then GCD is also the right model, independently of the Tanner graph of the code.

In conclusion, we see that the locality, which makes MPID a low-complexity algorithm, is also the main weakness of MPID.

5 Properties of Fundamental Polytopes and Cones

The fundamental polytope was introduced in Def. 8. In the meantime we have seen that it is one of the objects of central interest in this paper, namely it turns up when considering

GCD and LPD and because of the closeness of MPID and GCD it seems to be also important for MPID. It is therefore natural to try to better understand this object. To that end, this section will look at different ways of describing the fundamental polytope and will discuss various properties of it. Actually, we will mostly look at the fundamental cone which is the fundamental polytope around the vertex $\mathbf{0}$ and blown up to infinity, in other words, the conic hull of the fundamental polytope. Understanding the fundamental cone is sufficient because we restrict ourself to using binary-input output-symmetric memoryless channels, as was outlined in Sec. 3.

Definition 23 *The fundamental cone $\mathcal{K}(\mathbf{H})$ is defined to be the conic hull of the fundamental polytope $\mathcal{P}(\mathbf{H})$, i.e.*

$$\mathcal{K}(\mathbf{H}) \triangleq \text{conic}(\mathcal{P}(\mathbf{H})).$$

□

From this definition it follows easily that $\mathcal{P}(\mathbf{H}) \subset \mathcal{K}(\mathbf{H})$ and that for any $\boldsymbol{\omega} \in \mathcal{K}(\mathbf{H})$ there is an $\alpha \in \mathbb{R}_{++}$ (in fact, a whole interval of α 's) such that $\alpha \cdot \boldsymbol{\omega} \in \mathcal{P}(\mathbf{H})$.

In Ex. 18 we saw that the set of cost vectors where $\boldsymbol{\omega}^{(i)}$ is in the optimal set is given by the set $(\text{conic}(\mathcal{A} - \boldsymbol{\omega}^{(1)}))^\perp$. In the case of LPD and GCD, we see that $\mathbf{0}$ is in the optimal set when $\boldsymbol{\lambda}$ lies in $-(\text{conic}(\mathcal{P}(\mathbf{H}) - \mathbf{0}))^\perp$, which equals $-\mathcal{K}(\mathbf{H})^\perp$.²² This observation emphasize the fact that the fundamental cone contains all the relevant information and it is sufficient to study the fundamental cone (instead of the fundamental polytope). For that reason, all vectors in $\mathcal{K}(\mathbf{H})$ will be called pseudo-codewords. Moreover, if $\boldsymbol{\omega} \in \mathcal{K}(\mathbf{H})$ and $\{\alpha \cdot \boldsymbol{\omega} \mid \alpha \in \mathbb{R}_+\}$ is an edge of the fundamental cone then we call $\boldsymbol{\omega}$ a *minimal* pseudo-codeword. This generalizes the notion of minimal codewords [45, 46, 47, 48]²³ which are the edges of $\text{conic}(\mathcal{C})$.²⁴ Note that although all codewords are vertices of the fundamental polytope [31, 32], a minimal codeword need *not* necessarily be a minimal pseudo-codeword! (Given a minimal codeword there are simple conditions to check if it is a minimal pseudo-codeword; however, we are not aware of a general result that says when a minimal codeword is also a minimal pseudo-codeword. Having e.g. a Tanner graph with girth six is neither sufficient nor necessary to have all minimal codewords being minimal pseudo-codewords.)

In Sec. 2 we have seen that $\mathcal{Q}(\mathbf{H})$ and $\mathcal{P}(\mathbf{H})$ are tightly related. Not surprisingly, there is a connection between $\tilde{\mathcal{Q}}(\mathbf{H})$ and $\mathcal{K}(\mathbf{H})$, a connection that is explored in the following lemma.

Lemma 24 *Remember that if $\tilde{\mathbf{x}}$ is a codeword in some M -cover $\tilde{\mathbb{T}}$ of $\mathbb{T}(\mathbf{H})$, then $M\boldsymbol{\omega}(\tilde{\mathbf{x}}) \in \mathbb{Z}_+^n$ is called the *unscaled pseudo-codeword* corresponding to $\tilde{\mathbf{x}}$. Let*

$$\mathcal{Z}(\mathbf{H}) \triangleq \bigcup_{(M, \tilde{\mathbb{T}}, \tilde{\mathbf{x}}) \in \tilde{\mathcal{Q}}(\mathbf{H})} \{M\boldsymbol{\omega}(\tilde{\mathbf{x}})\} \quad (33)$$

be the set of all these unscaled pseudo-codewords. This set fulfills $\mathcal{Z}(\mathbf{H}) = \mathcal{K}(\mathbf{H}) \cap \mathbb{Z}^n$ and $\mathcal{Z}(\mathbf{H}) = \mathcal{C}$ (in \mathbb{F}_2). Moreover, for every minimal pseudo-codeword $\boldsymbol{\omega}$ there is an $\alpha \in \mathbb{R}_{++}$ (in fact, a whole set of α 's) such that $\alpha\boldsymbol{\omega} \in \mathcal{Z}(\mathbf{H})$.

²²Note that LPD/GCD is formulated as a minimization and not as a maximization problem, therefore the minuses in front of the dual cones.

²³A side remark: interestingly, Decoding Algorithm 1 in [45] can be seen as a simplex-type algorithm on $\text{conv}(\mathcal{C})$ to solve the LP in (19).

²⁴For a further discussion of minimal pseudo-codewords and minimal pseudo-codeword enumerators, see [49, 50, 51].

Object	Number of variables	Number of (in)equalities
\mathcal{P} in Lemma 25	$n + \mathcal{J} 2^{w_{\text{row}}-1}$	$2n + \mathcal{J} (w_{\text{row}} + 2^{w_{\text{row}}-1} + 1)$
\mathcal{K} in Lemma 25	$n + \mathcal{J} \binom{w_{\text{row}}}{2}$	$n + \mathcal{J} (w_{\text{row}} + \binom{w_{\text{row}}}{2})$
\mathcal{P} in Lemma 26	n	$2n + \mathcal{J} 2^{w_{\text{row}}-1}$
\mathcal{K} in Lemma 26	n	$n + \mathcal{J} w_{\text{row}}$

Table 1: The description complexity of the fundamental polytope and cone for a $(w_{\text{col}}, w_{\text{row}})$ -regular LDPC code of length n . Here, $|\mathcal{J}| = nw_{\text{col}}/w_{\text{row}}$.

Proof: See Sec. A.3. □

The following lemmas discuss different representations of the fundamental polytope and cone.

Lemma 25 *Let $\mathbf{P}'^{(j)}$ be a $2^{|\mathcal{I}_j|-1} \times \mathcal{I}_j$ matrix containing all the binary vectors of length $|\mathcal{I}_j|$ with even Hamming weight, i.e. the codewords of \mathcal{C}'_j , i.e. the codewords of a single-parity-check code of length $|\mathcal{I}_j|$. Let $\mathbf{P}''^{(j)}$ be a $\binom{|\mathcal{I}_j|}{2} \times \mathcal{I}_j$ matrix containing all the binary vectors of length $|\mathcal{I}_j|$ with Hamming weight two. The fundamental polytope $\mathcal{P} \triangleq \mathcal{P}(\mathbf{H})$ and the fundamental cone $\mathcal{K} \triangleq \mathcal{K}(\mathbf{H})$ can be described by the following sets of linear inequalities, respectively:*

$$\mathcal{P} = \left\{ \boldsymbol{\omega} \in \mathbb{R}^n \left| \begin{array}{l} \forall i \in \mathcal{I} : 0 \leq \omega_i \leq 1 \\ \forall j \in \mathcal{J} : \boldsymbol{\omega}_{\mathcal{I}_j} = \boldsymbol{\alpha}^{(j)} \mathbf{P}'^{(j)}, \boldsymbol{\alpha}^{(j)} \in \mathbb{R}^{2^{|\mathcal{I}_j|-1}}, \mathbf{0} \leq \boldsymbol{\alpha}^{(j)}, \langle \boldsymbol{\alpha}^{(j)}, \mathbf{1} \rangle = 1 \end{array} \right. \right\}, \quad (34)$$

$$\mathcal{K} = \left\{ \boldsymbol{\omega} \in \mathbb{R}^n \left| \begin{array}{l} \forall i \in \mathcal{I} : 0 \leq \omega_i \\ \forall j \in \mathcal{J} : \boldsymbol{\omega}_{\mathcal{I}_j} = \boldsymbol{\alpha}^{(j)} \mathbf{P}''^{(j)}, \boldsymbol{\alpha}^{(j)} \in \mathbb{R}^{\binom{|\mathcal{I}_j|}{2}}, \mathbf{0} \leq \boldsymbol{\alpha}^{(j)} \end{array} \right. \right\}. \quad (35)$$

Proof: The expression for \mathcal{P} is a direct consequence of the definition given in (12) and the expression for \mathcal{K} is obtained by taking the conic hull of \mathcal{P} . Note that because all binary vectors of even Hamming weight with Hamming weight larger than two can be written as the (integer) sum of several binary vectors of Hamming weight two, we were able to replace the matrices $\{\mathbf{P}'^{(j)}\}$ by the matrices $\{\mathbf{P}''^{(j)}\}$ in the expression for \mathcal{K} . □

Lemma 26 *The fundamental polytope $\mathcal{P} \triangleq \mathcal{P}(\mathbf{H})$ and the fundamental cone $\mathcal{K} \triangleq \mathcal{K}(\mathbf{H})$ can be described by the following sets of linear inequalities, respectively:*

$$\mathcal{P} = \left\{ \boldsymbol{\omega} \in \mathbb{R}^n \left| \begin{array}{l} \forall i \in \mathcal{I} : 0 \leq \omega_i \leq 1 \\ \forall j \in \mathcal{J}(\mathbf{H}), \forall \mathcal{I}'_j \subseteq \mathcal{I}_j, |\mathcal{I}'_j| \text{ odd} : \sum_{i \in \mathcal{I}'_j} \omega_i + \sum_{i \in (\mathcal{I}_j \setminus \mathcal{I}'_j)} (1 - \omega_i) \leq |\mathcal{I}_j| - 1 \end{array} \right. \right\}$$

$$\mathcal{K} = \left\{ \boldsymbol{\omega} \in \mathbb{R}^n \left| \begin{array}{l} \forall i \in \mathcal{I} : 0 \leq \omega_i \\ \forall j \in \mathcal{J}(\mathbf{H}), \forall i' \in \mathcal{I}_j : \omega_{i'} - \sum_{i \in (\mathcal{I}_j \setminus \{i'\})} \omega_i \leq 0 \end{array} \right. \right\}$$

Proof: We do not go into the details of deriving these inequalities. For a discussion, see e.g. [32, 52]. Note that the inequalities that describe $\mathcal{K}(\mathbf{H})$ are exactly those inequalities describing $\mathcal{P}(\mathbf{H})$ which are homogenous, i.e. that define half-spaces that go through the origin. □

Let us consider the description complexities of the various characterizations of the fundamental polytope and cone in Lemmas 25 and 26. For reasons of simplicity we consider a

$(w_{\text{col}}, w_{\text{row}})$ -regular binary LDPC code, but similar expressions can be obtained for irregular binary LDPC codes. The number of variables and (in)equalities that are needed are listed in Tab. 1. For the fundamental polytope we observe a linear behavior in the block length n but an exponential behavior in the row weight w_{row} . For binary LDPC codes, where w_{row} is a small number this is usually not a problem because $2^{w_{\text{row}}}$ is of reasonable magnitude. But for codes where w_{row} is on the order of the block length n the description complexity obviously grows exponentially in n . Interestingly, as shown in [32, Appendix II], there is a way to obtain a description of the fundamental polytope where the number of variables and the number of (in)equalities grow only polynomially and not exponentially in w_{row} . Indeed, the description complexity for that representation turns out to be on the order of $O(n|\mathcal{J}| + |\mathcal{J}|w_{\text{row}}^2 + nw_{\text{col}}w_{\text{row}})$. While this representation is obviously favorable for w_{row} 's on the order of n , it is clearly inferior for codes with small w_{row} .

Because understanding GCD and LPD is tightly related to understanding the fundamental cone, the following lemma lists some reformulations on the (in)equalities that describe the fundamental cone.

Lemma 27 *For a vector $\boldsymbol{\omega} \in \mathbb{R}^n$, $\boldsymbol{\omega} \geq \mathbf{0}$, the following conditions are equivalent*

- $\boldsymbol{\omega} \in \mathcal{K}(\mathbf{H})$.
- For each $j \in \mathcal{J}$ we have

$$\begin{aligned}
-\omega'_1 + \omega'_2 + \omega'_3 + \cdots + \omega'_{|\mathcal{I}_j|} &\geq 0, \\
+\omega'_1 - \omega'_2 + \omega'_3 + \cdots + \omega'_{|\mathcal{I}_j|} &\geq 0, \\
+\omega'_1 + \omega'_2 - \omega'_3 + \cdots + \omega'_{|\mathcal{I}_j|} &\geq 0, \\
&\vdots \\
+\omega'_1 + \omega'_2 + \omega'_3 + \cdots - \omega'_{|\mathcal{I}_j|} &\geq 0,
\end{aligned}$$

where $\boldsymbol{\omega}' \triangleq \boldsymbol{\omega}_{\mathcal{I}_j}$.

- For each $j \in \mathcal{J}$ we have $(\mathbf{1}_{|\mathcal{I}_j| \times |\mathcal{I}_j|} - 2 \cdot \mathbf{I}_{|\mathcal{I}_j| \times |\mathcal{I}_j|}) \cdot \boldsymbol{\omega}_{\mathcal{I}_j}^{\text{T}} \geq \mathbf{0}^{\text{T}}$, where $\mathbf{1}_{|\mathcal{I}_j| \times |\mathcal{I}_j|}$ is the all-ones matrix of size $|\mathcal{I}_j| \times |\mathcal{I}_j|$ and where $\mathbf{I}_{|\mathcal{I}_j| \times |\mathcal{I}_j|}$ is the identity matrix of size $|\mathcal{I}_j| \times |\mathcal{I}_j|$.
- For each $j \in \mathcal{J}$ we have for each $i' \in \mathcal{I}_j$: $\sum_{i \in \mathcal{I}_j \setminus \{i'\}} \omega_i \geq \omega_{i'}$, or, equivalently, $\sum_{i \in \mathcal{I}_j} \omega_i \geq 2\omega_{i'}$.
- For each $j \in \mathcal{J}$ we have: $\sum_{i \in \mathcal{I}_j} \omega_i \geq 2 \cdot (\max_{i \in \mathcal{I}_j} \omega_i)$, which can also be written as $\|\boldsymbol{\omega}_{\mathcal{I}_j}\|_1 \geq 2 \cdot \|\boldsymbol{\omega}_{\mathcal{I}_j}\|_{\infty}$.

Lemma 28 *Assume that the Tanner graph $\mathbb{T}(\mathbf{H})$ of a code with parity-check matrix \mathbf{H} is a forest, i.e. it has no cycles. Then $\mathcal{P}(\mathbf{H}) = \text{conv}(\mathcal{C})$, i.e. $\mathcal{P}(\mathbf{H})$ is the convex hull of all the codewords.*

Proof: See Sec. A.4. □

One of the consequences of Lemma 28 is that GCD and LPD equal MAPD/MLD for codes that are described by cycle-free Tanner graphs. Moreover, as is well-known from graphical

models, the max-product algorithm is also equal to the MAPD/MLD in the cycle-free Tanner case. Unfortunately, as was shown in [53], cycle-free Tanner graphs of binary codes, where all constraint nodes are simple parity-checks, support only weak codes.

Example 29 It is usually difficult to show a picture of the fundamental polytope because it is a polytope in \mathbb{R}^n and even small codes have usually a block length n that is larger than 3. In this example we discuss a code of length $n = 7$ where all the essential features of the fundamental polytope can be shown in a three-dimensional space because the effective dimension of the fundamental polytope is three.

The code \mathcal{C} under consideration is the $[7, 2, 3]$ binary linear code with parity-check matrix²⁵

$$\mathbf{H} = \begin{pmatrix} 1 & 1 & 0 & 0 & 0 & 0 & 0 \\ 1 & 0 & 1 & 0 & 0 & 0 & 0 \\ 0 & 1 & 1 & 1 & 0 & 0 & 0 \\ 0 & 0 & 0 & 1 & 1 & 0 & 1 \\ 0 & 0 & 0 & 0 & 1 & 1 & 0 \\ 0 & 0 & 0 & 0 & 0 & 1 & 1 \end{pmatrix},$$

whose Tanner graph $\mathsf{T}(\mathbf{H})$ is shown in Fig. 14 (left). Because all bit nodes have degree two this is a so-called cycle code. It can easily be verified that the code \mathcal{C} consists of the four codewords

$$\mathbf{x}^{(1)} = (0000000), \quad \mathbf{x}^{(2)} = (1110000), \quad \mathbf{x}^{(3)} = (0000111), \quad \mathbf{x}^{(4)} = (1110111).$$

Fig. 14 (right) shows a possible double cover. One can check that $\tilde{\mathbf{x}} = (1:0, 1:0, 1:0, 1:1, 1:0, 1:0, 1:0)$ is an (unscaled) pseudo-codeword with $\boldsymbol{\omega}^{(5)} \triangleq \boldsymbol{\omega}(\tilde{\mathbf{x}}) = (\frac{1}{2}, \frac{1}{2}, \frac{1}{2}, 1, \frac{1}{2}, \frac{1}{2}, \frac{1}{2})$. Using Lemma 26, and applying some simplifications, the fundamental polytope can be expressed as

$$\mathcal{P}(\mathbf{H}) = \left\{ \boldsymbol{\omega} \in \mathbb{R}^n \left| \begin{array}{l} 0 \leq \omega_i \leq 1 \quad \forall i \in [7] \\ \omega_1 = \omega_2 = \omega_3, \quad \omega_5 = \omega_6 = \omega_7 \\ \omega_4 \leq 2 \min(\omega_2, 1 - \omega_2, \omega_5, 1 - \omega_5) \end{array} \right. \right\}.$$

It turns out that this fundamental polytope has five vertices: the four codewords listed above and the pseudo-codeword just mentioned. Because $\omega_1 = \omega_2 = \omega_3$ and $\omega_5 = \omega_6 = \omega_7$, the effective dimension of $\mathcal{P}(\mathbf{H})$ is three and it is sufficient to focus on the three-dimensional subspace spanned by $(\omega_{123}, \omega_4, \omega_{567})$ where $\omega_{123} \triangleq \omega_1 = \omega_2 = \omega_3$ and $\omega_{567} \triangleq \omega_5 = \omega_6 = \omega_7$. Fig. 15 (right) shows the fundamental polytope in this space. For comparison purposes, Fig. 15 (left) shows the four codewords and the convex hull thereof (whose effective dimension is two).

When drawing the decision regions for MAPD/MLD and LPD it turns out to be sufficient to consider the three-dimensional space spanned by $(\lambda_{123}, \lambda_4, \lambda_{567})$ where $\lambda_{123} \triangleq \lambda_1 + \lambda_2 + \lambda_3$ and $\lambda_{567} \triangleq \lambda_5 + \lambda_6 + \lambda_7$. This follows from the fact that $(\lambda_{123}, \lambda_4, \lambda_{567})$ is a sufficient statistic for MAPD/MLD and LPD because $\sum_{i \in [7]} \omega_i \lambda_i = \omega_{123} \lambda_{123} + \omega_4 \lambda_4 + \omega_{567} \lambda_{567}$ for any $\boldsymbol{\omega} \in \mathcal{P}(\mathbf{H})$. For any λ_4 the MAPD/MLD the decision regions are shown in Fig. 16 (left). It is not surprising that the value of λ_4 has no influence on the decision since x_4 is known to be equal to zero in all codewords. For LPD the decision regions are shown Fig. 16 (left) when $\lambda_4 \geq 0$ and in Fig. 16 (right) when $\lambda_4 < 0$. Finally, for MSA and SPA decoding the decision regions are shown in Fig. 17 for $\lambda_4 = -2$. We note that in contrast to MAPD/MLD,

²⁵Some of the features of this code were also discussed in [54, 52].

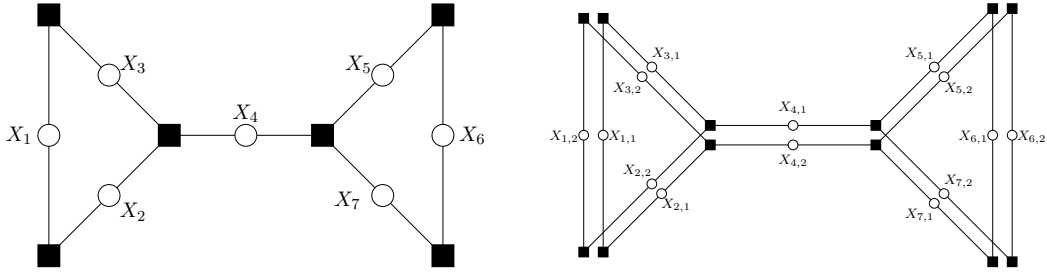


Figure 14: Left: Tanner graph $\mathbb{T}(\mathbf{H})$ for the parity-check matrix \mathbf{H} in Ex. 29. Right: a (possible) double $\tilde{\mathbb{T}}$ cover of $\mathbb{T}(\mathbf{H})$.

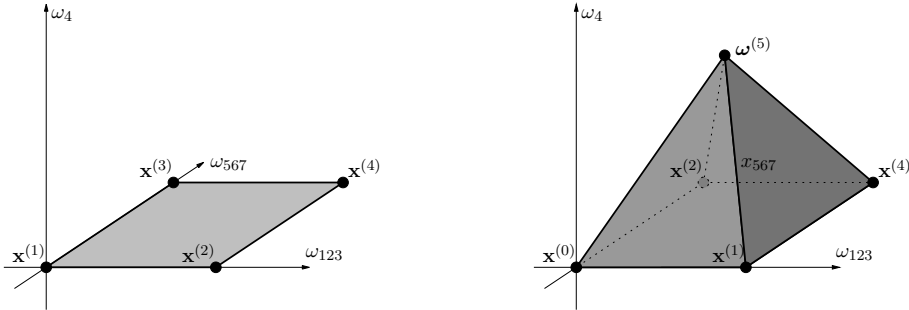


Figure 15: Left: codewords of \mathcal{C} and the polytope $\text{conv}(\mathcal{C})$ for the code in Ex. 29. Right: fundamental polytope $\mathcal{P}(\mathbf{H})$.

MSA and SPA decoding cannot exploit that x_4 equals zero for all valid codewords since *no* locally-operating, message-passing algorithm can come to this conclusion. Because \mathbf{H} is the parity-check matrix of a cycle code, MSA decoding should behave as predicted by GCD, which is indeed the case as shown in Fig. 17 (left). Fig. 17 (right) indicates that GCD gives also quite accurate predictions for SPA decoding for the present code. \square

Example 30 We consider a $(3, 5)$ -regular $[155, 62]$ binary LDPC code based on a parity-check matrix of size 93×155 for data transmission over an AWGNC. The parity-check matrix has been *randomly* generated and four-cycles have been eliminated. Moreover, the matrix has full rank and so the code has rate is exactly $2/5$.

The full space of LLR vectors is 155-dimensional. However, for obvious practical problems we can only show a two-dimensional slice through that space. Two interesting slices have been picked as follows. We first looked for a low-weight minimal pseudo-codeword in the fundamental cone: the one we selected has AWGNC pseudo-weight 13.65. Next, we laid the unit vectors λ'_1 and λ'_2 such that the pairwise decision region boundary is the hyperplane defined by $\lambda'_1 = 0$ and such that $\mathbb{E}[\mathbf{A} \mid \mathbf{X}=\mathbf{0}]$ lies in the plane spanned by λ'_1 and λ'_2 . Moreover, the unit vector λ'_3 has been chosen randomly such that it is orthogonal to λ'_1 and λ'_2 . Given this setup, two slices are shown in Figs. 18 and 19, respectively. In both cases we compare SPA decoding (with max. 100 iterations) and LPD. Both plots indicate that the decoding regions of LPD give a very good “first-order” approximation of SPA decoding.

Some final comments:

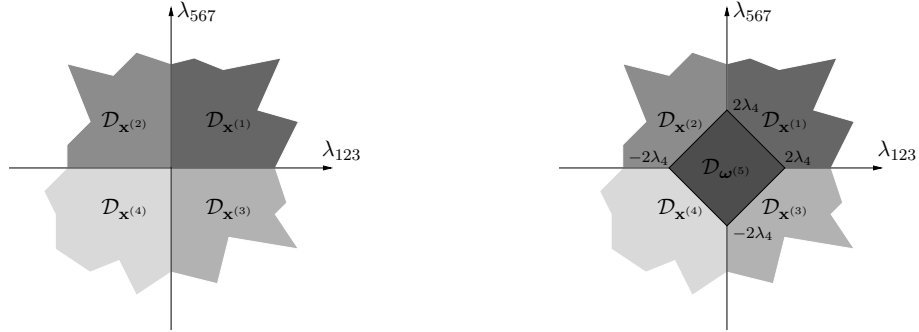


Figure 16: Decision regions for the code \mathcal{C} described by the parity-check matrix \mathbf{H} in Ex. 29. Left: Decision regions for MAPD/MLD (for any λ_4). These are also the decision regions for GCD and LPD if $\lambda_4 \geq 0$. Right: Decision regions for GCD and LPD if $\lambda_4 < 0$. (The decision region $\mathcal{D}_{\omega^{(5)}}$ is the square spanned by $(2\lambda_4, 0)$, $(0, 2\lambda_4)$, $(-2\lambda_4, 0)$, and $(0, -2\lambda_4, 0)$.)

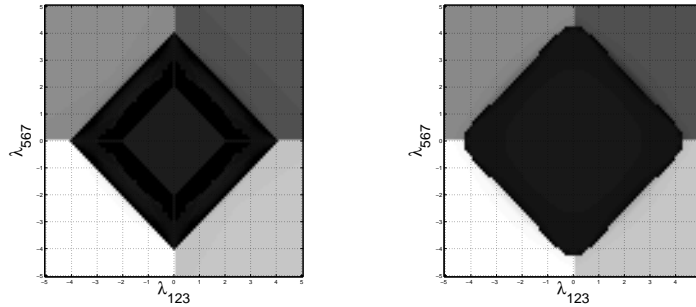


Figure 17: Decision regions under iterative decoding for $\lambda_4 = -2$ for the code \mathcal{C} described by the parity-check matrix \mathbf{H} in Ex. 29. For all simulated λ -vectors 30 iterations were performed. The shade of the gray indicates the codeword decision; within the regions the light differences in the shade of gray indicate the convergence time. Note that in the middle square corresponding to $\mathcal{D}_{\omega^{(5)}}$ the decoders did not converge to a codeword. Left: Decision regions under MSA decoding. Right: Decision regions under SPA decoding.

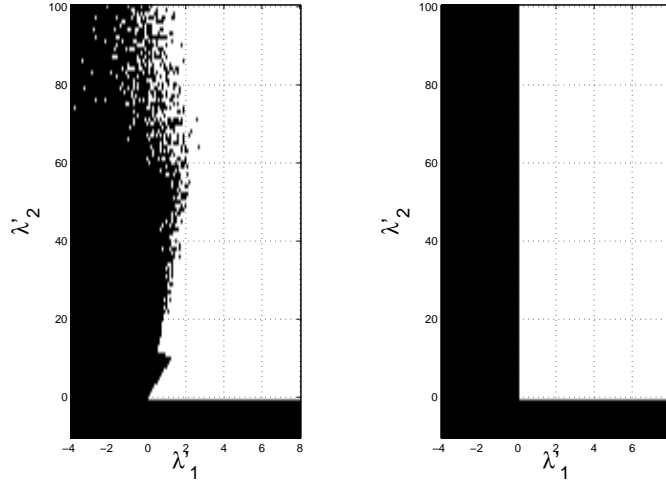


Figure 18: Decision region plots for the $[155, 62]$ binary linear LDPC code in Ex. 30. Shown is a slice in the plane spanned by λ'_1 and λ'_2 and with $\lambda'_3 = 0$. Observe that the λ'_1 -axis is stretched compared to the λ'_2 -axis. (See main text for more explanations.) Left: SPA decoding decision regions (max. 100 iterations). Right LPD decision regions (white: all-zeros codeword/black: non-zero (pseudo-)codeword).

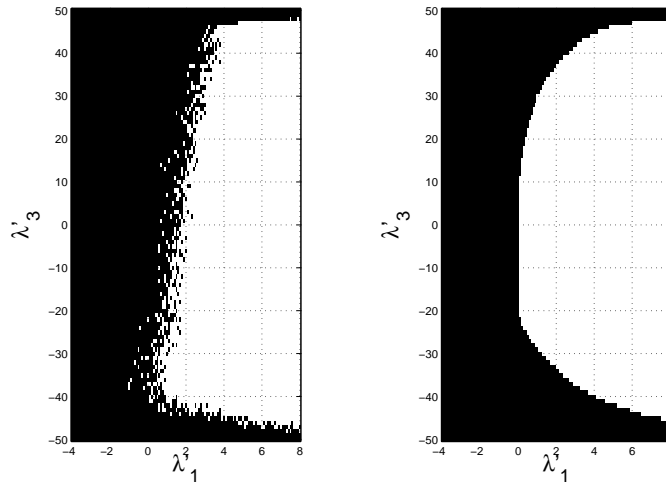


Figure 19: Decision region plots for the $[155, 62]$ binary linear LDPC code in Ex. 30. Shown is a slice with $\lambda'_2 = 50$ that is parallel to the plane spanned by λ'_1 and λ'_3 . Observe that the λ'_1 -axis is stretched compared to the λ'_3 -axis. (See main text for explanations.) Left: SPA decoding decision regions (max. 100 iterations). Right LPD decision regions (white: all-zeros codeword/black: non-zero (pseudo-)codeword).

- Using the results of Ex. 12 we see that for a signal-to-noise ratio of $E_b/N_0 = 4.197\text{dB}$ we have $E[\lambda'_1 | \mathbf{X}=\mathbf{0}] = 15.54$, $E[\lambda'_2 | \mathbf{X}=\mathbf{0}] = 50.00$, and $E[\lambda'_i | \mathbf{X}=\mathbf{0}] = 0$ for $i \in \mathcal{I} \setminus \{1, 2\}$. Moreover, $\sqrt{\text{Var}[\lambda'_i | \mathbf{X}=\mathbf{0}]} = 2.90$ for $i \in \mathcal{I}$.
- Let us briefly comment on the white triangle in Fig. 18 in the rectangle $0 \leq \lambda'_1 \lesssim 1$ and $0 \leq \lambda'_2 \lesssim 10$. It can easily be shown that for $\boldsymbol{\lambda}$ in the vicinity of the $\mathbf{0}$, the SPA decoder can only decode successfully if $\boldsymbol{\lambda} > \mathbf{0}$. The above-mentioned white triangle corresponds to the region where $\boldsymbol{\lambda} > \mathbf{0}$ and where $\|\boldsymbol{\lambda}\|_2$ is small.
- Similar plots as in Figs. 18 and 19 can be obtained under MSA decoding. Similarly to SPA decoding, the closer $\boldsymbol{\lambda}$ lies to the decision boundary, the more iterations are necessary. However, simulations show that the number of required iterations before convergence to the zero codeword increases much more in the case of MSA decoding.

□

Without going much into the details, let us mention some connections of the fundamental polytope to concepts like the marginal polytope (and relaxations thereof), Bethe free energy, and the cycle/metric polytope in matroid theory. Marginal polytope: when translated to coding theory, the marginal polytope [55] is the polytope spanned by all codewords, i.e. $\text{conv}(\mathcal{C})$; the fundamental polytope is then a relaxation of this marginal polytope. Bethe free energy: consider the set of all possible vectors $(\{b_{X_i}(x_i)\}_{i \in \mathcal{I}(\mathbf{H})}, \{b_{B_j}(b_j)\}_{j \in \mathcal{J}(\mathbf{H})})$ of beliefs on the variable and check nodes of a Tanner graph. A vector in this set yields a smaller-than-infinity Bethe free energy [56] if and only if the sub-vector containing the beliefs $(\{b_{X_i}(1)\}_{i \in \mathcal{I}(\mathbf{H})})$ corresponds to a point in the fundamental polytope. Cycle/metric polytope in matroid theory:²⁶ the cycle polytope of a binary matroid [57] is the polytope spanned by all codewords, i.e. $\text{conv}(\mathcal{C})$. The metric polytope is then a certain relaxation of this cycle polytope. In fact, this relaxation equals $\mathcal{R}_r(\mathbf{H})$ in Def. 11 for $r = |\mathcal{J}(\mathbf{H})|$ and is therefore the fundamental polytope of the parity-check matrix where all codewords of the dual code are included. Equivalently, it can also be seen as the intersection of all fundamental polytopes associated to all possible parity-check matrices for the given code.

6 Definition and Properties of Pseudo-Weights

After having seen different descriptions and properties of the fundamental polytope and cone, we turn our attention now to the question of “how bad” a certain pseudo-codeword is, i.e. we want to quantify pairwise error probabilities. Towards this end, let the pairwise error probability $P_{\mathbf{x} \rightarrow \mathbf{x}'}^{\text{MLD}}$ between two codewords \mathbf{x} and \mathbf{x}' be the probability that upon sending the codeword \mathbf{x} , MLD decides in favor of \mathbf{x}' (assuming that only \mathbf{x} and \mathbf{x}' are competing at the decoder). Similarly, we let the pairwise error probability $P_{\mathbf{x} \rightarrow \boldsymbol{\omega}}^{\text{GCD/LPD}}$ between a codeword \mathbf{x} and a pseudo-codeword $\boldsymbol{\omega}$ be the probability that upon sending the codeword \mathbf{x} , GCD/LPD decides in favor of $\boldsymbol{\omega}$ (assuming that only \mathbf{x} and $\boldsymbol{\omega}$ are competing at the decoder).

In the case of MLD of a binary code, the Hamming distance $d_{\text{H}}(\mathbf{x}, \mathbf{x}') = w_{\text{H}}(\mathbf{x}' - \mathbf{x})$ between two codewords \mathbf{x} and \mathbf{x}' is sufficient to deduce the pairwise error probability $P_{\mathbf{x} \rightarrow \mathbf{x}'}^{\text{MLD}}$

²⁶Here is a small translation table from coding theory to matroid theory language: codes are binary matroids, codewords are cycles, and cycle codes are graphic binary matroids.

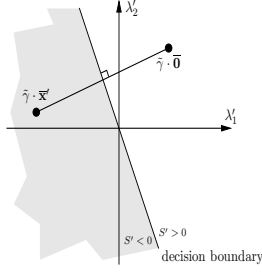


Figure 20: Decision regions under MLD when only the zero codeword is competing against the codeword \mathbf{x} . (See text for more details.)

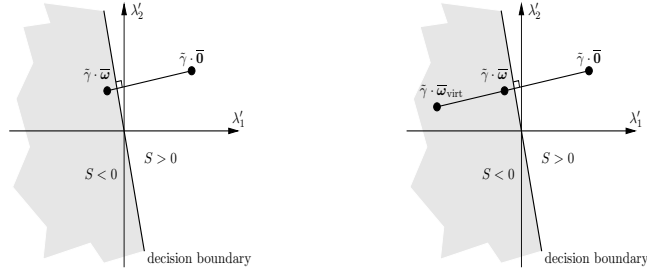


Figure 21: Left: decision regions under GCD/LPD when only the zero codeword is competing against the pseudo-codeword ω . (See text for more details.) Right: same as left part, however, in order to obtain a setup similar to the MLD case in Fig. 20 we defined $\omega_{\text{virt}} \triangleq \frac{\|\omega\|_1}{\|\omega\|_2} \cdot \omega$ such that the decision hyperplane is at the same Euclidean distance from $\tilde{\gamma} \cdot \bar{\mathbf{0}}$ and from $\tilde{\gamma} \cdot \bar{\omega}_{\text{virt}}$.

when transmitting over an AWGNC, a BSC, or a BEC. However, in the case of GCD/LPD we need different measures for characterizing the pairwise error probability $P_{\mathbf{x}' \rightarrow \omega}^{\text{GCD/LPD}}$ of a codeword \mathbf{x} and a pseudo-codeword ω . Therefore, in the following we will discuss the AWGNC, the BSC, and the BEC separately.

6.1 AWGNC Pseudo-Weight

We first consider the case of an AWGNC, where we will first study the MLD pairwise error probability and then the GCD/LPD pairwise error probability. So, let $\mathbf{x}' \neq \mathbf{0}$ be a codeword and define the random variable $S' \triangleq \langle \mathbf{x}', \mathbf{\Lambda} \rangle - \langle \mathbf{0}, \mathbf{\Lambda} \rangle = \sum_{i \in \mathcal{I}: x'_i=1} \Lambda_i$. Knowing that the Λ_i 's are statistically independent given $\mathbf{X} = \mathbf{0}$ (cf. Footnote 14) and using the results of Ex. 12, we can easily find the distribution of $\mathbf{\Lambda}$ given $\mathbf{X} = \mathbf{0}$, i.e.

$$S' |_{\mathbf{X}=\mathbf{0}} \sim \mathcal{N} \left(4R \frac{E_b}{N_0} w_H(\mathbf{x}'), 8R \frac{E_b}{N_0} w_H(\mathbf{x}') \right).$$

Because MLD decides in favor of \mathbf{x}' and against $\mathbf{0}$ when $S' \leq 0$ (cf. (19)), the pairwise error probability turns out to be²⁷

$$P_{\mathbf{0} \rightarrow \mathbf{x}'}^{\text{MLD}} = P(S' \leq 0 | \mathbf{X} = \mathbf{0}) = Q \left(\frac{4R \frac{E_b}{N_0} w_H(\mathbf{x}')}{\sqrt{8R \frac{E_b}{N_0} w_H(\mathbf{x}')}} \right) = Q \left(\sqrt{2R \frac{E_b}{N_0} w_H(\mathbf{x}')} \right), \quad (36)$$

where $Q(\theta)$ is as usual the integral from θ to ∞ of the normal distribution with mean 0 and variance 1. We see that it is sufficient to know the Hamming weight of \mathbf{x}' in order to compute the MLD pairwise error probability. (In the general case, we need only to know the Hamming distance between \mathbf{x} and \mathbf{x}' in order to compute $P_{\mathbf{x} \rightarrow \mathbf{x}'}^{\text{MLD}}$.)

Graphically, the pairwise error probability can be represented as follows. First, let $\gamma \triangleq \sqrt{E_c} = \sqrt{RE_b}$ and $\tilde{\gamma} \triangleq 4\sqrt{\frac{E_c}{N_0}} = 4\sqrt{\frac{RE_b}{N_0}}$ (note that $\gamma\tilde{\gamma} = 4\frac{E_c}{N_0} = 4R\frac{E_b}{N_0}$). Secondly, define $\bar{\mathbf{0}} \triangleq \gamma \cdot (\mathbf{1} - 2 \cdot \mathbf{0})$ and $\bar{\mathbf{x}}' \triangleq \gamma \cdot (\mathbf{1} - 2 \cdot \mathbf{x}')$ (cf. Ex. 12). Fig. 20 shows the plane of the LLR space that contains the origin, the point $\tilde{\gamma} \cdot \bar{\mathbf{0}}$, and the point $\tilde{\gamma} \cdot \bar{\mathbf{x}}'$. (The point $\tilde{\gamma} \cdot \bar{\mathbf{0}}$ corresponds to the LLR vector that is obtained at the receiver if $\mathbf{X} = \mathbf{0}$ is transmitted and no noise is added.) Rewriting S' as

$$S' \triangleq \langle \mathbf{x}', \mathbf{\Lambda} \rangle - \langle \mathbf{0}, \mathbf{\Lambda} \rangle = \langle \mathbf{x}' - \mathbf{0}, \mathbf{\Lambda} \rangle = \left\langle \bar{\mathbf{0}} - \bar{\mathbf{x}}', \frac{\mathbf{\Lambda}}{2\gamma} \right\rangle = \frac{1}{2\gamma\tilde{\gamma}} \langle \tilde{\gamma}(\bar{\mathbf{0}} - \bar{\mathbf{x}}'), \mathbf{\Lambda} \rangle \quad (37)$$

we see that S' is proportional to the projection of $\mathbf{\Lambda}$ onto the vector connecting $\tilde{\gamma} \cdot \bar{\mathbf{x}}'$ to $\tilde{\gamma} \cdot \bar{\mathbf{0}}$, that $S' = 0$ on the line labeled “decision boundary”, and that $S' < 0$ in the shaded area. It can easily be verified that the squared Euclidean distance from $\tilde{\gamma} \cdot \bar{\mathbf{0}}$ to the decision boundary is $\tilde{\gamma}^2 \cdot w_H(\mathbf{x}')$. (The second-to-last inner product in (37) can be seen as doing the projection in signal space, i.e. $\mathbf{\Lambda}/(2\gamma)$ is projected onto the vector connecting the signal space point $\bar{\mathbf{x}}'$ to the signal space point $\bar{\mathbf{0}}$.)

In general, MLD results in a decision hyperplane that consists of all points that are equally far away from the two competing codewords and so the this hyperplane does not need to go through the origin. However, when using binary codes and BPSK signaling all signals have the same energy and so the decision hyperplane goes through the origin as in Fig. 20.

Now we want to compute the pairwise error probability in the case of GCD/LPD. Let $\boldsymbol{\omega} \in \mathcal{P}(\mathbf{H})$ be a pseudo-codeword and define $S \triangleq \langle \boldsymbol{\omega}, \mathbf{\Lambda} \rangle - \langle \mathbf{0}, \mathbf{\Lambda} \rangle = \sum_{i \in \mathcal{I}} \omega_i \Lambda_i$. Again, because of the statistical independence of the Λ_i 's given $\mathbf{X} = \mathbf{0}$ we find that

$$S |_{\mathbf{X}=\mathbf{0}} \sim \mathcal{N} \left(4R \frac{E_b}{N_0} \sum_{i \in \mathcal{I}} \omega_i, 8R \frac{E_b}{N_0} \sum_{i \in \mathcal{I}} \omega_i^2 \right).$$

Because GCD/LPD decides in favor of $\boldsymbol{\omega}$ and against $\mathbf{0}$ when $S \leq 0$ (cf. (20)), the pairwise error probability turns out to be²⁸

$$P_{\mathbf{0} \rightarrow \boldsymbol{\omega}}^{\text{GCD/LPD}} = P(S \leq 0 | \mathbf{X} = \mathbf{0}) = Q \left(\frac{4R \frac{E_b}{N_0} \sum_{i \in \mathcal{I}} \omega_i}{\sqrt{8R \frac{E_b}{N_0} \sum_{i \in \mathcal{I}} \omega_i^2}} \right) = Q \left(\sqrt{2R \frac{E_b}{N_0} \frac{(\sum_{i \in \mathcal{I}} \omega_i)^2}{\sum_{i \in \mathcal{I}} \omega_i^2}} \right) \quad (38)$$

It was the idea of Wiberg [12] to define a generalization of the Hamming weight such that (38) looks formally like (36).

²⁷The case $S' = 0$ results in a tie. Depending on how ties are resolved, MLD might actually decide in favor of $\mathbf{0}$. However, $P(S' = 0 | \mathbf{X} = \mathbf{0}) = 0$.

²⁸A comment similar to Footnote 27 applies here.

Definition 31 ([12, 30]) Let $\boldsymbol{\omega} \in \mathbb{R}_+^n$. The AWGNC pseudo-weight $w_p^{\text{AWGNC}}(\boldsymbol{\omega})$ of $\boldsymbol{\omega}$ is given by

$$w_p^{\text{AWGNC}}(\boldsymbol{\omega}) \triangleq \frac{\|\boldsymbol{\omega}\|_1^2}{\|\boldsymbol{\omega}\|_2^2} = \frac{\left(\sum_{i \in [n]} \omega_i\right)^2}{\sum_{i \in [n]} \omega_i^2}, \quad (39)$$

where we define $w_p^{\text{AWGNC}}(\boldsymbol{\omega}) \triangleq 0$ if $\boldsymbol{\omega} = \mathbf{0}$. Wiberg [12, Ch. 6] called this quantity the “generalized weight”, whereas Forney et al. [30] called it the “effective weight”. (Note that in contrast to the Hamming weight, the AWGNC pseudo-weight is not a norm.) \square

With this, Eq. (38) can be written as

$$P_{\mathbf{0} \rightarrow \boldsymbol{\omega}}^{\text{GCD/LPD}} = Q \left(\sqrt{2R \frac{E_b}{N_0} w_p^{\text{AWGNC}}(\boldsymbol{\omega})} \right)$$

which indeed looks formally like (36). With suitable definitions, the general case $P_{\mathbf{x} \rightarrow \boldsymbol{\omega}}^{\text{GCD/LPD}}$ can also be formulated by using a generalization of Hamming distance. However, in contrast to the Hamming distance, the resulting generalization of the Hamming distance will not be a distance in the mathematical sense.

Similar to the MLD case we can also give a graphical interpretation of the decision regions in the GCD/LPD case. Fig. 21 shows the plane through the origin, the point $\tilde{\gamma} \cdot \bar{\mathbf{0}}$, and the point $\tilde{\gamma} \cdot \bar{\mathbf{x}}$. Rewriting S as

$$S \triangleq \langle \boldsymbol{\omega}, \boldsymbol{\Lambda} \rangle - \langle \mathbf{0}, \boldsymbol{\Lambda} \rangle = \langle \boldsymbol{\omega} - \mathbf{0}, \boldsymbol{\Lambda} \rangle = \left\langle \bar{\mathbf{0}} - \bar{\boldsymbol{\omega}}, \frac{\boldsymbol{\Lambda}}{2\gamma} \right\rangle = \frac{1}{2\gamma\tilde{\gamma}} \langle \tilde{\gamma}(\bar{\mathbf{0}} - \bar{\boldsymbol{\omega}}), \boldsymbol{\Lambda} \rangle \quad (40)$$

we see that S is proportional to the projection of $\boldsymbol{\Lambda}$ onto the vector connecting $\tilde{\gamma} \cdot \bar{\boldsymbol{\omega}}$ to $\tilde{\gamma} \cdot \bar{\mathbf{0}}$, that $S = 0$ on the line labeled “decision boundary”, and that $S < 0$ in the shaded area. (The second-to-last inner product in (40) can be seen as doing the projection in signal space, i.e. $\boldsymbol{\Lambda}/(2\gamma)$ is projected onto the vector connecting the signal space point $\bar{\mathbf{x}}$ to the signal space point $\bar{\mathbf{0}}$.) In contrast to MLD, the two points $\tilde{\gamma} \cdot \bar{\mathbf{0}}$ and $\tilde{\gamma} \cdot \bar{\boldsymbol{\omega}}$ do not have the same distance from the decision boundary in general; in fact, it can even happen that the two points lie on the same side of the decision boundary. Finally, note that the squared Euclidean distance of $\tilde{\gamma} \cdot \bar{\mathbf{0}}$ to the decision boundary is now given by $\tilde{\gamma}^2 \cdot w_p^{\text{AWGNC}}(\boldsymbol{\omega})$, which looks formally like the formula that we obtained in the case of MLD.

It is clear that these geometrical observations can be connected to the discussion on linear programming at the end of Sec. 3; the details of this connection are left to the reader as an exercise.

6.2 BSC Pseudo-Weight

We first discuss MLD. Defining S' as in Sec. 6.1 for a codeword $\mathbf{x}' \neq \mathbf{0}$, we see that a necessary condition for $S'|_{\mathbf{x}=\mathbf{0}}$ to be non-positive is that the number of bit flips on the channel is at least $\frac{1}{2}w_H(\mathbf{x}')$. The BSC pseudo-weight is defined such that we can formally make the same statement for GCD/LPD.

Definition 32 ([30]) Let $\boldsymbol{\omega} \in \mathbb{R}_+^n$. Let $\boldsymbol{\omega}'$ be a vector of length n with the same components as $\boldsymbol{\omega}$ but in non-increasing order. Introducing

$$\begin{aligned} f(\xi) &\triangleq \omega'_i \quad (i-1 < \xi \leq i, \quad 0 < \xi \leq n), \\ F(\xi) &\triangleq \int_0^\xi f(\xi') \, d\xi', \\ e &\triangleq F^{-1}\left(\frac{F(n)}{2}\right), \end{aligned}$$

the BSC pseudo-weight $w_p^{\text{BSC}}(\boldsymbol{\omega})$ is defined to be $w_p^{\text{BSC}}(\boldsymbol{\omega}) \triangleq 2e$.²⁹ \square

With this definition and S defined as in Sec. 6.1 we see that a necessary condition for $S|_{\mathbf{x}=\mathbf{0}}$ to be non-positive is that the number of bit flips on the channels is at least $w_p^{\text{BSC}}(\boldsymbol{\omega})/2$. Note however that the BSC pairwise error probability formulas for GCD/LPD are not simply obtained from the BSC pairwise error probability formulas for MLD by replacing the Hamming weight by the BSC pseudo-weight. Namely, whereas in the case of MLD it only matters how many channel bit flips correspond to positions in $\text{supp}(\mathbf{x}')$, in the case of GCD/LPD it not only matters how many channel bit flips correspond to positions in $\text{supp}(\boldsymbol{\omega})$ but also at which position these bit flips are.

Another way to generalize the Hamming weight in the case of the BSC is given by the fractional and max-fractional weight.

Definition 33 ([31]) The fractional and max-fractional weight of a vector $\boldsymbol{\omega} \in \mathbb{R}_+^n$ are defined to be, respectively,

$$w_{\text{frac}}(\boldsymbol{\omega}) = \|\boldsymbol{\omega}\|_1. \quad (41)$$

$$w_{\text{max-frac}}(\boldsymbol{\omega}) \triangleq \frac{w_{\text{frac}}(\boldsymbol{\omega})}{\|\boldsymbol{\omega}\|_\infty} = \frac{\|\boldsymbol{\omega}\|_1}{\|\boldsymbol{\omega}\|_\infty}. \quad (42)$$

For $\boldsymbol{\omega} = \mathbf{0}$ we define $w_{\text{max-frac}}(\boldsymbol{\omega}) \triangleq 0$. We actually use a slightly different notation than [31]. Here, w_{frac} and $w_{\text{max-frac}}$ are defined for any vector in \mathbb{R}_+^n , whereas in [31], w_{frac} and $w_{\text{max-frac}}$ already denote the minimum of these values over all nonzero vertices of the fundamental polytope. \square

Fix some non-zero vector $\boldsymbol{\omega} \in [0, 1]^n$. Using the above definition, it can be seen that a necessary condition for $S|_{\mathbf{x}=\mathbf{0}}$ to be non-positive is that the number of bit flips on the channel is at least $\frac{1}{2}w_{\text{frac}}(\boldsymbol{\omega})$. Similarly, fix some non-zero vector $\boldsymbol{\omega} \in \mathbb{R}_+^n$. Then, a necessary condition for $S|_{\mathbf{x}=\mathbf{0}}$ to be non-positive is that the number of bit flips on the channel is at least $\frac{1}{2}w_{\text{max-frac}}(\boldsymbol{\omega})$. (The details of these two statements can be found in Sec. A.5.)

6.3 BEC Pseudo-Weight

We first discuss the MLD. Defining S' as in Sec. 6.1 for a codeword $\mathbf{x}' \neq \mathbf{0}$, we see that a necessary condition for $S'|_{\mathbf{x}=\mathbf{0}}$ to be non-positive³⁰ is that the number of erasures on the channel is at least $w_H(\mathbf{x}')$. The BEC pseudo-weight is defined such that we can formally make the same statement for GCD/LPD.

²⁹Note that the quantity e is obviously related to the median of the ‘‘pdf’’ given by $f(\xi)/F(n)$. However, let us remark that this is a different ‘‘distribution’’ than used later on in Lemma 39 when characterizing the AWGNC pseudo-weight.

³⁰Because of special properties of the BEC, S can never be negative.

Definition 34 ([30]) *Let $\boldsymbol{\omega} \in \mathbb{R}_+^n$. The BEC pseudo-weight $w_p^{\text{BEC}}(\boldsymbol{\omega})$ is defined to be*

$$w_p^{\text{BEC}}(\boldsymbol{\omega}) = |\text{supp}(\boldsymbol{\omega})|.$$

□

With this definition and S defined as in Sec. 6.1 we see that a necessary condition for $S|_{\mathbf{x}=\mathbf{0}}$ to be non-positive is that the number of bit flips on the channels is at least $w_p^{\text{BEC}}(\boldsymbol{\omega})$. In contrast to the BSC, the BEC pairwise error probability formulas for GCD/LPD are simply obtained from the BEC pairwise error probability formulas for MLD by replacing the Hamming weight by the BEC pseudo-weight. (Note that the exact formulas depend on how ties are resolved.)

6.4 Pseudo-Weight Properties

This section collects different lemmas that characterize the different pseudo-weights and the fractional and max-fractional weights.

Lemma 35 *The AWGNC, BSC, and BEC pseudo-weights and the max-fractional weight are invariant under scaling by a positive scalar, i.e.*

$$\begin{aligned} w_p^{\text{AWGNC}}(\alpha \cdot \boldsymbol{\omega}) &= w_p^{\text{AWGNC}}(\boldsymbol{\omega}), \\ w_p^{\text{BSC}}(\alpha \cdot \boldsymbol{\omega}) &= w_p^{\text{BSC}}(\boldsymbol{\omega}), \\ w_p^{\text{BEC}}(\alpha \cdot \boldsymbol{\omega}) &= w_p^{\text{BEC}}(\boldsymbol{\omega}), \\ w_{\text{max-frac}}(\alpha \cdot \boldsymbol{\omega}) &= w_{\text{max-frac}}(\boldsymbol{\omega}), \end{aligned}$$

for any $\alpha \in \mathbb{R}_{++}$ and any $\boldsymbol{\omega} \in \mathbb{R}_+^n$. Note that the fractional weight is not scaling-invariant.

Proof: Follows easily from the definitions. □

Lemma 36 *If $\boldsymbol{\omega} \in \{0, 1\}^n$ then the AWGNC, the BSC, and the BEC pseudo-weights and the fractional and max-fractional weight reduce to the Hamming weight, i.e. $w_p^{\text{AWGNC}}(\boldsymbol{\omega}) = w_H(\boldsymbol{\omega})$, etc.*

Proof: This is straightforward. E.g. in the case of an AWGNC the result follows from observing that $\|\boldsymbol{\omega}\|_1 = w_H(\boldsymbol{\omega})$ and that $\|\boldsymbol{\omega}\|_2 = \sqrt{w_H(\boldsymbol{\omega})}$ which implies that $w_p^{\text{AWGNC}}(\boldsymbol{\omega}) = \|\boldsymbol{\omega}\|_1^2 / \|\boldsymbol{\omega}\|_2^2 = w_H(\boldsymbol{\omega})^2 / w_H(\boldsymbol{\omega}) = w_H(\boldsymbol{\omega})$. □

The following definitions generalize the notion of the minimum Hamming weight of a binary linear code.

Definition 37 *The minimum AWGNC, BSC, and BEC pseudo-weight and the minimum*

fractional and max-fractional weights are defined to be, respectively,

$$\begin{aligned}
w_p^{\text{AWGNC},\min}(\mathbf{H}) &\triangleq \min_{\boldsymbol{\omega} \in \mathcal{V}(\mathcal{P}(\mathbf{H})) \setminus \{0\}} w_p^{\text{AWGNC}}(\boldsymbol{\omega}), \\
w_p^{\text{BSC},\min}(\mathbf{H}) &\triangleq \min_{\boldsymbol{\omega} \in \mathcal{V}(\mathcal{P}(\mathbf{H})) \setminus \{0\}} w_p^{\text{BSC}}(\boldsymbol{\omega}), \\
w_p^{\text{BEC},\min}(\mathbf{H}) &\triangleq \min_{\boldsymbol{\omega} \in \mathcal{V}(\mathcal{P}(\mathbf{H})) \setminus \{0\}} w_p^{\text{BEC}}(\boldsymbol{\omega}), \\
w_{\text{frac}}^{\min}(\mathbf{H}) &\triangleq \min_{\boldsymbol{\omega} \in \mathcal{V}(\mathcal{P}(\mathbf{H})) \setminus \{0\}} w_{\text{frac}}(\boldsymbol{\omega}), \\
w_{\text{max-frac}}^{\min}(\mathbf{H}) &\triangleq \min_{\boldsymbol{\omega} \in \mathcal{V}(\mathcal{P}(\mathbf{H})) \setminus \{0\}} w_{\text{max-frac}}(\boldsymbol{\omega}),
\end{aligned}$$

where $\mathcal{V}(\mathcal{P}(\mathbf{H})) \setminus \{0\}$ is the set of all non-zero vertices of the fundamental polytope $\mathcal{P}(\mathbf{H})$. \square

It is important to note that the above minimal weights depend on the choice of parity-check matrix \mathbf{H} , i.e. different parity-check matrices for the same code can lead to different minimal weights. This is in contrast to the minimal Hamming weight of a code which is independent of the specific choice of parity-check matrix by which a binary linear code is represented.

Lemma 38

$$\begin{aligned}
w_p^{\text{AWGNC},\min}(\mathbf{H}) &= \min_{\boldsymbol{\omega} \in \mathcal{P}(\mathbf{H}) \setminus \{0\}} w_p^{\text{AWGNC}}(\boldsymbol{\omega}) = \min_{\boldsymbol{\omega} \in \mathcal{K}(\mathbf{H}) \setminus \{0\}} w_p^{\text{AWGNC}}(\boldsymbol{\omega}), \\
w_p^{\text{BSC},\min}(\mathbf{H}) &= \min_{\boldsymbol{\omega} \in \mathcal{P}(\mathbf{H}) \setminus \{0\}} w_p^{\text{BSC}}(\boldsymbol{\omega}) = \min_{\boldsymbol{\omega} \in \mathcal{K}(\mathbf{H}) \setminus \{0\}} w_p^{\text{BSC}}(\boldsymbol{\omega}), \\
w_p^{\text{BEC},\min}(\mathbf{H}) &= \min_{\boldsymbol{\omega} \in \mathcal{P}(\mathbf{H}) \setminus \{0\}} w_p^{\text{BEC}}(\boldsymbol{\omega}) = \min_{\boldsymbol{\omega} \in \mathcal{K}(\mathbf{H}) \setminus \{0\}} w_p^{\text{BEC}}(\boldsymbol{\omega}), \\
w_{\text{max-frac}}^{\min}(\mathbf{H}) &= \min_{\boldsymbol{\omega} \in \mathcal{P}(\mathbf{H}) \setminus \{0\}} w_{\text{max-frac}}(\boldsymbol{\omega}) = \min_{\boldsymbol{\omega} \in \mathcal{K}(\mathbf{H}) \setminus \{0\}} w_{\text{max-frac}}(\boldsymbol{\omega}).
\end{aligned}$$

Note that there is no such statement for the fractional weight.

Proof: These are simple consequences of the fact that the AWGNC, BSC, and BEC pseudo-weights and the max-fractional weight are scaling-invariant, that Lemma 41 holds, and that $\mathcal{K}(\mathbf{H}) \setminus \{0\} = \text{conic}(\mathcal{P}(\mathbf{H})) \setminus \{0\}$. \square

In the following, our standard channel will be the AWGNC. Therefore, when nothing else is specified, pseudo-weight will mean AWGNC pseudo-weight and we will write $w_p(\boldsymbol{\omega})$ and $w_p^{\min}(\mathbf{H})$ instead of $w_p^{\text{AWGNC}}(\boldsymbol{\omega})$ and $w_p^{\text{AWGNC},\min}(\mathbf{H})$, respectively.

Lemma 39 Let $\boldsymbol{\omega} \in \mathbb{R}_+^n$ and let $\mathcal{S} \triangleq \text{supp}(\boldsymbol{\omega})$ be its support. Consider the non-zero entries of $\boldsymbol{\omega}$ to be $|\mathcal{S}|$ samples of a positive random variable Ω . Introducing the empirical first moment (mean) $\hat{\mathbb{E}}[\Omega] = (1/|\mathcal{S}|) \sum_{i \in \mathcal{S}} \omega_i = (1/|\mathcal{S}|) \|\boldsymbol{\omega}\|_1$, the empirical second moment $\hat{\mathbb{E}}[\Omega^2] = (1/|\mathcal{S}|) \sum_{i \in \mathcal{S}} \omega_i^2 = (1/|\mathcal{S}|) \|\boldsymbol{\omega}\|_2^2$, and the empirical variance $\widehat{\text{Var}}[\Omega] = \hat{\mathbb{E}}[\Omega^2] - (\hat{\mathbb{E}}[\Omega])^2$, we can rewrite the AWGNC pseudo-weight as

$$w_p(\boldsymbol{\omega}) = |\mathcal{S}| \cdot \frac{(\hat{\mathbb{E}}[\Omega])^2}{\hat{\mathbb{E}}[\Omega^2]}. \tag{43}$$

In the case that $\boldsymbol{\omega}$ is scaled such that $\hat{\mathbb{E}}[\Omega] = 1$ (i.e. $\|\boldsymbol{\omega}\|_1 = |\mathcal{S}|$), we can write

$$w_p(\boldsymbol{\omega}) = |\mathcal{S}| \cdot \frac{1}{\widehat{\text{Var}}[\Omega] + 1}. \quad (44)$$

Therefore, the more the non-zero components of $\boldsymbol{\omega}$ are apart, the smaller is the AWGNC pseudo-weight.

Proof: See Sec. A.6. □

Lemma 40 Let $\boldsymbol{\omega} \in \mathbb{R}_+^n$ and let $\angle(\boldsymbol{\omega}, \mathbf{1})$ be the angle between the vectors $\boldsymbol{\omega}$ and $\mathbf{1}$. Interestingly, $w_p(\boldsymbol{\omega})$ is only a function of n and the angle $\angle(\boldsymbol{\omega}, \mathbf{1})$:

$$w_p(\boldsymbol{\omega}) = n \cdot \cos(\angle(\boldsymbol{\omega}, \mathbf{1}))^2 \quad (45)$$

We see that the larger the angle $\angle(\boldsymbol{\omega}, \mathbf{1})$ becomes, the smaller is $w_p(\boldsymbol{\omega})$. Alternatively, if we let $\mathbf{1}_\omega$ be the indicator vector of $\boldsymbol{\omega}$, i.e. the i -th position is 1 if ω_i is non-zero and it is 0 otherwise, then

$$w_p(\boldsymbol{\omega}) = |\text{supp}(\boldsymbol{\omega})| \cdot \cos(\angle(\boldsymbol{\omega}, \mathbf{1}_\omega))^2 \quad (46)$$

Proof: See Sec. A.7. □

Lemma 41 For any positive integer L , let $\{\boldsymbol{\omega}^{(\ell)}\}_{\ell \in [L]}$ be a set of vectors where $\boldsymbol{\omega}^{(\ell)} \in \mathbb{R}_+^n$, $\ell \in [L]$. Then,

$$\begin{aligned} w_p^{\text{AWGNC}} \left(\sum_{\ell \in [L]} \alpha_\ell \boldsymbol{\omega}^{(\ell)} \right) &\geq \min_{\ell \in [L]} w_p^{\text{AWGNC}}(\boldsymbol{\omega}^{(\ell)}) \\ w_p^{\text{BSC}} \left(\sum_{\ell \in [L]} \alpha_\ell \boldsymbol{\omega}^{(\ell)} \right) &\geq \min_{\ell \in [L]} w_p^{\text{BSC}}(\boldsymbol{\omega}^{(\ell)}), \\ w_p^{\text{BEC}} \left(\sum_{\ell \in [L]} \alpha_\ell \boldsymbol{\omega}^{(\ell)} \right) &\geq \min_{\ell \in [L]} w_p^{\text{BEC}}(\boldsymbol{\omega}^{(\ell)}), \\ w_{\text{max-frac}} \left(\sum_{\ell \in [L]} \alpha_\ell \boldsymbol{\omega}^{(\ell)} \right) &\geq \min_{\ell \in [L]} w_{\text{max-frac}}(\boldsymbol{\omega}^{(\ell)}), \end{aligned}$$

for any $\alpha_\ell \geq 0$, $\ell \in [L]$ where not all α_i are zero. This means that the AWGNC pseudo-weight of any conic combination of an arbitrary set of vectors in \mathbb{R}_+^n is at least as large as the smallest AWGNC pseudo-weight of any of these vectors. This property is intuitively clear from the geometrical meaning of the AWGNC pseudo-weight. (Similar statements can be made for the BSC and BEC pseudo-weight and for the max-fractional weight.)

Proof: See Sec. A.8. □

Lemma 42 For any positive integer L , let $\{\boldsymbol{\omega}^{(\ell)}\}_{\ell \in [L]}$ be a set of vectors where $\boldsymbol{\omega}^{(\ell)} \in \mathbb{R}_+^n$, $\ell \in [L]$. If $\|\boldsymbol{\omega}^{(\ell)}\|_1 = 1$ for all $\ell \in [L]$ then

$$\frac{1}{\sqrt{w_p\left(\sum_{\ell \in [L]} \alpha_\ell \boldsymbol{\omega}^{(\ell)}\right)}} \leq \sum_{\ell \in [L]} \frac{\alpha_\ell}{\sqrt{w_p(\boldsymbol{\omega}^{(\ell)})}} \quad (47)$$

for any $\alpha_\ell \geq 0$, $\ell \in [L]$, such that $\sum_{\ell \in [L]} \alpha_\ell = 1$.

Proof: See Sec. A.9. □

Lemma 43 Let $\boldsymbol{\omega} \in \mathbb{R}_+^n$. Then

$$\frac{\partial}{\partial \omega_i} w_p(\boldsymbol{\omega}) \begin{cases} > 0 & \text{if } \omega_i < \|\boldsymbol{\omega}\|_1 / w_p(\boldsymbol{\omega}) \\ = 0 & \text{if } \omega_i = \|\boldsymbol{\omega}\|_1 / w_p(\boldsymbol{\omega}) \\ < 0 & \text{if } \omega_i > \|\boldsymbol{\omega}\|_1 / w_p(\boldsymbol{\omega}) \end{cases}.$$

Proof: See Sec. A.10. □

Roughly speaking, the above lemma means that if we are given a vector $\boldsymbol{\omega} \in \mathbb{R}_+^n$ and want to decrease its AWGNC pseudo-weight then we must either decrease the small components or increase the large components. In both cases the empirical variance increases which is in agreement with the observations in Lemma 39.

Lemma 44 Let $\boldsymbol{\omega} \in \mathbb{R}_+^n$ with $\mathbf{0} \leq \boldsymbol{\omega} \leq \mathbf{1}$. Remember that $w_p(\boldsymbol{\omega}) = w_p^{\text{AWGNC}}(\boldsymbol{\omega})$ by definition. Then

$$w_{\text{frac}}(\boldsymbol{\omega}) \leq w_{\text{max-frac}}(\boldsymbol{\omega}) \leq w_p(\boldsymbol{\omega}) \leq w_p^{\text{BEC}}(\boldsymbol{\omega}), \quad (48)$$

$$w_{\text{frac}}(\boldsymbol{\omega}) \leq w_{\text{max-frac}}(\boldsymbol{\omega}) \leq w_p^{\text{BSC}}(\boldsymbol{\omega}) \leq w_p^{\text{BEC}}(\boldsymbol{\omega}), \quad (49)$$

and

$$w_{\text{frac}}^{\min}(\mathbf{H}) \leq w_{\text{max-frac}}^{\min}(\mathbf{H}) \leq w_p^{\min}(\mathbf{H}) \leq w_p^{\text{BEC}, \min}(\mathbf{H}), \quad (50)$$

$$w_{\text{frac}}^{\min}(\mathbf{H}) \leq w_{\text{max-frac}}^{\min}(\mathbf{H}) \leq w_p^{\text{BSC}, \min}(\mathbf{H}) \leq w_p^{\text{BEC}, \min}(\mathbf{H}), \quad (51)$$

Proof: See Sec. A.11. □

Note that there is no hierarchy between $w_p(\boldsymbol{\omega})$ and $w_p^{\text{BSC}}(\boldsymbol{\omega})$, i.e. one can find $\boldsymbol{\omega}$'s such that either one is larger. Consider for example $\boldsymbol{\omega} = (1, 1, \frac{1}{2}, \frac{1}{2}, \frac{1}{2}, \frac{1}{2})$ for which the AWGNC pseudo-weight is larger: $w_p(\boldsymbol{\omega}) = \frac{4^2}{3} = \frac{16}{3} = 5.333 > w_p^{\text{BSC}}(\boldsymbol{\omega}) = 2 \cdot 2 = 4$. However, the vector $\boldsymbol{\omega} = (1, \frac{1}{4}, \dots, \frac{1}{4})$ of length 65 is an example where the BSC pseudo-weight is larger: $w_p(\boldsymbol{\omega}) = \frac{17^2}{5} = 57.8 < w_p^{\text{BSC}}(\boldsymbol{\omega}) = 2 \cdot 31 = 62$.

Asymptotically, i.e. for $n \rightarrow \infty$, the AWGNC and BSC pseudo-weight can vary drastically in the following sense. In Prop. 49 we will show that $w_p(\cdot)$ always grows sub-linearly for an ensemble of $(w_{\text{col}}, w_{\text{row}})$ -regular LDPC codes where $3 \leq w_{\text{col}} < w_{\text{row}}$. However, for properly chosen families of $(w_{\text{col}}, w_{\text{row}})$ -regular LDPC codes one can guarantee a linear behavior of $w_p^{\text{BSC}}(\cdot)$ as $n \rightarrow \infty$ [58]. Some of the reasons and implications of this fact are also discussed in [59].

The above considerations have also implications for the fractional and max-fractional weight (see Def. 33) that was introduced in [31] to analyze the decoding behavior when transmitting over a BSC. Using Lemma 44 we see that when considering the limit $n \rightarrow \infty$ the fractional and the max-fractional weight can grow at best like the AWGNC pseudo-weight. However, the comments in the previous paragraph show that the AWGNC and BSC pseudo-weight can behave quite differently for $n \rightarrow \infty$, therefore the fractional/max-fractional weight and the BSC pseudo-weight can also behave quite differently for $n \rightarrow \infty$. Note though that from an analysis point of view, the fractional weight might sometimes be a more manageable quantity since it is a linear function of the argument whereas the BSC pseudo-weight is more complicated function. Indeed, [31, Sec. 4.4.3] shows an efficient procedure for computing the minimal fractional weight of a code with given parity-check matrix.

7 A Simple Upper Bound on the Minimum AWGNC Pseudo-Weight

In this section we investigate the asymptotic behavior of the minimum pseudo-weight of families of $(w_{\text{col}}, w_{\text{row}})$ -regular LDPC codes, i.e. codes whose parity-check matrices have a fixed column and row weight.³¹ Our main result will be that the relative³² minimum AWGNC pseudo-weight of any $(w_{\text{col}}, w_{\text{row}})$ -regular code, $3 \leq w_{\text{col}} < w_{\text{row}}$, approaches zero as $n \rightarrow \infty$, a behavior which is in sharp contrast to the observation made by Gallager [2] that the relative minimum Hamming weight of a randomly generated $(w_{\text{col}}, w_{\text{row}})$ -regular LDPC code, $3 \leq w_{\text{col}} < w_{\text{row}}$, is lower bounded by a nonzero number with probability one for $n \rightarrow \infty$.

In the following, we associate the Tanner graph $\mathsf{T} \triangleq \mathsf{T}(\mathbf{H})$ to the parity-check matrix \mathbf{H} and denote its girth and diameter by $g(\mathsf{T})$ and $\delta(\mathsf{T})$, respectively.

Definition 45 *Let T be a Tanner graph of an arbitrary code (not necessarily $(w_{\text{col}}, w_{\text{row}})$ -regular). We let an arbitrary variable node V of T to be the root. We classify the remaining variable and check nodes according to their (graph) distance from the root, i.e. all nodes at distance 1 from the root will be called nodes of tier 1, all nodes at distance 2 from the root node will be called nodes of tier 2, etc. We call this ordering “breadth-first spanning-tree ordering with root V .” Because of the bipartite-ness of T , it follows easily that the nodes of the even tiers are variable nodes whereas the nodes of the odd tiers are check nodes. Furthermore, a check node at tier $2t + 1$ can only be connected to variable nodes in tier $2t$ and possibly to variable nodes in tier $2t + 2$. Note that the last tier is tier $\delta(\mathsf{T})$ and that the symbol nodes are at tiers $0, 2, \dots, 2\lfloor \delta(\mathsf{T})/2 \rfloor$. \square*

Let us upper bound the number of nodes for each tier when we perform breadth-first spanning-tree ordering according to Def. 45 with respect to an arbitrary node V of the Tanner graph T of an arbitrary $(w_{\text{col}}, w_{\text{row}})$ -regular LDPC code. Let $N_{V,t}(\mathsf{T})$ be the number of nodes at tier t and let $N_{V,t}^{\max} \triangleq N_{V,t,w_{\text{col}},w_{\text{row}}}^{\max}$ be the maximal number of nodes possible at tier t for any $(w_{\text{col}}, w_{\text{row}})$ -regular LDPC code. It is not difficult to see that $N_{V,0}^{\max} = 1$, $N_{V,1}^{\max} = w_{\text{col}}$, $N_{V,2}^{\max} = w_{\text{col}}(w_{\text{row}} - 1)$, $N_{V,3}^{\max} = w_{\text{col}}(w_{\text{row}} - 1)(w_{\text{col}} - 1)$, $N_{V,4}^{\max} = w_{\text{col}}(w_{\text{row}} - 1)(w_{\text{col}} - 1)(w_{\text{row}} - 1)$. In general, $N_{V,2t}^{\max} = w_{\text{col}}(w_{\text{col}} - 1)^{t-1}(w_{\text{row}} - 1)^t$ for $t > 0$ and $N_{V,2t+1}^{\max} = w_{\text{col}}(w_{\text{col}} - 1)^t(w_{\text{row}} - 1)^t$ for $t \geq 0$.

³¹Although similar methods can be devised for irregular LDPC codes, we focus on the regular case only.

³²In the same way as the relative Hamming weight of a vector is the Hamming weight of the vector divided by n , we can define relative pseudo-weights for all the pseudo-weights that were introduced in Sec. 6.

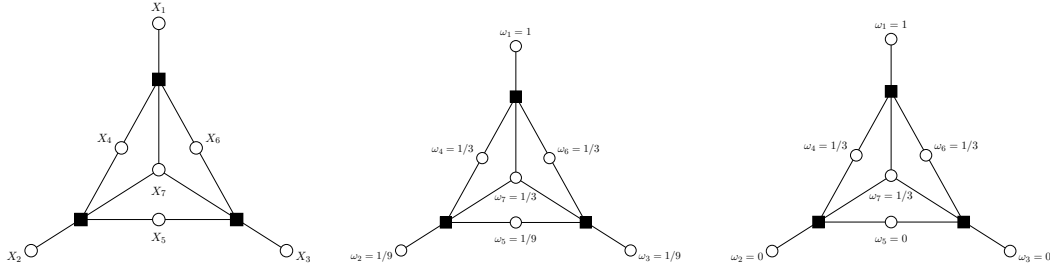


Figure 22: Left: Tanner graph for the $[7,4,3]$ code in Ex. 47. Middle: Canonical completion with respect to node X_1 . Right: Another pseudo-codeword.

Definition 46 Let \mathbb{T} be the Tanner graph of a code whose parity-check matrix \mathbf{H} has uniform row weight w_{row} . After performing the breadth-first spanning-tree ordering with an arbitrary variable node V as root we construct a pseudo-codeword ω in the following way. If bit i corresponds to a variable node in tier $2t$, then

$$\omega_i \triangleq \frac{1}{(w_{\text{row}} - 1)^t}. \quad (52)$$

We call this the canonical completion with root V . It will be shown in Lemma 48 that $\omega \in \mathcal{K}(\mathbf{H})$, i.e. ω is a pseudo-codeword. \square

Example 47 Fig. 22 (left) shows the Tanner graph of a $[7, 4, 3]$ binary linear code. (It is the length-7 Hamming code.) Note that in this Tanner graph, all check nodes have degree four, i.e. $w_{\text{row}} = 4$. Performing breadth-first spanning-tree ordering with root X_1 we see that tier 0 consists of $\{X_1\}$, tier 2 consists of $\{X_4, X_6, X_7\}$, and tier 4 consists of $\{X_2, X_3, X_5\}$. Correspondingly, the canonical completion with root X_1 yields the vector $\omega = (1, \frac{1}{9}, \frac{1}{9}, \frac{1}{3}, \frac{1}{9}, \frac{1}{3}, \frac{1}{3})$ shown in Fig. 22 (middle). It is easy to check that ω is inside the fundamental cone for this graph and is therefore a pseudo-codeword. The AWGNC pseudo-weight for ω equals

$$w_p(\omega) = \frac{(1 + \frac{1}{9} + \frac{1}{9} + \frac{1}{3} + \frac{1}{9} + \frac{1}{3} + \frac{1}{3})^2}{1 + \frac{1}{81} + \frac{1}{81} + \frac{1}{9} + \frac{1}{81} + \frac{1}{9} + \frac{1}{9}} = 3.973.$$

(As an aside, we note that the Tanner graph in Fig. 22 (left) also supports a pseudo-codeword ω' of type $\omega' = (1, 0, 0, \frac{1}{3}, 0, \frac{1}{3}, \frac{1}{3})$ whose AWGNC pseudo-weight equals only three and is thus at “minimum distance” for this code, see Fig. 22 (right).) \square

Without going into the details, let us mention that Def. 46 can be generalized in the following way: instead of doing a canonical completion with respect to a single variable node, one might do a canonical completion with respect to a set of variable nodes. The entries of the pseudo-vector will then be defined according to the graph distance to this set of nodes. This generalized notion of canonical completion was e.g. used in [60, 50].

Lemma 48 Let \mathbb{T} be the Tanner graph of a code whose parity-check matrix \mathbf{H} has uniform row weight w_{row} . The canonical completion with an arbitrary codeword symbol node V as root

yields a vector $\boldsymbol{\omega}$ such that $\boldsymbol{\omega}$ is in the fundamental cone $\mathcal{K}(\mathbf{H})$. The vector $\boldsymbol{\omega}$ has AWGNC pseudo-weight $w_p(\boldsymbol{\omega}) = \|\boldsymbol{\omega}\|_1^2 / \|\boldsymbol{\omega}\|_2^2$, where

$$\|\boldsymbol{\omega}\|_1 = \sum_{t=0}^{\lfloor \delta(\mathbb{T})/2 \rfloor} N_{V,2t}(\mathbb{T}) \frac{1}{(w_{\text{row}} - 1)^t}, \quad (53)$$

$$\|\boldsymbol{\omega}\|_2^2 = \sum_{t=0}^{\lfloor \delta(\mathbb{T})/2 \rfloor} N_{V,2t}(\mathbb{T}) \left(\frac{1}{(w_{\text{row}} - 1)^t} \right)^2. \quad (54)$$

Proof: See Sec. A.12. □

For a given \mathbb{T} , one can numerically calculate the pseudo-weight of the pseudo-codeword given by the canonical completion for any given root; this will always yield an upper bound on $w_p^{\min}(\mathcal{C})$. In the next proposition we will see that the canonical-completion approach is powerful enough to show that $w_p^{\min}(\mathcal{C})$ can at best only grow sub-linearly for $(w_{\text{col}}, w_{\text{row}})$ -regular LDPC codes with $3 \leq w_{\text{col}} < w_{\text{row}}$.

Proposition 49 *Let \mathbf{H} be the $(w_{\text{col}}, w_{\text{row}})$ -regular parity-check matrix of a length- n LDPC code \mathcal{C} with $3 \leq w_{\text{col}} < w_{\text{row}}$. Then the minimum pseudo-weight is upper bounded by*

$$w_p^{\min}(\mathbf{H}) \leq \beta' \cdot n^\beta, \quad (55)$$

where

$$\beta' \triangleq \beta'(w_{\text{col}}, w_{\text{row}}) \triangleq \left(\frac{w_{\text{col}}(w_{\text{col}} - 1)}{w_{\text{col}} - 2} \right)^2, \quad \beta \triangleq \beta(w_{\text{col}}, w_{\text{row}}) \triangleq \frac{\log((w_{\text{col}} - 1)^2)}{\log((w_{\text{col}} - 1)(w_{\text{row}} - 1))} < 1. \quad (56)$$

Proof: See Sec. A.13. □

Note that this proposition excludes two type of $(w_{\text{col}}, w_{\text{row}})$ -regular codes. The first type is the family of codes where $w_{\text{col}} = 2$, also known as cycle codes. In that case a much better upper bound can be given: the minimum distance, and therefore also the minimal AWGNC pseudo-weight, grow at best only logarithmically in the block length n .

The second type of codes that were excluded were families of codes where $w_{\text{col}} \geq w_{\text{row}}$. Note however that randomly generated $(w_{\text{col}}, w_{\text{row}})$ -regular LDPC codes are not too interesting since the dimension of the code will be zero or near-zero with high probability. Nevertheless, let us mention that there are interesting and practically useful families of algebraically constructed $(w_{\text{col}}, w_{\text{row}})$ -regular codes where the rate does not vanish, e.g. [61].

Corollary 50 *Consider a sequence of $(w_{\text{col}}, w_{\text{row}})$ -regular LDPC codes, $3 \leq w_{\text{col}} < w_{\text{row}}$, whose length goes to infinity. The relative minimum AWGNC pseudo-weight (i.e. the fraction of minimum pseudo-weight to code length) must go to zero. This is in sharp contrast to the fact that the relative minimum Hamming weight of a randomly generated $(w_{\text{col}}, w_{\text{row}})$ -regular LDPC code, $3 \leq w_{\text{col}} < w_{\text{row}}$, is lower bounded by a nonzero number with probability one for $n \rightarrow \infty$ [2].*

Let us finish this section with two observation. The first observation is about the “strange” shape of the fundamental cone. Using Lemma 40 we see that Prop. 49 says that for families of $(w_{\text{col}}, w_{\text{row}})$ -regular LDPC codes there are pseudo-codewords (i.e. vectors in the fundamental

cone) whose angle with the all-ones vector goes to 90° for $n \rightarrow \infty$. However, none of the polytopes associated to this family of codes contains the vector $(w_{\text{row}} - 1 + \varepsilon, 1, \dots, 1)$, where $\varepsilon > 0$, yet the angle of this vector with the all-ones vector goes to 0° for $n \rightarrow \infty$.

The second observation is that the BEC pseudo-weight of the canonical completion with respect to any variable node equals the block length. This means that although the fundamental cone characterizes the pseudo-codewords for the AWGNC and the BEC, the worst-case pseudo-codewords within the fundamental cone might be quite different depending on the channel.

8 The Relationship of the Fundamental Polytope to other Concepts that Explain the Behavior of Iterative Decoding

As we mentioned in the introduction to the paper, a variety of concepts have been introduced in the past that try to explain the behavior of MPID. In this section we would like to show how some of these are related to the fundamental polytope and the various pseudo-weights.

8.1 Stopping Sets

Let us recall the definition of a stopping set [22] for a Tanner graph T . A subset \mathcal{S} of the variable nodes of T is called a stopping set if and only if every check node in $\partial(\mathcal{S})$ is connected to at least two variable nodes in \mathcal{S} . Stopping sets are a means to understand the suboptimal behavior of iterative decoding techniques for the BEC, in fact they completely characterize iterative decoding in that case. It has been observed later that stopping sets seem to also reflect, to some degree, the performance of iteratively decoded codes for other channels.

Proposition 51 *On the one hand, if $\omega \in \mathcal{P}(\mathbf{H})$ then $\text{supp}(\omega)$ is a stopping set of $\mathsf{T}(\mathbf{H})$. On the other hand, if \mathcal{S} is a stopping set of $\mathsf{T}(\mathbf{H})$ then there exists a vector $\omega \in \mathcal{P}(\mathbf{H})$ such that $\text{supp}(\omega) = \mathcal{S}$.*

Proof: See Sec. A.14. □

In the light of Prop. 51 it seems quite intuitive that the BEC pseudo-weight of a vector $\omega \in \mathcal{P}(\mathbf{H})$ is defined to be $w_{\text{p}}^{\text{BEC}}(\omega) = |\text{supp}(\omega)|$, see Def. 34, but we will not go into the details here.

While the notion of stopping set is well suited to the BEC it is not refined enough to capture the situation for the AWGN channel. Consider the parity-check matrix \mathbf{H} whose Tanner graph $\mathsf{T} \triangleq \mathsf{T}(\mathbf{H})$ is shown in Fig. 23 and whose fundamental cone is

$$\mathcal{K}(\mathbf{H}) = \{\alpha_1 \cdot (2, 2, 1, 1) + \alpha_2 \cdot (1, 1, 2, 2) \mid \alpha_1, \alpha_2 \in \mathbb{R}_+\}.$$

While all the non-zero vectors in $\mathcal{K}(\mathbf{H})$ have BEC pseudo-weight 4 (i.e. their supports yield stopping sets of size 4), the AWGNC pseudo-weight is usually smaller than 4, e.g. the two minimal pseudo-codewords $(2, 2, 1, 1)$ and $(1, 1, 2, 2)$ have AWGNC pseudo-weight 3.6.

8.2 Near Codewords and Trapping Sets

Near-codewords were introduced by MacKay and Postol [23]: a vector $\mathbf{x} \in \mathbb{F}_2^n$ is called a (w, w') near-codeword in a Tanner graph $\mathsf{T} \triangleq \mathsf{T}(\mathbf{H})$ with n variable nodes if $w_{\mathbf{H}}(\mathbf{x}) = w$

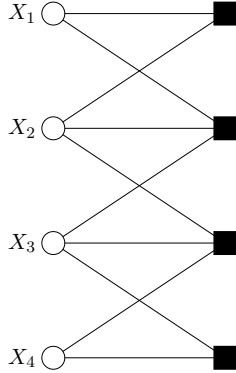


Figure 23: Tanner graph T .

and $w_H(\mathbf{s}) = w'$ where $\mathbf{s} = \mathbf{x} \cdot \mathbf{H}^T$ (in \mathbb{F}_2) is the syndrome of \mathbf{x} with respect to \mathbf{H} . In other words, the graph induced by the w non-zero components of \mathbf{x} contains w' check nodes of odd degree. Richardson’s definition of trapping sets is essentially identical [24]: $\mathbf{x} \in \mathbb{F}_2^n$ is a (w, w') near-codeword if and only if $\text{supp}(\mathbf{x})$ is a (w, w') trapping set.

As was remarked in [23]: “near codewords with small w' tend to be error states from which the sum-product decoding algorithm cannot escape.” Therefore it is important to understand the (w, w') near-codewords that have low w and low w' . To exemplify this with a simple, albeit extreme, example, consider an LDPC code \mathcal{C} represented by a parity-check matrix \mathbf{H} . Fix some $i' \in \mathcal{I}$ and let $\mathbf{x} \in \mathbb{F}_2^n$ be a vector where $x_{i'} = 1$ and $x_i = 0$ for $i \in \mathcal{I} \setminus \{i'\}$. It is easy to check that \mathbf{x} is a $(1, w')$ near-codeword where w' equals the Hamming weight of the i' column of \mathbf{H} . In fact, it can cause problems when transmitting over an AWGNC. Assume that the all-zeros codeword is transmitted ($+\sqrt{E_c}\mathbf{1}$ after modulation) and that the noise vector is the all-zeros vector except for the i' -th position that is negative. If it is negative enough then MPID will decide wrongly.

A connection between near-codewords and trapping sets on the one hand and pseudo-codewords on the other hand can be made in the following way. One way is to find the pseudo-codeword in the fundamental cone that is the closest to a (w, w') near-codeword \mathbf{x} . If w' is small, only small changes have to be applied to the components of the vector \mathbf{x} to get a pseudo-codeword. Alternatively, when trying to assign a pseudo-codeword to a near-codeword one might want to apply the canonical completion that is rooted at the near-codeword.

8.3 Why Four-Cycles are Potentially Bad

Already people like Wiberg realized that for MPID to work well one should have Tanner graphs that look locally tree-like which means that the girth of a graph should be reasonably large. A first step in that direction is to avoid four-cycles.³³ In this subsection we would like to explore what the fundamental-polytope view can contribute to this topic.

A simple observation towards this goal is the following: considering the proof of Prop. 49 we see that the smaller the girth of the graph is the smaller can be made the AWGNC pseudo-weight of the canonical completion.

³³Note though that some researchers have studied algebraically-constructed Tanner graphs with girth four, see e.g. [62, 63, 64], and exhibited some codes which work very well under iterative decoding.

A different avenue is pursued by the following lemma and its corollaries which explore the effect of girth on the fundamental polytope upon adding redundant rows to a parity-check matrix.

Lemma 52 *Let \mathcal{C} be a code with parity-check matrix \mathbf{H} . Basic coding theory tells us that the modified parity-check matrix*

$$\mathbf{H}' \triangleq \begin{pmatrix} \mathbf{H} \\ \mathbf{a} \cdot \mathbf{H} \end{pmatrix} \quad (\text{in } \mathbb{F}_2),$$

where $\mathbf{a} \in \mathbb{F}_2^{|\mathcal{J}(\mathbf{H})|}$ is an arbitrary vector, defines the same code \mathcal{C} . If the Tanner graph $\mathsf{T}(\mathbf{H})$ of \mathbf{H} is a forest, i.e. cycle-free, then $\mathcal{P}(\mathbf{H}) = \mathcal{P}(\mathbf{H}')$.

Proof: See Sec. A.15. □

Note that in the absence of cycle-freeness of $\mathsf{T}(\mathbf{H})$ one can easily exhibit a vector \mathbf{a} where $\mathcal{P}(\mathbf{H}') \subsetneq \mathcal{P}(\mathbf{H})$.

Corollary 53 *Similar to Lemma 52, consider a code \mathcal{C} with parity-check matrix \mathbf{H} and a modified parity-check matrix \mathbf{H}' , where $\mathbf{a} \in \mathbb{F}_2^n$ is an arbitrary vector. However, now we do not require that $\mathsf{T}(\mathbf{H})$ is a forest. Let \mathbf{H}_1 be the $|\text{supp}(\mathbf{a})| \times n$ submatrix of \mathbf{H} where we include the j -th row if and only if $a_j \neq 0$. If the Tanner graph $\mathsf{T}(\mathbf{H}_1)$ of \mathbf{H}_1 is a forest, i.e. cycle-free, then $\mathcal{P}(\mathbf{H}) = \mathcal{P}(\mathbf{H}')$.*

Proof: See Sec. A.16. □

Corollary 54 *Let \mathcal{C} be a code with parity-check matrix \mathbf{H} . Basic coding theory tells us that the modified parity-check matrix*

$$\mathbf{H}' \triangleq \begin{pmatrix} \mathbf{H} \\ \mathbf{A} \cdot \mathbf{H} \end{pmatrix} \quad (\text{in } \mathbb{F}_2),$$

where \mathbf{A} is an arbitrary matrix over \mathbb{F}_2 with $|\mathcal{J}(\mathbf{H})|$ columns, defines the same code \mathcal{C} . For each row r of \mathbf{A} , let \mathbf{H}_r be the submatrix of \mathbf{H} where we include the j -th row of \mathbf{H} if $[\mathbf{A}]_{r,j} = 1$. If $\mathsf{T}(\mathbf{H}_r)$ is a cycle-free Tanner graph for all rows r of \mathbf{A} , then $\mathcal{P}(\mathbf{H}) = \mathcal{P}(\mathbf{H}')$.

Proof: See Sec. A.17. □

Lemma 52 and its corollaries have some important consequences.³⁴

- Let \mathbf{H} be a parity-check matrix of a code \mathcal{C} where the Tanner graph $\mathsf{T}(\mathbf{H})$ has girth six. We can create a new parity-check matrix \mathbf{H}' that describes the same code in the following way: let \mathbf{H}' consist of all rows of \mathbf{H} and the modulo-2 sums of all pairs of rows of \mathbf{H} . Then $\mathcal{P}(\mathbf{H}) = \mathcal{P}(\mathbf{H}')$. (This observation follows from the fact that girth six for $\mathsf{T}(\mathbf{H})$ implies that $\mathsf{T}(\begin{pmatrix} \mathbf{h}_{j'} \\ \mathbf{h}_{j''} \end{pmatrix})$ is cycle-free for all pairs of rows j', j'' of \mathbf{H} .) Note that applying the same procedure to Tanner graphs $\mathsf{T}(\mathbf{H})$ with girth four will usually lead to $\mathcal{P}(\mathbf{H}') \subsetneq \mathcal{P}(\mathbf{H})$.

³⁴Similar observations were also made by Wainwright [65].

- More generally, let \mathbf{H} be a parity-check matrix of a code \mathcal{C} where the Tanner graph $\mathbb{T}(\mathbf{H})$ has girth g . We can create a new parity-check matrix \mathbf{H}' that describes the same code in the following way: let \mathbf{H}' consist of all rows of \mathbf{H} , the modulo-2 sums of all pairs of rows of \mathbf{H} , \dots , the modulo-2 sums of all $(g-2)/2$ -tuples of rows of \mathbf{H} . Then $\mathcal{P}(\mathbf{H}) = \mathcal{P}(\mathbf{H}')$.
- The above observations have some interesting consequences for $\mathcal{R}_r(\mathbf{H})$ as defined in Def. 11: if $\mathbb{T}(\mathbf{H})$ has girth g then $\mathcal{R}_r(\mathbf{H}) = \mathcal{P}(\mathbf{H})$ for $r \leq (g-2)/2$. This means that the larger the girth of the Tanner graph $\mathbb{T}(\mathbf{H})$ is, the more codewords from the dual code have to be added to the parity-check matrix so that the fundamental polytope changes. Parity-check matrices whose Tanner graphs have large girth therefore possess a good complexity-approximation tradeoff: it takes much more effort to get a better approximation of $\text{conv}(\mathcal{C})$.

The above considerations show that large girth seems to be a desirable design criterion when constructing LDPC codes. This supports for example the type of random LDPC code constructions as presented by Hu et al. in [66]. It is certainly also a desirable criterion when designing algebraically constructed LDPC codes, nevertheless one has to be careful beyond having simply a large girth: a Tanner graph with a cycle structure that is "too nice" can lead to either low-weight codewords (which is very bad) or low-weight pseudo-codewords (which might potentially be detected and avoided in a decoder). E.g. in the case of the Margulis construction with Ramanujan graphs one has large girth but also a minimum distance of 24 for $n = 4896$ [67, 23]. Obviously, adding any possible better constraints does not help as this minimum codeword will always be included. Although the original Margulis codes [6] do not seem to have low-weight codewords they exhibit some near-codewords [23]. These near-codewords might be avoided using better relaxations.

Another word of caution: when adding redundant rows to a parity-check matrix it is clear that the decoding performance of GCD and LPD can only become better. A question remains as how far GCD is still a good model of MPID when the parity-check matrix contains many more rows than columns. (Some initial explorations in this direction were presented in [68].)

9 Conclusions

We have introduced graph-cover decoding, a theoretical tool that helps to establish a bridge between linear-programming decoding and message-passing iterative decoding and explains why they perform similarly. The central object behind these decoding algorithms is the fundamental polytope which is a function of the graphical representation of the code (and not of the channel). Therefore, different representations of the same code yield (potentially) different fundamental polytopes. Vectors inside the fundamental polytope are called pseudo-codewords and their influence is measured by the pseudo-weight, a function that depends on the pseudo-codeword and the channel law. For all the cases where the behavior of message-passing decoding is known analytically, the graph-cover decoder gives the correct predictions and for the other cases the graph-cover decoder seems to be a good model of the behavior of message-passing decoding. Moreover, there are connections to Bethe free energy, the marginal polytope, and the metric polytope.

Some of the questions for future research that should be addressed are as follows. First, given a code and its representation, what analytical and computational tools can be used to

characterize the fundamental polytope? (Some initial work in this direction was presented in [69, 70] where a lower bound on the AWGNC pseudo-weight was given.) Secondly, how can one construct codes on graphs whose fundamental polytopes have good properties? Thirdly, one can always change the Tanner graph of a code, e.g. by repeating a check many times, so that the fundamental polytope and therefore also the linear programming decoding performance remains the same whereas the iterative decoding performance will change. So, up to what degree is the graph-cover decoding a good model for message-passing decoding? (Some initial work in this direction was presented in [33] and [68].)

A Proofs

This appendix contains a variety of proofs that were used in the main text.

A.1 Proof of Proposition 10

We prove Prop. 10 in three major steps. First, Lemma 55 will show that $\mathcal{Q}(\mathbf{H})$ is a subset of $\mathcal{P}(\mathbf{H})$. Secondly, Lemma 56 will prove that if a point in $\mathcal{P}(\mathbf{H})$ has only rational entries then it must also be in $\mathcal{Q}(\mathbf{H})$. Thirdly, Lemma 58 will prove that all vertices of $\mathcal{P}(\mathbf{H})$ are vectors with rational entries. Eq. (14) is then a simple consequence of these first two lemmas, (15) is a simple consequence of (14), and the statement that all vertices of $\mathcal{P}(\mathbf{H})$ are in $\mathcal{Q}(\mathbf{H})$ is a consequence of the third lemma.

Lemma 55 *It holds that*

$$\mathcal{Q}(\mathbf{H}) \subseteq \mathcal{P}(\mathbf{H}).$$

Proof: Let $\tilde{\mathbb{T}}$ be any M -fold cover of $\mathbb{T}(\mathbf{H})$ and let $\tilde{\mathcal{C}} \triangleq \mathcal{C}(\tilde{\mathbb{T}})$. Because of (11), if we can show that $\omega(\tilde{\mathbf{x}}) \in \text{conv}(\mathcal{C}_j)$ for all $\tilde{\mathbf{x}} \in \mathcal{C}(\tilde{\mathbb{T}})$ and for all $j \in \mathcal{J}$ we are done. Fix some $\tilde{\mathbf{x}} \in \mathcal{C}(\tilde{\mathbb{T}})$ and some $j \in \mathcal{J}$. As we saw in the remarks after Ex. 4, the Tanner graph $\tilde{\mathbb{T}}$ defines some permutations $\pi_{j,i}$ for all $i \in \mathcal{I}_j$ and so $\tilde{\mathbf{x}}$ fulfills

$$\sum_{i \in \mathcal{I}_j} \tilde{x}_{i, \pi_{j,i}(m)} = 0 \quad (\text{in } \mathbb{F}_2) \quad (57)$$

for all $m \in [M]$. In order to simplify the following expressions, let us introduce some dummy permutations $\pi_{j,i}$ for all $i \in \mathcal{I} \setminus \mathcal{I}_j$. Then, for $m \in [M]$, let us define the vectors $\mathbf{x}'^{(m)} \in \mathbb{R}^n$ with

$$x'_i{}^{(m)} \triangleq \tilde{x}_{i, \pi_{j,i}(m)}$$

for all $i \in \mathcal{I}$. Rewriting (57) as

$$\sum_{i \in \mathcal{I}_j} x'_i{}^{(m)} = 0 \quad (\text{in } \mathbb{F}_2) \quad (58)$$

we see that $\mathbf{x}'^{(m)} \in \mathcal{C}_j(\mathbf{H})$ for all $m \in [M]$. A convex sum of these M vectors must obviously lie in $\text{conv}(\mathcal{C}_j(\mathbf{H}))$:

$$\sum_{m \in [M]} \frac{1}{M} \mathbf{x}'^{(m)} \in \text{conv}(\mathcal{C}_j(\mathbf{H})). \quad (59)$$

Observing that the i -th position of the left-hand side in (59) takes on the value

$$\sum_{m \in [M]} \frac{1}{M} x_i'^{(m)} = \frac{1}{M} \sum_{m \in [M]} x_i'^{(m)} = \frac{1}{M} \sum_{m \in [M]} \tilde{x}_{i, \pi_{j,i}(m)} = \frac{1}{M} \sum_{m' \in [M]} \tilde{x}_{i, m'} = \omega_i(\tilde{\mathbf{x}}), \quad (60)$$

we conclude that $\omega(\tilde{\mathbf{x}}) \in \text{conv}(\mathcal{C}_j(\mathbf{H}))$. Because $\tilde{\mathbf{T}}$, $\tilde{\mathbf{x}}$, and j were arbitrary, this finishes the proof.

Note that when $\mathcal{P}(\mathbf{H})$ contains more than one point in \mathbb{R}^n then the subset relationship between $\mathcal{Q}(\mathbf{H})$ and $\mathcal{P}(\mathbf{H})$ is strict: $\mathcal{Q}(\mathbf{H}) \subsetneq \mathcal{P}(\mathbf{H})$. To prove this, simply choose a point ω in $\mathcal{P}(\mathbf{H})$ where at least one component is irrational: because all points in $\mathcal{Q}(\mathbf{H})$ have rational components it follows that $\omega \notin \mathcal{Q}(\mathbf{H})$. (Note that the case where $\mathcal{P}(\mathbf{H})$ contains only one point in \mathbb{R}^n can only happen for block length $n = 1$ and parity-check matrices like $\mathbf{H} = (1)$.) \square

Lemma 56 *If a point in $\mathcal{P}(\mathbf{H})$ has only rational entries then it must also be in $\mathcal{Q}(\mathbf{H})$.*

The main part of the following proof will consist of an algorithm; Ex. 57 (which can be found in the text after this proof) illustrates the involved concepts with the help of a code that we have already used earlier on.

Proof: We will prove this lemma as follows: for an arbitrary point $\nu \in \mathcal{P}(\mathbf{H}) \cap \mathbb{Q}^n$ we will show that there is an M -cover $\tilde{\mathbf{T}}$ of $\mathbf{T}(\mathbf{H})$ such that we can exhibit a codeword $\tilde{\mathbf{x}} \in \mathcal{C}(\tilde{\mathbf{T}})$ such that $\omega(\tilde{\mathbf{x}}) = \nu$.

So, let $\nu \in \mathcal{P}(\mathbf{H}) \cap \mathbb{Q}^n$. Because $\nu \in \mathcal{P}(\mathbf{H})$ we have $\nu \in \text{conv}(\mathcal{C}_j(\mathbf{H}))$ for $j \in \mathcal{J}$. Using Carathéodory's Theorem (see e.g. [40, p. 10]), we can conclude that for all $j \in \mathcal{J}$ we can write

$$\nu = \alpha^{(j)} \mathbf{P}^{(j)},$$

where $\mathbf{P}^{(j)}$ is an $(n+1) \times n$ matrix where the rows represent some vertices of $\text{conv}(\mathcal{C}_j(\mathbf{H}))$, i.e. codewords of $\mathcal{C}_j(\mathbf{H})$, and where $\alpha^{(j)}$ is a vector of length $n+1$ where all entries are nonzero and sum to one. For each $j \in \mathcal{J}$ these statements can be reformulated to

$$(\nu \quad \mathbf{1}) = \alpha^{(j)} (\mathbf{P}^{(j)} \quad \mathbf{1}^T).$$

This is a system of $n+1$ equations with $n+1$ unknowns. Because $\nu \in \mathbb{Q}^n$ and because all entries of $\mathbf{P}^{(j)}$ are either 0 or 1, we can conclude with the help of Cramér's rule for solving systems of linear equations (see e.g. [71]) that all entries of $\alpha^{(j)}$ must be rational.

Now we proceed to construct a finite cover $\tilde{\mathbf{T}}$ of $\mathbf{T}(\mathbf{H})$ and a codeword $\tilde{\mathbf{x}} \in \mathcal{C}(\tilde{\mathbf{T}})$. Let M be a common denominator of all the entries of all the vectors $\alpha^{(j)}$, $j \in \mathcal{J}$: from this we have that not only $M\alpha^{(j)} \in \mathbb{Z}_+^n$, $j \in \mathcal{J}$, but also that $M\nu \in \mathbb{Z}_+^n$. The graph $\tilde{\mathbf{T}}$ shall be an M -cover of $\mathbf{T}(\mathbf{H})$ with symbol nodes $X_{i,m}$, $(i, m) \in \mathcal{I} \times [M]$ and check nodes $B_{j,m}$, $(j, m) \in \mathcal{J} \times [M]$. The entries of the codeword $\tilde{\mathbf{x}}$ shall be

$$\tilde{x}_{i,m} = \begin{cases} 1 & (i \in \mathcal{I}, m \in [M\nu_i]) \\ 0 & (\text{otherwise}) \end{cases}.$$

It now remains to specify the connection pattern of $\tilde{\mathbf{T}}$, i.e. what symbol node is connected to what check node. Once this pattern is specified, it will be easy to see that $\tilde{\mathbf{T}}$ is indeed an M -cover of $\mathbf{T}(\mathbf{H})$ and that $\tilde{\mathbf{x}}$ is a codeword in $\mathcal{C}(\tilde{\mathbf{T}})$. We use the following algorithm:

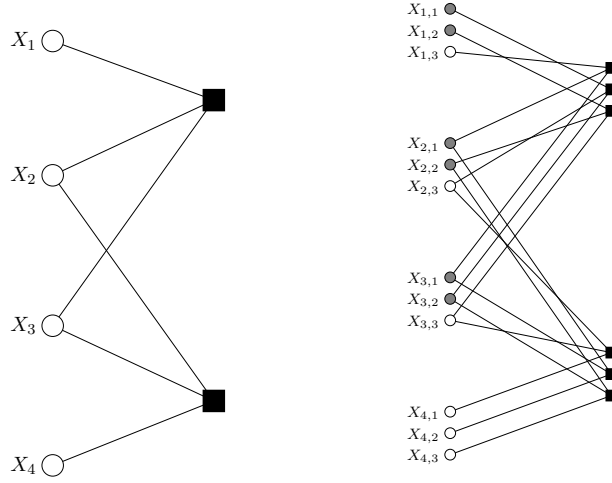


Figure 24: Left: Tanner graph $\mathbb{T}(\mathbf{H})$ of the simple binary linear code in Ex. 4. Right: 3-cover of $\mathbb{T}(\mathbf{H})$ as found in Ex. 57. The shading of the symbol nodes indicates the codeword found in this example.

- For all $j \in \mathcal{J}$ do:
 - Let $m_j \triangleq 1$. For all $i \in \mathcal{I}_j$, let $m'_i \triangleq 1$ and $m''_i \triangleq M\nu_i + 1$.
 - For ℓ from 1 to $n + 1$ do: for s from 1 to $M\alpha_\ell^{(j)}$ do:
 - * For all $i \in \mathcal{I}_j$ do:
 - If $[\mathbf{P}^{(j)}]_{\ell,i} = 1$ then connect X_{i,m'_i} to B_{j,m_j} and let $m'_i \triangleq m'_i + 1$.
 - If $[\mathbf{P}^{(j)}]_{\ell,i} = 0$ then connect X_{i,m''_i} to B_{j,m_j} and let $m''_i \triangleq m''_i + 1$.
 - * Let $m_j \triangleq m_j + 1$.

We leave it to the reader to check that this construction indeed yields the desired graph cover and codeword. □

Example 57 We continue Ex. 4. In Exs. 5 and 7 we saw that the vector $\boldsymbol{\nu} = (\frac{2}{3}, \frac{2}{3}, \frac{2}{3}, 0)$ is a pseudo-codeword. Let us show how the algorithm in the proof of Lemma 56 handles this vector. First of all, we must check that $\boldsymbol{\nu} \in \mathcal{P}(\mathbf{H}) \cap \mathbb{Q}^n$. This is indeed true. Next, we have to find the matrices $\mathbf{P}^{(1)}$ and $\mathbf{P}^{(2)}$. Note that the codes \mathcal{C}_1 and \mathcal{C}_2 are the sets

$$\mathcal{C}_1 = \left\{ \begin{pmatrix} (0, 0, 0) \\ (0, 1, 1) \\ (1, 0, 1) \\ (1, 1, 0) \end{pmatrix} \right\} \times \left\{ \begin{pmatrix} (0) \\ (1) \end{pmatrix} \right\} = \left\{ \begin{pmatrix} (0, 0, 0, 0) \\ (0, 0, 0, 1) \\ (0, 1, 1, 0) \\ (0, 1, 1, 1) \\ (1, 0, 1, 0) \\ (1, 0, 1, 1) \\ (1, 1, 0, 0) \\ (1, 1, 0, 1) \end{pmatrix} \right\}, \quad \mathcal{C}_2 = \left\{ \begin{pmatrix} (0) \\ (1) \end{pmatrix} \right\} \times \left\{ \begin{pmatrix} (0, 0, 0) \\ (0, 1, 1) \\ (1, 0, 1) \\ (1, 1, 0) \end{pmatrix} \right\} = \left\{ \begin{pmatrix} (0, 0, 0, 0) \\ (0, 0, 1, 1) \\ (0, 1, 0, 1) \\ (0, 1, 1, 0) \\ (1, 0, 0, 0) \\ (1, 0, 1, 1) \\ (1, 1, 0, 1) \\ (1, 1, 1, 0) \end{pmatrix} \right\}.$$

For the given vector $\boldsymbol{\nu}$ it turns out that $\boldsymbol{\nu} = \boldsymbol{\alpha}^{(1)}\mathbf{P}^{(1)}$ and $\boldsymbol{\nu} = \boldsymbol{\alpha}^{(2)}\mathbf{P}^{(2)}$ with³⁵

$$\boldsymbol{\alpha}^{(1)} = \left(0 \quad 0 \quad \frac{1}{3} \quad \frac{1}{3} \quad \frac{1}{3}\right), \quad \boldsymbol{\alpha}^{(2)} = \left(\frac{1}{3} \quad 0 \quad 0 \quad 0 \quad \frac{2}{3}\right),$$

$$\mathbf{P}^{(1)} = \begin{pmatrix} 0 & 0 & 0 & 0 \\ 0 & 0 & 0 & 1 \\ 0 & 1 & 1 & 0 \\ 1 & 0 & 1 & 0 \\ 1 & 1 & 0 & 0 \end{pmatrix}, \quad \mathbf{P}^{(2)} = \begin{pmatrix} 0 & 0 & 0 & 0 \\ 0 & 0 & 1 & 1 \\ 0 & 1 & 0 & 1 \\ 0 & 1 & 1 & 0 \\ 1 & 1 & 1 & 0 \end{pmatrix}$$

Note that the first two lines of $\mathbf{P}^{(1)}$ and the three middle lines of $\mathbf{P}^{(2)}$ are dummy lines so that $\boldsymbol{\alpha}^{(1)}$ and $\boldsymbol{\alpha}^{(2)}$ have $n + 1 = 5$ entries.

We see that $M = 3$ is the smallest common denominator of all the entries in $\boldsymbol{\alpha}^{(1)}$ and $\boldsymbol{\alpha}^{(2)}$, therefore let us find a 3-cover of $\mathbb{T}(\mathbf{H})$ that has a codeword $\tilde{\mathbf{x}} \in \mathcal{C}(\tilde{\mathbb{T}})$ such that $\boldsymbol{\omega}(\tilde{\mathbf{x}}) = \boldsymbol{\nu}$. Applying the rest of the algorithm in Lemma 56 we find the 3-cover graph $\tilde{\mathbb{T}}$ in Fig. 24 (right) and the codeword $\tilde{\mathbf{x}} = (1:1:0, 1:1:0, 1:1:0, 0:0:0) \in \mathcal{C}(\tilde{\mathbb{T}})$. \square

Lemma 58 *All vertices of $\mathcal{P}(\mathbf{H})$ are vectors with rational entries.*

Proof: Remember that $\mathcal{P}(\mathbf{H}) = \bigcap_{j \in \mathcal{J}(\mathbf{H})} \text{conv}(\mathcal{C}_j(\mathbf{H}))$ is defined as the intersection of $|\mathcal{J}(\mathbf{H})|$ polytopes. However, all polytopes $\text{conv}(\mathcal{C}_j(\mathbf{H}))$, $j \in \mathcal{J}(\mathbf{H})$ can be defined with linear inequalities that involve only integer coefficients, cf. Lemmas 25 and 26. Therefore, also $\mathcal{P}(\mathbf{H})$ can be defined with linear inequalities that involve only integer coefficients. Now, any vertex of $\mathcal{P}(\mathbf{H})$ is a point in $\mathcal{P}(\mathbf{H})$ where n inequalities hold with equality and where these n equalities form a system of linear equations with full rank. Using Cramér's rule for solving systems of linear equations (see e.g. [71]) we see that indeed all vertices of $\mathcal{P}(\mathbf{H})$ are vectors with rational entries. \square

A.2 Proof of Proposition 22

Let $\lambda_i \triangleq \lambda_i(y_i)$ be defined as in (17). Let us first prove the following lemma.

Lemma 59

$$\hat{\boldsymbol{\omega}}^{\text{GCD}(\mathbf{H})}(\mathbf{y}) = \arg \min_{\boldsymbol{\omega} \in \mathcal{Q}(\mathbf{H})} \sum_{i \in \mathcal{I}} \omega_i \lambda_i. \quad (61)$$

³⁵Other choices for $\boldsymbol{\alpha}^{(1)}$, $\boldsymbol{\alpha}^{(2)}$, $\mathbf{P}^{(1)}$, and $\mathbf{P}^{(2)}$ can also yield $\boldsymbol{\nu}$.

Proof: Let us first rewrite the right-hand side of (30). Because $P_{\tilde{\mathbf{Y}}|\tilde{\mathbf{X}}}(\mathbf{y}^{\uparrow M}|\mathbf{0}^{\uparrow M})$ is a constant for a given \mathbf{y} , instead of maximizing $(1/M) \log P_{\tilde{\mathbf{Y}}|\tilde{\mathbf{X}}}(\mathbf{y}^{\uparrow M}|\tilde{\mathbf{x}})$ in (30) we can also maximize

$$\begin{aligned}
\frac{1}{M} \log \frac{P_{\tilde{\mathbf{Y}}|\tilde{\mathbf{X}}}(\mathbf{y}^{\uparrow M}|\tilde{\mathbf{x}})}{P_{\tilde{\mathbf{Y}}|\tilde{\mathbf{X}}}(\mathbf{y}^{\uparrow M}|\mathbf{0}^{\uparrow M})} &= \frac{1}{M} \sum_{i \in \mathcal{I}} \sum_{m \in [M]} \log \frac{P_{Y_{i,m}|X_{i,m}}(y_i|\tilde{x}_{i,m})}{P_{Y_{i,m}|X_{i,m}}(y_i|0)} \\
&= \frac{1}{M} \sum_{i \in \mathcal{I}} \sum_{m \in [M]} \log \frac{P_{Y_i|X_i}(y_i|\tilde{x}_{i,m})}{P_{Y_i|X_i}(y_i|0)} \\
&= -\frac{1}{M} \sum_{i \in \mathcal{I}} \sum_{m \in [M]} \tilde{x}_{i,m} \lambda_i \\
&= -\sum_{i \in \mathcal{I}} \left(\frac{1}{M} \sum_{m \in [M]} \tilde{x}_{i,m} \right) \lambda_i \\
&\stackrel{(*)}{=} -\sum_{i \in \mathcal{I}} \omega_i(\tilde{\mathbf{x}}) \cdot \lambda_i,
\end{aligned}$$

where at step (*) we used (4). With this we can extend (30) to read

$$\begin{aligned}
(\hat{M}, \hat{T}, \hat{\tilde{\mathbf{x}}})^{\text{GCD}(\mathbf{H})}(\mathbf{y}) &= \arg \max_{(M, \tilde{\mathbf{T}}, \tilde{\mathbf{x}}) \in \tilde{\mathcal{Q}}(\mathbf{H})} \frac{1}{M} \log P_{\tilde{\mathbf{Y}}|\tilde{\mathbf{X}}}(\mathbf{y}^{\uparrow M}|\tilde{\mathbf{x}}) \\
&= \arg \min_{(M, \tilde{\mathbf{T}}, \tilde{\mathbf{x}}) \in \tilde{\mathcal{Q}}(\mathbf{H})} \sum_{i \in \mathcal{I}} \omega_i(\tilde{\mathbf{x}}) \cdot \lambda_i.
\end{aligned}$$

Remembering the relationship between $\tilde{\mathcal{Q}}(\mathbf{H})$ and $\mathcal{Q}(\mathbf{H})$ as defined in (5) and (6), respectively, we can write

$$\hat{\omega}^{\text{GCD}(\mathbf{H})}(\mathbf{y}) \triangleq \omega(\hat{\tilde{\mathbf{x}}}^{\text{GCD}(\mathbf{H})}(\mathbf{y})) = \arg \min_{\omega \in \mathcal{Q}(\mathbf{H})} \sum_{i \in \mathcal{I}} \omega_i \cdot \lambda_i,$$

which proves the lemma. \square

Lemma 59 allows us now to prove Prop. 22. Using the convexity of $\mathcal{P}(\mathbf{H})$ and a result that we found in Prop. 10, namely that all vertices of $\mathcal{P}(\mathbf{H})$ are in $\mathcal{Q}(\mathbf{H})$, we can extend (61) to read

$$\hat{\omega}^{\text{GCD}(\mathbf{H})}(\mathbf{y}) = \arg \min_{\omega \in \mathcal{Q}(\mathbf{H})} \sum_{i \in \mathcal{I}} \omega_i \lambda_i = \arg \min_{\omega \in \mathcal{P}(\mathbf{H})} \sum_{i \in \mathcal{I}} \omega_i \lambda_i,$$

which proves the proposition.

A.3 Proof of Lemma 24

Let $\tilde{\mathbf{T}}$ be an M -cover of $\mathbb{T}(\mathbf{H})$ and let $\tilde{\mathbf{x}} \in \mathcal{C}(\tilde{\mathbf{T}})$. We know that $M\omega(\tilde{\mathbf{x}}) \in \mathbb{Z}_+^n$ and from Prop. 10 we know that $\omega(\tilde{\mathbf{x}}) \in \mathcal{P}(\mathbf{H}) \cap \mathbb{Q}^n$. Because $\mathcal{K}(\mathbf{H}) = \text{conic}(\mathcal{P}(\mathbf{H}))$ we conclude that $M\omega(\tilde{\mathbf{x}}) \in \mathcal{K}(\mathbf{H})$. Therefore, $M\omega(\tilde{\mathbf{x}}) \in \mathcal{K}(\mathbf{H}) \cap \mathbb{Z}^n$, which proves the first statement.

Similar to the proof of Lemma 55, let us fix some $j \in \mathcal{J}$ and let us associate the vectors $\mathbf{x}'^{(m)}$, $m \in [M]$ to $\tilde{\mathbf{x}}$. There it was shown that $\mathbf{x}'^{(m)} \in \mathcal{C}_j(\mathbf{H})$ for all $m \in [M]$. Rewriting (60) to read $M\omega(\tilde{\mathbf{x}}) = \sum_{m \in [M]} \mathbf{x}'^{(m)}$, we see that $M\omega(\tilde{\mathbf{x}}) \in \mathcal{C}_j$ (in \mathbb{F}_2). Because j was arbitrary

and because $\mathcal{C} = \bigcap_{j \in \mathcal{J}} \mathcal{C}_j(\mathbf{H})$, we have $\mathcal{Z}(\mathbf{H}) \subseteq \mathcal{C}$ (in \mathbb{F}_2). Moreover, it is clear that $\mathcal{Z}(\mathbf{H}) \supseteq \mathcal{C}$ (in \mathbb{F}_2). Combining these two results proves the second statement.

Let $\boldsymbol{\omega}$ be a minimal pseudo-codeword and consider the half-ray given by $\{\alpha \boldsymbol{\omega} \mid \alpha \in \mathbb{R}_+\}$. Because the fundamental cone $\mathcal{K}(\mathbf{H})$ is the conic hull of the fundamental polytope $\mathcal{P}(\mathbf{H})$ we know that there is a non-zero vertex of the fundamental polytope lying on this half-ray. However, in Prop. 10 we have seen that all vertices of $\mathcal{P}(\mathbf{H})$ have rational entries and are therefore also in $\mathcal{Q}(\mathbf{H})$. Looking at one of the pre-images $(M, \tilde{\mathbf{T}}, \tilde{\mathbf{x}}) \in \tilde{\mathcal{Q}}(\mathbf{H})$ of this vertex we finally see that there must be an $\alpha \in \mathbb{R}_{++}$ such that $\alpha \cdot \boldsymbol{\omega} = \tilde{\mathbf{x}} \in \mathcal{Z}(\mathbf{H})$. This proves the third statement.

A.4 Proof of Lemma 28

Let us study the set $\mathcal{Q}(\mathbf{H})$ as defined in (6) and (7); Prop. 10, which shows a connection between $\mathcal{Q}(\mathbf{H})$ and $\mathcal{P}(\mathbf{H})$, will then give the desired result. (Note that we only discuss the case where $\mathsf{T}(\mathbf{H})$ is a tree. The case where $\mathsf{T}(\mathbf{H})$ is a forest, i.e. a collection of trees, is a straightforward extension.)

So, let $\tilde{\mathbf{T}}$ be an M -cover $\tilde{\mathbf{T}}$ of $\mathsf{T}(\mathbf{H})$. Because $\mathsf{T}(\mathbf{H})$ is a tree it is easy to see that $\tilde{\mathbf{T}}$ is a collection of M disjoint trees that are copies of $\mathsf{T}(\mathbf{H})$. With suitable labeling of the vertices of $\tilde{\mathbf{T}}$ we have $\mathcal{C}(\tilde{\mathbf{T}}) = \{\tilde{\mathbf{x}} \in \mathbb{F}_2^{nM} \mid (\tilde{x}_{1,m}, \dots, \tilde{x}_{n,m}) \in \mathcal{C} \text{ for all } m \in [M]\}$ and it follows that

$$\mathcal{Q}(\mathbf{H}) = \bigcup_{\tilde{\mathbf{T}}: \tilde{\mathbf{T}} \text{ is a finite-cover graph of } \mathsf{T}(\mathbf{H})} \boldsymbol{\omega}(\mathcal{C}(\tilde{\mathbf{T}}))$$

equals $\text{conv}(\mathcal{C}) \cap \mathbb{Q}^n$. Using Prop. 10 we see that $\mathcal{P}(\mathbf{H}) = \overline{\mathcal{Q}(\mathbf{H})} = \overline{\text{conv}(\mathcal{C}) \cap \mathbb{Q}^n} = \text{conv}(\mathcal{C})$ as promised.

A.5 Proof of Statements after Definition 33

The first statement is proven as follows. Note that $\boldsymbol{\omega} \in [0, 1]^n$. Let $\mathcal{E} \subseteq \mathcal{I}$ be set of positions where the channel bit flips happened. $S|_{\mathbf{x}=0}$ is non-negative if and only if $\sum_{i \in \mathcal{I}} \omega_i \lambda_i \leq 0$ if and only if $-\sum_{i \in \mathcal{E}} \omega_i + \sum_{i \in \mathcal{I} \setminus \mathcal{E}} \omega_i \leq 0$ if and only if $-2 \sum_{i \in \mathcal{E}} \omega_i + \sum_{i \in \mathcal{I}} \omega_i \leq 0$. Therefore, a necessary condition for $S|_{\mathbf{x}=0}$ to be non-positive is that $|\mathcal{E}| \geq \frac{1}{2} w_{\text{frac}}(\boldsymbol{\omega})$. This follows by observing that $|\mathcal{E}| \geq \sum_{i \in \mathcal{E}} \omega_i \geq \frac{1}{2} \sum_{i \in \mathcal{I}} \omega_i = \frac{1}{2} w_{\text{frac}}(\boldsymbol{\omega})$.

The second statement follows by replacing $\boldsymbol{\omega}$ by $\boldsymbol{\omega} / \|\boldsymbol{\omega}\|_\infty$ in the above argument and by observing that $\boldsymbol{\omega} / \|\boldsymbol{\omega}\|_\infty \in [0, 1]^n$.

A.6 Proof of Lemma 39

The expressions in the lemma are obtained doing the following manipulations:

$$w_p(\boldsymbol{\omega}) \triangleq \frac{\|\boldsymbol{\omega}\|_1^2}{\|\boldsymbol{\omega}\|_2^2} = \frac{|\mathcal{S}|^2 \cdot (\hat{\mathbb{E}}[\Omega])^2}{|\mathcal{S}| \cdot \hat{\mathbb{E}}[\Omega^2]} = |\mathcal{S}| \cdot \frac{(\hat{\mathbb{E}}[\Omega])^2}{\hat{\mathbb{E}}[\Omega^2]} = |\mathcal{S}| \cdot \frac{1}{\frac{\hat{\mathbb{E}}[\Omega^2] - (\hat{\mathbb{E}}[\Omega])^2}{(\hat{\mathbb{E}}[\Omega])^2} + 1} = |\mathcal{S}| \cdot \frac{1}{\frac{\widehat{\text{Var}}[\Omega]}{(\hat{\mathbb{E}}[\Omega])^2} + 1}. \quad (62)$$

A.7 Proof of Lemma 40

From vector analysis it is well known that $\langle \boldsymbol{\omega}, \mathbf{1} \rangle = \|\mathbf{1}\|_2 \|\boldsymbol{\omega}\|_2 \cos(\angle(\boldsymbol{\omega}, \mathbf{1}))$. With this, we can write

$$w_p(\boldsymbol{\omega}) = \frac{\langle \boldsymbol{\omega}, \mathbf{1} \rangle^2}{\|\boldsymbol{\omega}\|_2^2} = \frac{\|\mathbf{1}\|_2^2 \|\boldsymbol{\omega}\|_2^2 \cos^2(\angle(\boldsymbol{\omega}, \mathbf{1}))}{\|\boldsymbol{\omega}\|_2^2} = n \cdot \cos^2(\angle(\boldsymbol{\omega}, \mathbf{1})). \quad (63)$$

The proof of the second part of the lemma statement is analogous.

A.8 Proof of Lemma 41

We only consider the AWGNC pseudo-weight case, the other cases are left to the reader as an exercise. The proof for the AWGNC pseudo-weight case is done in two steps: first we prove a simplified statement (Lemma 60), then we prove the general case.

Lemma 60 *Consider the same setup as in Lemma 41. Assuming additionally that $\|\boldsymbol{\omega}^{(\ell)}\|_1 = 1$ for all $\ell \in [L]$ and that $\sum_{\ell \in [L]} \alpha_\ell = 1$ we have*

$$w_p\left(\sum_{\ell \in [L]} \alpha_\ell \boldsymbol{\omega}^{(\ell)}\right) \geq \min_{\ell \in [L]} w_p(\boldsymbol{\omega}^{(\ell)}) \quad (64)$$

Proof: Let $\boldsymbol{\nu} \triangleq \sum_{\ell \in [L]} \alpha_\ell \boldsymbol{\omega}^{(\ell)}$. Using the assumptions, it is easy to see that $\|\boldsymbol{\nu}\|_1 = 1$. Moreover,

$$\begin{aligned} \|\boldsymbol{\nu}\|_2^2 &= \left\| \sum_{\ell \in [L]} \alpha_\ell \boldsymbol{\omega}^{(\ell)} \right\|_2^2 = \sum_{i \in [n]} \left(\sum_{\ell_1 \in [L]} \alpha_{\ell_1} \omega_i^{(\ell_1)} \right) \left(\sum_{\ell_2 \in [L]} \alpha_{\ell_2} \omega_i^{(\ell_2)} \right) \\ &= \sum_{\ell_1 \in [L]} \sum_{\ell_2 \in [L]} \alpha_{\ell_1} \alpha_{\ell_2} \sum_{i \in [n]} \omega_i^{(\ell_1)} \omega_i^{(\ell_2)} \\ &\stackrel{(*)}{\leq} \sum_{\ell_1 \in [L]} \sum_{\ell_2 \in [L]} \alpha_{\ell_1} \alpha_{\ell_2} \sqrt{\left(\sum_{i \in [n]} (\omega_i^{(\ell_1)})^2 \right)} \sqrt{\left(\sum_{i \in [n]} (\omega_i^{(\ell_2)})^2 \right)} \\ &= \sum_{\ell_1 \in [L]} \sum_{\ell_2 \in [L]} \alpha_{\ell_1} \alpha_{\ell_2} \|\boldsymbol{\omega}^{(\ell_1)}\|_2 \|\boldsymbol{\omega}^{(\ell_2)}\|_2 = \left(\sum_{\ell \in [L]} \alpha_\ell \|\boldsymbol{\omega}^{(\ell)}\|_2 \right)^2 \end{aligned} \quad (65)$$

$$\leq \left(\max_{\ell' \in [L]} \|\boldsymbol{\omega}^{(\ell')}\|_2 \cdot \sum_{\ell \in [L]} \alpha_\ell \right)^2 = \max_{\ell \in [L]} \|\boldsymbol{\omega}^{(\ell)}\|_2^2, \quad (66)$$

where step (*) follows from the Cauchy-Schwarz inequality. Concluding,

$$w_p(\boldsymbol{\nu}) = \frac{\|\boldsymbol{\nu}\|_1^2}{\|\boldsymbol{\nu}\|_2^2} = \frac{1}{\|\boldsymbol{\nu}\|_2^2} \stackrel{(*)}{\geq} \frac{1}{\max_{\ell \in [L]} \|\boldsymbol{\omega}^{(\ell)}\|_2^2} = \min_{\ell \in [L]} \frac{1}{\|\boldsymbol{\omega}^{(\ell)}\|_2^2} = \min_{\ell \in [L]} \frac{\|\boldsymbol{\omega}^{(\ell)}\|_1^2}{\|\boldsymbol{\omega}^{(\ell)}\|_2^2} = \min_{\ell \in [L]} w_p(\boldsymbol{\omega}^{(\ell)}), \quad (67)$$

where step (*) follows from (66). \square

Now we prove Lemma 41. For $\ell \in [L]$, let $\alpha'_\ell \triangleq \alpha_\ell \|\boldsymbol{\omega}^{(\ell)}\|_1 / \left(\sum_{\ell' \in [L]} \alpha_{\ell'} \|\boldsymbol{\omega}^{(\ell')}\|_1 \right)$ and let $\boldsymbol{\omega}'_\ell \triangleq \boldsymbol{\omega}^{(\ell)} / \|\boldsymbol{\omega}^{(\ell)}\|_1$. Note that $\sum_{\ell \in [L]} \alpha'_\ell = 1$ and that $\|\boldsymbol{\omega}'_\ell\|_1 = 1$, $\ell \in [L]$. Then

$$w_p(\boldsymbol{\nu}) \stackrel{(*)}{=} w_p \left(\frac{\boldsymbol{\nu}}{\sum_{\ell' \in [L]} \alpha_{\ell'} \|\boldsymbol{\omega}^{(\ell')}\|_1} \right) = w_p \left(\sum_{\ell \in [L]} \frac{\alpha_\ell \|\boldsymbol{\omega}^{(\ell)}\|_1}{\sum_{\ell' \in [L]} \alpha_{\ell'} \|\boldsymbol{\omega}^{(\ell')}\|_1} \cdot \frac{\boldsymbol{\omega}^{(\ell)}}{\|\boldsymbol{\omega}^{(\ell)}\|_1} \right) \quad (68)$$

$$= w_p \left(\sum_{\ell \in [L]} \alpha'_\ell \boldsymbol{\omega}'_\ell \right) \stackrel{(**)}{\geq} \min \left(w_p(\boldsymbol{\omega}^{(1)}), \dots, w_p(\boldsymbol{\omega}^{(L)}) \right). \quad (69)$$

where at step (*) we used the scaling-invariance of $w_p(\cdot)$ and at step (**) we used the above lemma and the fact that $w_p(\boldsymbol{\omega}^{(\ell)}) = w_p(\boldsymbol{\omega}'_\ell)$ for $\ell \in [L]$.

A.9 Proof of Lemma 42

Proof: Let $\boldsymbol{\nu} \triangleq \sum_{\ell \in [L]} \alpha_\ell \boldsymbol{\omega}^{(\ell)}$. Note that the assumptions in the lemma statement imply that $\|\boldsymbol{\nu}\|_1 = 1$. The inequality follows then by using partial results of the proof of Lemma 60. Specifically, we use (65) which says that

$$\|\boldsymbol{\nu}\|_2^2 \leq \left(\sum_{\ell \in [L]} \alpha_\ell \|\boldsymbol{\omega}^{(\ell)}\|_2 \right)^2 \quad \text{or, equivalently,} \quad \|\boldsymbol{\nu}\|_2 \leq \sum_{\ell \in [L]} \alpha_\ell \|\boldsymbol{\omega}^{(\ell)}\|_2. \quad (70)$$

For $\|\boldsymbol{\nu}\|_1 = 1$ and $\|\boldsymbol{\omega}^{(\ell)}\|_1 = 1$ we have $\|\boldsymbol{\nu}\|_2 = 1/\sqrt{w_p(\boldsymbol{\nu})}$ and $\|\boldsymbol{\omega}^{(\ell)}\|_2 = 1/\sqrt{w_p(\boldsymbol{\omega}^{(\ell)})}$, respectively, and the result follows then immediately from the assumptions in the lemma statement and the above considerations. \square

A.10 Proof of Lemma 43

Proof: We have

$$\begin{aligned} \frac{\partial}{\partial \omega_i} w_p(\boldsymbol{\omega}) &= \frac{\partial}{\partial \omega_i} \frac{\left(\sum_{i' \in [n]} \omega_{i'} \right)^2}{\sum_{i' \in [n]} \omega_{i'}^2} = \frac{2 \left(\sum_{i' \in [n]} \omega_{i'} \right)}{\sum_{i' \in [n]} \omega_{i'}^2} - \frac{\left(\sum_{i' \in [n]} \omega_{i'} \right)^2 2\omega_i}{\left(\sum_{i' \in [n]} \omega_{i'}^2 \right)^2} \\ &= 2 \frac{\left(\sum_{i' \in [n]} \omega_{i'} \right)^2}{\left(\sum_{i' \in [n]} \omega_{i'}^2 \right)^2} \left[\left(\sum_{i' \in [n]} \omega_{i'} \right) \frac{\sum_{i' \in [n]} \omega_{i'}^2}{\left(\sum_{i' \in [n]} \omega_{i'} \right)^2} - \omega_i \right]. \end{aligned}$$

The lemma follows then by analyzing the expression in the square brackets. \square

A.11 Proof of Lemma 44

Proof: For $\boldsymbol{\omega} = \mathbf{0}$ the statement is trivial. So, assume that $\boldsymbol{\omega} \neq \mathbf{0}$. Because we assume in the lemma that $\boldsymbol{\omega} \leq \mathbf{1}$ we must have $\max_{i \in [n]} \omega_i \leq 1$, which proves the first inequality in (48).

The second inequality in (48) follows upon observing that

$$\begin{aligned} w_{\max\text{-frac}}(\boldsymbol{\omega}) &= \frac{\sum_{i \in [n]} \omega_i}{\max_{i \in [n]} \omega_i} = \frac{\left(\sum_{i \in [n]} \omega_i\right)^2}{\left(\max_{i \in [n]} \omega_i\right) \left(\sum_{i \in [n]} \omega_i\right)} = \frac{\left(\sum_{i \in [n]} \omega_i\right)^2}{\sum_{i \in [n]} (\omega_i \max_{i' \in [n]} \omega_{i'})} \\ &\leq \frac{\left(\sum_{i \in [n]} \omega_i\right)^2}{\sum_{i \in [n]} \omega_i^2} = w_p(\boldsymbol{\omega}). \end{aligned}$$

The third inequality in (48) can be proven as follows. Let $\mathbf{1}_\omega$ be the indicator vector of $\boldsymbol{\omega}$, i.e. the i -th position is 1 if ω_i is non-zero and it is 0 otherwise. Then, using the Cauchy-Schwarz inequality we see that $\|\boldsymbol{\omega}\|_1^2 = \langle \boldsymbol{\omega}, \mathbf{1} \rangle^2 = \langle \boldsymbol{\omega}, \mathbf{1}_\omega \rangle^2 \leq \|\boldsymbol{\omega}\|_2^2 \cdot \|\mathbf{1}_\omega\|_2^2 = \|\boldsymbol{\omega}\|_2^2 \cdot |\text{supp}(\boldsymbol{\omega})| = \|\boldsymbol{\omega}\|_2^2 \cdot w_p^{\text{BEC}}(\boldsymbol{\omega})$ and dividing by $\|\boldsymbol{\omega}\|_2^2$ yields the desired expression.

The inequalities in (50) follow from the inequalities in (48) by observing that $w_p(\cdot)$ and $w_p^{\text{BEC}}(\cdot)$ are scaling-invariant and therefore, when finding $w_p^{\min}(\mathbf{H})(\cdot)$ and $w_p^{\text{BEC}, \min}(\mathbf{H})(\cdot)$, it is sufficient to minimize over the non-zero vertices of the fundamental polytope.

The first inequality in (49) is the same as the first inequality in (48). In order to prove the second inequality in (49) consider the functions $f(\cdot)$ and $F(\cdot)$ and the value e in Def. 32. On the one hand, the area under $f(\cdot)$ from 0 to e equals $(1/2) \cdot F(n) = (1/2) \cdot \|\boldsymbol{\omega}\|_1$ by definition. On the other hand, because $f(\cdot)$ is non-increasing, the same area is upper bounded by $e \cdot \|\boldsymbol{\omega}\|_\infty$. Solving for $2e$ we obtain $2e \geq \|\boldsymbol{\omega}\|_1 / \|\boldsymbol{\omega}\|_\infty$. The third inequality in (49) is obtained as follows. First, note that $F(|\text{supp}(\boldsymbol{\omega})|) = F(n)$. Secondly, consider the chord from $(0, F(0) = 0)$ to $(|\text{supp}(\boldsymbol{\omega})|, F(|\text{supp}(\boldsymbol{\omega})|)) = \|\boldsymbol{\omega}\|_1$. Because $F(\cdot)$ is concave, the chord is always below $F(\cdot)$ in the domain of interest. Therefore, $F(e)$, which by definition must be equal to $(1/2) \cdot \|\boldsymbol{\omega}\|_1$, is not smaller than $(\|\boldsymbol{\omega}\|_1 / |\text{supp}(\boldsymbol{\omega})|) \cdot e$. Combining these observations we obtain $2e \leq |\text{supp}(\boldsymbol{\omega})|$.

The inequalities in (51) follow from the inequalities in (49) by observing that $w_p(\cdot)$ and $w_p^{\text{BSC}}(\cdot)$ are scaling-invariant and therefore, when finding $w_p^{\min}(\mathbf{H})(\cdot)$ and $w_p^{\text{BSC}, \min}(\mathbf{H})(\cdot)$, it is sufficient to minimize over the non-zero vertices of the fundamental polytope. \square

A.12 Proof of Lemma 48

The expressions in (53) and (54) for the AWGNC pseudo-weight are an immediate consequence of Defs. 45 and 46. Our main task is therefore to show that $\boldsymbol{\omega} \in \mathcal{K}(\mathbf{H})$. To that end, let us use the fundamental cone description of Lemma 26. It is obvious that $\omega_i \geq 0$ for all $i \in \mathcal{I}(\mathbf{H})$. Now, consider a check node B_j at tier $2t + 1$ for some $t \geq 0$ that is connected to variable nodes at tier $2t$ and possibly some variable nodes at tier $2t + 2$. We distinguish two cases:

- The check node B_j is connected to only one variable node, say X_{i_1} at tier $2t$, and $w_{\text{row}} - 1$ variable nodes, say $X_{i_2}, \dots, X_{i_{w_{\text{row}}}}$, at tier $2t + 2$. From Def. 46 it follows that $\omega_{i_1} = 1/(w_{\text{row}} - 1)^t$ and that $\omega_{i_2} = \dots = \omega_{i_{w_{\text{row}}}} = 1/(w_{\text{row}} - 1)^{t+1}$. It is easy to check that $\omega_{i'} \leq \sum_{i \in \mathcal{I}_j \setminus \{i'\}} \omega_i$ is satisfied for all $i' \in \mathcal{I}_j = \{i_1, \dots, i_{w_{\text{row}}}\}$. Indeed, the most crucial of them being for $i' = i_1$ where we have the inequality $1/(w_{\text{row}} - 1)^t \leq (w_{\text{row}} - 1) \cdot 1/(w_{\text{row}} - 1)^{t+1}$ that is satisfied with equality.
- The check node B_j is connected to at least two variable nodes, say X_{i_1}, \dots, X_{i_h} at tier $2t$, and $w_{\text{row}} - h$ variable nodes, say $X_{i_{h+1}}, \dots, X_{i_{w_{\text{row}}}}$, at tier $2t + 2$ where $2 \leq h \leq w_{\text{row}}$. From Def. 46 it follows that $\omega_{i_1} = \dots = \omega_{i_h} = 1/(w_{\text{row}} - 1)^t$ and that $\omega_{i_{h+1}} = \dots =$

$\omega_{i_{w_{\text{row}}}} = 1/(w_{\text{row}} - 1)^{t+1}$. It is easy to check that $\omega_{i'} \leq \sum_{i \in \mathcal{I}_j \setminus \{i'\}} \omega_i$ is satisfied for all $i' \in \mathcal{I}_j = \{i_1, \dots, i_{w_{\text{row}}}\}$. Actually, unless $w_{\text{row}} = 2$, none of them is satisfied with equality.

Because the check node B_j was arbitrary, this concludes the proof that $\boldsymbol{\omega} \in \mathcal{K}(\mathbf{H})$.

A.13 Proof of Proposition 49

Let $\mathbb{T} \triangleq \mathbb{T}(\mathbf{H})$ be the Tanner graph corresponding to \mathbf{H} . To prove the upper bound on $w_{\text{p}}^{\min}(\mathbf{H})$ we proceed as follows. By definition, the AWGNC pseudo-weight of any non-zero pseudo-codeword is larger than or equal to $w_{\text{p}}^{\min}(\mathbf{H})$. Therefore, any upper bound on the pseudo-weight of any non-zero pseudo-codeword will yield an upper bound on $w_{\text{p}}^{\min}(\mathbf{H})$.

Our choice for a non-zero pseudo-codeword is a pseudo-codeword that was obtained by the canonical completion rooted at an arbitrary variable node V , see Def. 46. Its AWGNC pseudo-weight was established in Lemma 48. To get an upper bound on $w_{\text{p}}(\boldsymbol{\omega})$, we need a lower bound on $\|\boldsymbol{\omega}\|_2^2$ and an upper bound on $\|\boldsymbol{\omega}\|_1$. We start with the lower bound on $\|\boldsymbol{\omega}\|_2^2$. We have³⁶

$$\|\boldsymbol{\omega}\|_2^2 = \sum_{t=0}^{\lfloor \delta(\mathbb{T})/2 \rfloor} N_{V,2t}(\mathbb{T}) \left(\frac{1}{(k-1)^t} \right)^2 \geq \sum_{t=0}^0 N_{V,2t}(\mathbb{T}) \left(\frac{1}{(k-1)^t} \right)^2 = 1, \quad (71)$$

where we used $N_{V,0}(\mathbb{T}) = 1$. A side note: if we can assume that the girth $g(\mathbb{T})$ of \mathbb{T} is at least six, we have $N_{V,0}(\mathbb{T}) = N_{V,0}^{\max}(\mathbb{T})$ and $N_{V,2}(\mathbb{T}) = N_{V,2}^{\max}(\mathbb{T})$, and therefore we get the better lower bound

$$\begin{aligned} \|\boldsymbol{\omega}\|_2^2 &= \sum_{t=0}^{\lfloor \delta(\mathbb{T})/2 \rfloor} N_{V,2t}(\mathbb{T}) \left(\frac{1}{(k-1)^t} \right)^2 \geq \sum_{t=0}^1 N_{V,2t}(\mathbb{T}) \left(\frac{1}{(k-1)^t} \right)^2 \\ &= \sum_{t=0}^1 N_{V,2t}^{\max}(\mathbb{T}) \left(\frac{1}{(k-1)^t} \right)^2 = 1 + j(k-1) \frac{1}{(k-1)^2} = 1 + \frac{j}{k-1}. \end{aligned}$$

For even larger girth, we could give even better lower bounds, but we will not pursue this any further.

Now we turn to the problem of obtaining an upper bound on $\|\boldsymbol{\omega}\|_1 = \sum_{t=0}^{\lfloor \delta(\mathbb{T})/2 \rfloor} N_{V,2t}(\mathbb{T}) \frac{1}{(k-1)^t}$. Because $N_{V,2t}(\mathbb{T}) \leq N_{V,2t}^{\max}$ for all $t \geq 0$, this sum is clearly upper bounded by the same sum for a Tanner graph which has the same number of variable nodes but which has maximal expansion, i.e.,

$$\|\boldsymbol{\omega}\|_1 = \sum_{t=0}^{\lfloor \delta(\mathbb{T})/2 \rfloor} N_{V,2t}(\mathbb{T}) \frac{1}{(k-1)^t} \leq \sum_{t=0}^{t'} N'_{V,2t} \frac{1}{(k-1)^t},$$

where we introduced $N'_{V,2t} \triangleq N_{V,2t}^{\max}$ for $0 \leq t \leq t'$ where t' is some constant such that $\sum_{t=0}^{t'-1} N'_{V,2t} < n = \sum_{t=0}^{\lfloor \delta(\mathbb{T})/2 \rfloor} N_{V,2t}(\mathbb{T}) \leq \sum_{t=0}^{t'} N'_{V,2t}$. By construction, t' will fulfill $t' \leq$

³⁶In order to shorten the notation used in this proof we will use $j \triangleq w_{\text{col}}$ and $k \triangleq w_{\text{row}}$.

$\lfloor \delta(T)/2 \rfloor$. Continuing,

$$\begin{aligned}
\|\boldsymbol{\omega}\|_1 &\leq \sum_{t=0}^{t'} N'_{V,2t} \frac{1}{(k-1)^t} = 1 + \sum_{t=1}^{t'} j(j-1)^{t-1} (k-1)^t \frac{1}{(k-1)^t} \\
&= 1 + \sum_{t=1}^{t'} j(j-1)^{t-1} = 1 + \frac{j}{j-2} \cdot \left((j-1)^{t'} - 1 \right) \\
&\leq \frac{j}{j-2} \cdot (j-1)^{t'}.
\end{aligned} \tag{72}$$

Combining (71) and (72) we obtain

$$w_p^{\min}(\mathbf{H}) \leq w_p(\boldsymbol{\omega}) = \frac{\|\boldsymbol{\omega}\|_1^2}{\|\boldsymbol{\omega}\|_2^2} \leq \frac{\left(\frac{j}{j-2} \cdot (j-1)^{t'} \right)^2}{1} \leq \left(\frac{j}{j-2} \right)^2 \cdot (j-1)^{2t'} \tag{73}$$

In order to complete the proof, we need an upper bound (in function of the code size n) on t' . Remembering the definition of t' , such a bound can be obtained as follows:

$$n \geq \sum_{t=0}^{t'-1} N_{V,2t}^{\max} = 1 + \sum_{t=1}^{t'-1} j(j-1)^{t-1} (k-1)^t = 1 + j(k-1) \frac{\gamma_{j,k}^{t'-1} - 1}{\gamma_{j,k} - 1} \tag{74}$$

$$= 1 + \underbrace{\left(\frac{jk - j}{jk - j - k + 1 - 1} \right)}_{\geq 1} \left(\gamma_{j,k}^{t'-1} - 1 \right) \geq \gamma_{j,k}^{t'-1}, \tag{75}$$

where $\gamma_{j,k} = (j-1)(k-1)$. Therefore,

$$t' \leq 1 + \frac{\log(n)}{\log(\gamma_{j,k})}. \tag{76}$$

Finally,

$$w_p^{\min}(\mathbf{H}) \leq \left(\frac{j}{j-2} \right)^2 \cdot (j-1)^{2t'} \leq \left(\frac{j}{j-2} \right)^2 \cdot (j-1)^{2+2\frac{\log(n)}{\log(\gamma_{j,k})}} \tag{77}$$

$$= \left(\frac{j(j-1)}{j-2} \right)^2 \cdot (j-1)^{2\frac{\log(n)}{\log(\gamma_{j,k})}} = \beta'(j,k) \cdot n^{\beta(j,k)}, \tag{78}$$

where

$$\beta'(j,k) \triangleq \left(\frac{j(j-1)}{j-2} \right)^2, \quad \beta(j,k) \triangleq 2 \frac{\log(j-1)}{\log(\gamma_{j,k})} = \frac{\log((j-1)^2)}{\log((j-1)(k-1))}. \tag{79}$$

For $k > j$ we have $\beta(j,k) < 1$.

A.14 Proof of Proposition 51

Let us prove the first statement. Because $\boldsymbol{\omega}$ is in the fundamental polytope $\mathcal{P}(\mathbf{H})$, it is also in the fundamental cone $\mathcal{K}(\mathbf{H})$ and so, for each $j \in \mathcal{J}$ and for each $i' \in \mathcal{I}_j$ it fulfills (see Def. 27): $\sum_{i \in \mathcal{I}_j \setminus \{i'\}} \omega_i \geq \omega_{i'}$. This means that for all $j \in \mathcal{J}$, if there is an $i'_j \in \mathcal{I}_j$ such that

$\omega_{i'_j} > 0$ then there are at least two distinct $i'_j, i''_j \in \mathcal{I}_j$ such that $\omega_{i'_j} > 0$ and $\omega_{i''_j} > 0$. But this is equivalent to the condition that each check node in $\partial(\text{supp}(\boldsymbol{\omega}))$ is connected to at least two variable nodes in $\text{supp}(\boldsymbol{\omega})$.

Let us now prove the second statement. Let \mathcal{S} be a stopping set and let $\boldsymbol{\nu} \in \mathbb{R}_+^n$ be a vector where $\nu_i \triangleq 1$ if $i \in \mathcal{S}$ and $\nu_i \triangleq 0$ otherwise. It can easily be seen that this vector fulfills all the conditions for being in the fundamental cone $\mathcal{K}(\mathbf{H})$, using e.g. the inequalities in Lemma 26. Following the comment after Def. 23, there is an $\alpha \in \mathbb{R}_{++}$ (in fact, a whole interval of α 's) such that $\boldsymbol{\omega} \triangleq \alpha \boldsymbol{\nu}$ is in the fundamental polytope $\mathcal{P}(\mathbf{H})$.

A.15 Proof of Lemma 52

It follows from the definition of the fundamental polytope (Def. 8) and the discussion before and after (21) that $\text{conv}(\mathcal{C}) \subseteq \mathcal{P}(\mathbf{H}') \subseteq \mathcal{P}(\mathbf{H})$. However, using Lemma 28 we can conclude that $\mathcal{P}(\mathbf{H}) = \text{conv}(\mathcal{C})$ which proves that $\mathcal{P}(\mathbf{H}) = \mathcal{P}(\mathbf{H}')$ as desired.

An alternative proof would be to show that (under the conditions in the lemma statement) $\boldsymbol{\omega} \in \mathcal{P}(\mathbf{H})$ implies $\boldsymbol{\omega} \in \mathcal{P}(\mathbf{H}')$ where for $\mathcal{P}(\mathbf{H})$ and $\mathcal{P}(\mathbf{H}')$ we use the description given in Lemma 26. Some manipulations of the involved inequalities lead to the desired result. We leave the details to the reader.

A.16 Proof of Corollary 53

Let $\overline{\mathbf{H}}_1$ be the matrix that contains the rows of \mathbf{H} that are not included in \mathbf{H}_1 . We have

$$\begin{aligned} \mathcal{P}(\mathbf{H}) &= \mathcal{P}(\mathbf{H}_1) \cap \mathcal{P}(\overline{\mathbf{H}}_1), \\ \mathcal{P}(\mathbf{H}') &= \mathcal{P}\left(\begin{pmatrix} \mathbf{H}_1 \\ \mathbf{a} \cdot \mathbf{H} \end{pmatrix}\right) \cap \mathcal{P}(\overline{\mathbf{H}}_1). \end{aligned}$$

Using Lemma 52 we conclude that $\mathcal{P}\left(\begin{pmatrix} \mathbf{H}_1 \\ \mathbf{a} \cdot \mathbf{H} \end{pmatrix}\right)$ equals $\mathcal{P}(\mathbf{H}_1)$ and that therefore $\mathcal{P}(\mathbf{H}')$ equals $\mathcal{P}(\mathbf{H})$.

A.17 Proof of Corollary 54

Let \mathbf{A} have L rows, let \mathbf{a}_ℓ , $\ell \in [L]$, be the vector containing the ℓ -th row of \mathbf{A} , and let $\overline{\mathbf{H}}_\ell$, $\ell \in [L]$, be the matrix that contains the rows of \mathbf{H} that are not included in \mathbf{H}_ℓ . We have

$$\begin{aligned} \mathcal{P}(\mathbf{H}) &= \bigcap_{\ell \in [L]} (\mathcal{P}(\mathbf{H}_\ell) \cap \mathcal{P}(\overline{\mathbf{H}}_\ell)), \\ \mathcal{P}(\mathbf{H}') &= \bigcap_{\ell \in [L]} \left(\mathcal{P}\left(\begin{pmatrix} \mathbf{H}_\ell \\ \mathbf{a}_\ell \cdot \mathbf{H} \end{pmatrix}\right) \cap \mathcal{P}(\overline{\mathbf{H}}_\ell) \right). \end{aligned}$$

Using Lemma 52 we conclude that $\mathcal{P}\left(\begin{pmatrix} \mathbf{H}_\ell \\ \mathbf{a}_\ell \cdot \mathbf{H} \end{pmatrix}\right)$ equals $\mathcal{P}(\mathbf{H}_\ell)$ for all $\ell \in [L]$ and that therefore $\mathcal{P}(\mathbf{H}')$ equals $\mathcal{P}(\mathbf{H})$.

References

- [1] R. G. Gallager, “Low-density parity-check codes,” *IRE Trans. Inform. Theory*, vol. 8, pp. 21–28, Jan. 1962.
- [2] R. G. Gallager, *Low-Density Parity-Check Codes*. M.I.T. Press, Cambridge, MA, 1963. Available online under <http://web.mit.edu/gallager/www/pages/ldpc.pdf>.
- [3] V. V. Zyablov, “An estimate of the complexity of constructing binary linear cascade codes,” *Probl. Inform. Transm.*, vol. 7, no. 1, pp. 3–10, 1971.
- [4] V. V. Zyablov and M. S. Pinsker, “Estimation of error-correction complexity of Gallager low-density codes,” *Probl. Inform. Transm.*, vol. 11, no. 1, pp. 18–28, 1976.
- [5] R. M. Tanner, “A recursive approach to low-complexity codes,” *IEEE Trans. on Inform. Theory*, vol. IT-27, pp. 533–547, Sept. 1981.
- [6] G. A. Margulis, “Explicit constructions of graphs without short cycles and low density codes,” *Combinatorica*, vol. 2, no. 1, pp. 71–78, 1982.
- [7] C. Berrou, A. Glavieux, and P. Thitimajshima, “Near Shannon Limit Error-Correcting Coding and Decoding: Turbo-Codes (1),” in *Proc. IEEE Int. Conf. Communications*, (Geneva, Switzerland), pp. 1064–1070, May 1993.
- [8] D. J. C. MacKay and R. M. Neal, “Near Shannon limit performance of low density parity check codes,” *Electronics Letters*, vol. 32, p. 1645, 29 Aug. 1996.
- [9] D. J. C. MacKay and R. M. Neal, “Near Shannon limit performance of low density parity check codes,” *Electronics Letters*, vol. 33, pp. 457–458, 13 Mar. 1997.
- [10] D. J. C. MacKay, “Good error-correcting codes based on very sparse matrices,” *IEEE Trans. on Inform. Theory*, vol. IT-45, no. 2, pp. 399–431, 1999.
- [11] N. Wiberg, H.-A. Loeliger, and R. Kötter, “Codes and iterative decoding on general graphs,” *Europ. Trans. on Telecomm.*, vol. 6, pp. 513–525, Sept./Oct. 1995.
- [12] N. Wiberg, *Codes and Decoding on General Graphs*. PhD thesis, Linköping University, Sweden, 1996.
- [13] S. M. Aji and R. J. McEliece, “The generalized distributive law,” *IEEE Trans. on Inform. Theory*, vol. IT-46, no. 2, pp. 325–343, 2000.
- [14] F. R. Kschischang, B. J. Frey, and H.-A. Loeliger, “Factor graphs and the sum-product algorithm,” *IEEE Trans. on Inform. Theory*, vol. IT-47, no. 2, pp. 498–519, 2001.
- [15] H.-A. Loeliger, “An introduction to factor graphs,” *IEEE Sig. Proc. Mag.*, vol. 21, no. 1, pp. 28–41, 2004.
- [16] M. G. Luby, M. Mitzenmacher, M. A. Shokrollahi, and D. A. Spielman, “Improved low-density parity-check codes using irregular graphs and belief propagation,” in *Proc. IEEE Intern. Symp. on Inform. Theory*, (MIT, Cambridge, MA, USA), p. 117, Aug. 16-21 1998.

- [17] T. Richardson and R. Urbanke, “Thresholds for turbo codes,” in *Proc. IEEE Intern. Symp. on Inform. Theory*, (Sorrento, Italy), p. 317, June 25–30 2000.
- [18] T. J. Richardson, M. A. Shokrollahi, and R. L. Urbanke, “Design of capacity-approaching irregular low-density parity-check codes,” *IEEE Trans. on Inform. Theory*, vol. IT-47, no. 2, pp. 619–637, 2001.
- [19] J. B. Anderson and S. M. Hladik, “Tailbiting MAP decoders,” *IEEE J. Sel. Areas Comm.*, vol. JSAC-16, no. 2, pp. 297–302, 1998.
- [20] S. M. Aji, G. B. Horn, and R. J. McEliece, “Iterative decoding on graphs with a single cycle,” in *Proc. IEEE Intern. Symp. on Inform. Theory*, (MIT, Cambridge, MA, USA), p. 276, Aug. 16-21 1998.
- [21] G. D. Forney, Jr., F. R. Kschischang, B. Marcus, and S. Tuncel, “Iterative decoding of tail-biting trellises and connections with symbolic dynamics,” in *Codes, Systems, and Graphical Models (Minneapolis, MN, 1999)* (B. Marcus and J. Rosenthal, eds.), pp. 239–264, Springer Verlag, New York, Inc., 2001.
- [22] C. Di, D. Proietti, I. E. Telatar, T. J. Richardson, and R. L. Urbanke, “Finite-length analysis of low-density parity-check codes on the binary erasure channel,” *IEEE Trans. on Inform. Theory*, vol. IT-48, no. 6, pp. 1570–1579, 2002.
- [23] D. J. C. MacKay and M. S. Postol, “Weaknesses of Margulis and Ramanujan-Margulis low-density parity-check codes,” *Electronic Notes in Theoretical Computer Science*, vol. 74, 2003.
- [24] T. Richardson, “Error floors of LDPC codes,” in *Proc. 41st Allerton Conf. on Communications, Control, and Computing*, (Allerton House, Monticello, Illinois, USA), October 1–3 2003.
- [25] T. Tian, C. R. Jones, J. D. Villasenor, and R. D. Wesel, “Selective avoidance of cycles in irregular LDPC code construction,” *IEEE Trans. on Comm.*, vol. COM-52, no. 8, pp. 1242–1247, 2004.
- [26] A. Ramamoorthy and R. D. Wesel, “Analysis of an algorithm for irregular LDPC code construction,” in *Proc. IEEE Intern. Symp. on Inform. Theory*, (Chicago, IL, USA), p. 69, June 27–July 2 2004.
- [27] V. Chernyak, M. Chertkov, M. Stepanov, and B. Vasic, “Instanton method of post-error-correction analytical evaluation,” in *Proc. IEEE Inform. Theory Workshop*, (San Antonio, TX, USA), pp. 220–224, Oct. 24–29 2004.
- [28] M. Stepanov, V. Chernyak, M. Chertkov, and B. Vasic, “Diagnosis of weaknesses in modern error correction codes: a physics approach,” *available online under <http://www.arxiv.org/cond-mat/0506037>*, June 2005.
- [29] B. J. Frey, R. Koetter, and A. Vardy, “Signal-space characterization of iterative decoding,” *IEEE Trans. on Inform. Theory*, vol. IT-47, no. 2, pp. 766–781, 2001.

- [30] G. D. Forney, Jr., R. Koetter, F. R. Kschischang, and A. Reznik, “On the effective weights of pseudocodewords for codes defined on graphs with cycles,” in *Codes, Systems, and Graphical Models (Minneapolis, MN, 1999)* (B. Marcus and J. Rosenthal, eds.), vol. 123 of *IMA Vol. Math. Appl.*, pp. 101–112, Springer Verlag, New York, Inc., 2001.
- [31] J. Feldman, *Decoding Error-Correcting Codes via Linear Programming*. PhD thesis, Massachusetts Institute of Technology, Cambridge, MA, 2003. Available online under <http://www.columbia.edu/~jf2189/pubs.html>.
- [32] J. Feldman, M. J. Wainwright, and D. R. Karger, “Using linear programming to decode binary linear codes,” *IEEE Trans. on Inform. Theory*, vol. IT-51, no. 3, pp. 954–972, 2005.
- [33] P. O. Vontobel and R. Koetter, “On the relationship between linear programming decoding and min-sum algorithm decoding,” in *Proc. Intern. Symp. on Inform. Theory and its Applications (ISITA)*, (Parma, Italy), pp. 991–996, Oct. 10–13 2004.
- [34] <http://www.pseudocodewords.info>.
- [35] R. M. Tanner, “On quasi-cyclic repeat-accumulate codes,” in *Proc. of the 37th Allerton Conference on Communication, Control, and Computing*, (Allerton House, Monticello, Illinois, USA), pp. 249–259, Sep. 22–24 1999.
- [36] R. M. Tanner, D. Sridhara, and T. Fuja, “A class of group-structured LDPC codes,” in *Proc. of ICSTA 2001*, (Ambleside, England), 2001.
- [37] S. Laendner and O. Milenkovic, “Algorithmic and combinatorial analysis of trapping sets in structured LDPC codes,” in *Proc. 2005 International Conference on Wireless Networks, Communications, and Mobile Computing (Wirelesscom 2005)*, (Maui, HI, USA), Jun. 13–16 2005.
- [38] F. J. MacWilliams and N. J. A. Sloane, *The Theory of Error-Correcting Codes*. New York: North-Holland, 1998.
- [39] S. Boyd and L. Vandenberghe, *Convex Optimization*. Cambridge, UK: Cambridge University Press, 2004.
- [40] A. Barvinok, *A Course in Convexity*, vol. 54 of *Graduate Studies in Mathematics*. Providence, RI: American Mathematical Society, 2002.
- [41] W. S. Massey, *Algebraic Topology: an Introduction*. New York: Springer-Verlag, 1977. Reprint of the 1967 edition, Graduate Texts in Mathematics, Vol. 56.
- [42] H. M. Stark and A. A. Terras, “Zeta functions of finite graphs and coverings,” *Adv. Math.*, vol. 121, no. 1, pp. 124–165, 1996.
- [43] J. Polderman and J. Willems, *Introduction to Mathematical Systems Theory*. Springer-Verlag New York, Inc., 1998.
- [44] J. Feldman, D. R. Karger, and M. J. Wainwright, “LP decoding,” in *Proc. 41st Allerton Conf. on Communications, Control, and Computing*, (Allerton House, Monticello, Illinois, USA), October 1–3 2003. Available online under <http://www.columbia.edu/~jf2189/pubs.html>.

- [45] T. Y. Hwang, “Decoding linear block codes for minimizing word error rate,” *IEEE Trans. on Inform. Theory*, vol. IT-25, no. 6, pp. 733–737, 1979.
- [46] E. Agrell, “Voronoi regions for binary linear block codes,” *IEEE Trans. on Inform. Theory*, vol. IT-42, no. 1, pp. 310–316, 1996.
- [47] A. Ashikhmin and A. Barg, “Minimal vectors in linear codes,” *IEEE Trans. on Inform. Theory*, vol. IT-44, no. 5, pp. 2010–2017, 1998.
- [48] Y. Borissov, N. Manev, and S. Nikova, “On the non-minimal codewords in the binary Reed-Muller code,” in *Proc. IEEE Intern. Symp. on Inform. Theory*, (Washington, D.C., USA), p. 39, June 24-29 2001.
- [49] P. O. Vontobel, R. Smarandache, N. Kiyavash, J. Teutsch, and D. Vukobratovic, “On the minimal pseudo-codewords of codes from finite geometries,” in *Proc. IEEE Intern. Symp. on Inform. Theory*, (Adelaide, Australia), pp. 980–984, Sep. 4–9 2005. Available online under <http://www.arxiv.org/abs/cs.IT/0508019>.
- [50] P. O. Vontobel and R. Smarandache, “On minimal pseudo-codewords of Tanner graphs from projective planes,” in *Proc. 43rd Allerton Conf. on Communications, Control, and Computing*, (Allerton House, Monticello, Illinois, USA), Sep. 28–30 2005. Available online under <http://www.arxiv.org/abs/cs.IT/0510043>.
- [51] R. Smarandache and M. Wauer, “Bounds on the pseudo-weight of minimal pseudo-codewords of projective geometry codes,” *submitted, available online under* <http://www.arxiv.org/abs/cs.IT/0510049>, Oct. 2005.
- [52] R. Koetter, W.-C. W. Li, P. O. Vontobel, and J. L. Walker, “Characterizations of pseudo-codewords of LDPC codes,” *submitted, available online under* <http://www.arxiv.org/abs/cs.IT/0508049>, Aug. 2005.
- [53] T. Etzion, A. Trachtenberg, and A. Vardy, “Which codes have cycle-free Tanner graphs?,” *IEEE Trans. on Inform. Theory*, vol. IT-45, pp. 2173–2183, Sept. 1999.
- [54] R. Koetter, W.-C. W. Li, P. O. Vontobel, and J. L. Walker, “Pseudo-codewords of cycle codes via zeta functions,” in *Proc. IEEE Inform. Theory Workshop*, (San Antonio, TX, USA), pp. 7–12, Oct. 24–29 2004. Available online under <http://www.arxiv.org/abs/cs.IT/0502033>.
- [55] M. J. Wainwright and M. I. Jordan, “Variational inference in graphical models: the view from the marginal polytope,” in *Proc. 41st Allerton Conf. on Communications, Control, and Computing*, (Allerton House, Monticello, Illinois, USA), October 1–3 2003.
- [56] J. S. Yedidia, W. T. Freeman, and Y. Weiss, “Constructing free-energy approximations and generalized belief propagation algorithms,” *IEEE Trans. on Inform. Theory*, vol. IT-51, no. 7, pp. 2282–2312, 2005.
- [57] M. M. Deza and M. Laurent, *Geometry of cuts and metrics*, vol. 15 of *Algorithms and Combinatorics*. Berlin: Springer-Verlag, 1997.

- [58] J. Feldman, T. Malkin, C. Stein, R. A. Servedio, and M. J. Wainwright, “LP decoding corrects a constant fraction of errors,” in *Proc. IEEE Intern. Symp. on Inform. Theory*, (Chicago, IL, USA), p. 68, June 27–July 2 2004.
- [59] J. Feldman, R. Koetter, and P. O. Vontobel, “The benefit of thresholding in LP decoding of LDPC codes,” in *Proc. IEEE Intern. Symp. on Inform. Theory*, (Adelaide, Australia), pp. 307–311, Sep. 4–9 2005. Available online under <http://www.arxiv.org/abs/cs.IT/0508014>.
- [60] D. Haley and A. Grant, “Improved reversible LDPC codes,” in *Proc. IEEE Intern. Symp. on Inform. Theory*, (Adelaide, Australia), pp. 1367–1371, Sep. 4–9 2005.
- [61] Y. Kou, S. Lin, and M. P. C. Fossorier, “Low-density parity-check codes based on finite geometries: a rediscovery and new results,” *IEEE Trans. on Inform. Theory*, vol. IT-47, pp. 2711–2736, Nov. 2001.
- [62] R. Lucas, M. Bossert, and M. Breitbart, “On iterative soft-decision decoding of linear binary block codes and product codes,” *IEEE J. Sel. Areas Comm.*, vol. JSAC-16, no. 2, pp. 276–296, 1998.
- [63] J. Xu, H. Tang, Y. Kou, S. Lin, and K. Abdel-Ghaffar, “A general class of LDPC finite geometry codes and their performance,” in *Proc. IEEE Intern. Symp. on Inform. Theory*, (Lausanne, Switzerland), p. 309, June 30–July 5 2002.
- [64] M. Fossorier, R. Palanki, and J. Yedidia, “Iterative decoding of multi-step majority logic decodable codes,” in *Proc. 3rd Intern. Symp. on Turbo Codes and Related Topics*, (Brest, France), Sept. 1–5 2003.
- [65] M. J. Wainwright, “Codeword polytopes and linear programming relaxations for error-control coding.” Talk at Workshop on “Applications of Statistical Physics to Coding Theory”, Santa Fe, New Mexico, USA, Jan. 11 2005. Available online under http://cnls.lanl.gov/~chertkov/EC_Talks/Wainwright/.
- [66] X.-Y. Hu, E. Eleftheriou, and D. M. Arnold, “Regular and irregular progressive edge-growth Tanner graphs,” *IEEE Trans. on Inform. Theory*, vol. IT-51, no. 1, pp. 386–398, 2005.
- [67] J. Rosenthal and P. O. Vontobel, “Constructions of LDPC codes using Ramanujan graphs and ideas from Margulis,” in *Proc. of the 38th Allerton Conference on Communication, Control, and Computing*, (Allerton House, Monticello, Illinois, USA), pp. 248–257, Oct. 4–6 2000.
- [68] C. Kelley and D. Sridhara, “Pseudocodewords of Tanner graphs,” *submitted to IEEE Trans. Inform. Theory*, available online under <http://www.arxiv.org/abs/cs.IT/0504013>, Apr. 2005.
- [69] P. O. Vontobel and R. Koetter, “Lower bounds on the minimum pseudo-weight of linear codes,” in *Proc. IEEE Intern. Symp. on Inform. Theory*, (Chicago, IL, USA), p. 70, June 27–July 2 2004.

- [70] P. Chaichanavong and P. H. Siegel, “Relaxation bounds on the minimum pseudo-weight of linear block codes,” in *Proc. IEEE Intern. Symp. on Inform. Theory*, (Adelaide, Australia), pp. 805–809, Sep. 4–9 2005. Available online under <http://www.arxiv.org/abs/cs.IT/0508046>.
- [71] R. A. Horn and C. R. Johnson, *Matrix Analysis*. Cambridge: Cambridge University Press, 1990. Corrected reprint of the 1985 original.